A High-speed Reconfigurable Free Space Optical Communication System Utilizing Software Defined Radio Environment

Zun Maung Maung Htay

A thesis submitted in partial fulfilment of the requirements of Northumbria University for the degree of Doctor of Philosophy

Research undertaken in the Faculty of Engineering and Environment

Jan 2023

Dedication

To life that was given by my darling mother Mrs. Khin Lay Tin.

To my thinnest patience that got thicker during this time.

To the unfathomable amount of food, drinks, and the company

I've enjoyed,

and lastly, to you.

Abstract

Free space optical (FSO) communication allows for high-speed data transmissions while also being extremely cost-effective by using visible or infrared wavelengths to transmit and receive data wirelessly through the free space channel. However, FSO links are highly susceptible to the effects of the atmosphere, particularly turbulence, smoke, and fog. On the other hand, FSO itself does not provide enough flexibility to address the issue of such blockage and obstruction caused by objects and atmospheric conditions. This research investigates, proposes, and evaluates a software defined multiple input multiple output (MIMO) FSO system to ensure link availability and reliability under weather conditions as part of the last mile access in the 5^{th} generation, 6^{th} generation, and beyond. Software defined radio (SDR) technology is adopted in order to provide a certain degree of flexibility to the optical wireless communications system. The scope of this research focuses on the design, validation, implementation, and evaluation of a novel adaptive switching algorithm i.e., activating additional transmitters of a MIMO FSO system using a software defined ecosystem. The main issues are the compactness of the experimental design; the limitation of software-oriented signal generation; robustness; reliability; and the quality of service. As part of the system design, the thresholding method, a decision-making process via the feedback link, and a spatial diversity technique is adopted to carry out the adaptive switching. The adaptive switching is performed via a feedback link in which the atmospheric loss and scintillation index are calculated for fog and turbulence respectively. The initial design is implemented in SDR/ GNURadio for a real-time emulation of the proposed system to enhance the system flexibility of a traditional MIMO FSO system. A bit-by-bit comparison is performed with the GNURadio signal processing block and BERT for a real-time BER estimation. However, based on the initial results, the switching mechanism can only overcome the effect of turbulence at a certain level. A new design to mainly mitigate the varying fog conditions is proposed based on the SDR-based adaptive switching for a gigabit ethernet (GbE) MIMO FSO system and tested in a 5 m dedicated atmospheric chamber. The proposed system is implemented using off-the-shelf components such as a media converter, small form pluggable transceivers, optical switch, and

power meter to estimate the channel state information. A new Schmitt trigger-based thresholding method is also introduced. The proposed software defined GbE MIMO FSO with an adaptive switching algorithm is fabricated, implemented, and investigated. The results are also compared with the real-time simulated data. Since the purpose of this Ph.D. is to explain and demonstrate the proof of concept for the proposed SDR-MIMO FSO system, the emphasis has been on the design, evaluation, and minimal performance requirements rather than maximizing the data rate. The outcome of the thesis will be a huge degree of flexibility and mitigation property MIMO FSO can offer with the help of SDR. It will be shown that the designed system has the capability to provide data transmission with 99.999% availability with a packet error rate and data rate of 7.2×10^{-2} and ~120 Mbps respectively, under extremely harsh fog conditions with visibility V of < 11 m.

Acknowledgment

This Ph.D. has been a roller coaster ride but firstly, I would like to show my love and appreciation to each and individual one of those who have made this a lot easier. Top of my list is Prof. Fary Ghassemlooy (my principal supervisor) who has guided me through the journey patiently. His outstanding mentoring, support, motivation, and encouragement have been keeping this PhD and myself alive. He has been an amazing colleague, a father, and a wonderful friend. His supervision and guidance have shaped me the way I am today in both scientific and personal point of view. Throughout the research process, his vital advice is evident that I have produced various collaborations and research output.

Sincere thanks to Dr Mojtaba Mansour Abadi (my second supervisor) for his mental and technical support, I have received throughout the journey. His extremely questionable patience and a big heart has always been something I thrive to have one day during my future academic path. Beside my advisors, I would like to thank the valuable comments and feedback from Dr Andrew Burton (ISOCOM Ltd.) and Prof. Stanislav Zvánovec at the Czech Technical University in Prague and his team. Furthermore, I would like to thank Dr Hoa Le Minh for his support and encouragement to pursue this PhD.

I would also like to thank my friends, colleagues and lab mates for the countless discussions, the sleepless nights, all the food and fun we have had through thick and thin, specifically, Mr. Carlos Guerra-Yánez, Dr Othman Younus, Dr Neha Chaudhary, Dr Xicong Li, Ms. Rida Zia-ul-Mustafa, the optical communications research group members, European collaborative research network and all the visiting researchers.

A great deal of gratitude goes to my friends, Dr Hernan Barrio-Zhang, Ms. Moe Yadanar Oo, and Mr. Michael George for their valuable support and love for me and my academic career.

In addition, I specially thank my grandmother, my aunt, my dearest late mother who always encouraged, loved, and supported me during this PhD until her final breath, my father, for his

immeasurable sacrifices made for me and the rest of my family. Many thanks to my sister, Zin and my nephew, Lu for the moral support and the smile they never failed to put on me during the difficult time.

Declaration

I declare that the work contained in this thesis is entirely mine and that no portion of it has been submitted in support of an application for another degree or qualification in this, or any other university, or institute of learning, or industrial organization.

Any ethical clearance for the research presented in this commentary has been approved. Approval has been sought and granted through the Researcher's submission to Northumbria University's Ethics Online System / external committee [Submission Ref: 21509] on 29th January 2020.

I declare that the Word Count of this Thesis is 29,352 words.

Zun Htay

31st Jan 2023

Table of Contents

Abstract i
Acknowledgment iii
Declaration v
Table of Contents vi
List of Tables ix
List of Figures x
List of Abbreviations xiii
Glossary of Symbols xvi
Chapter 1. Introduction 19
1.1 Background 19
1.2 Motivation 23
1.3 Aim and Objectives 25
1.4 Original Contributions 26
1.5 Thesis Structure 29
1.6 Publications and Awards 30
1.6.1 Journal Papers 30
1.6.2 Conference Papers 31
1.6.3 Awards 31
Chapter 2. The FSO System 32
2.1 Introduction 32
2.2 An Overview 32
2.2.1 Application Areas 33
2.3 FSO Features 36
2.4 FSO Structure 38
2.4.1 The Transmitter 38
2.4.2 The Channel 40
2.4.3 The Receiver 42
2.5 Atmospheric Conditions 43
2.5.1 Turbulence 43
2.5.2 Mitigation Techniques 48
2.5.3 Combining Methods 50
2.5.4 Fog and Visibility 55
2.5.5 Mitigation Techniques 58
2.6 Link Budget Analysis 59

2.7 Summary 60
Chapter 3. Software Defined Systems 61
3.1 Introduction 61
3.2 Software Defined Radio (SDR) 62
3.2.1 Areas of Applications 65
3.2.2 Structure of SDR 67
3.2.3 SDR Frontends 69
3.3 Software Defined Networking 74
3.3.1 Application Areas 75
3.3.2 Structure of SDN 76
3.3.3 SDN Frontends 77
3.3.4 SDN Software 78
3.4 Summary 79
Chapter 4. Software Defined Optical Wireless Communication 80
4.1 Introduction 80
4.2 SDR-based OWC 81
4.3 An Adaptive SDR 82
4.4 SDR-based Adaptive Equalization for OWC Systems 83
4.4.1 SDR-based Adaptive Modulation for OWC Systems 86
4.4.2 SDR-based Adaptive Power Control OWC Systems 87
4.5 SDR-based MIMO FSO System with Adaptive Switching 88
4.5.1 System Design Configuration 88
4.5.2 Implementation of SDR-based MIMO FSO with Adaptive Switching 93
4.5.3 Recorded Data 96
4.6 Summary 99
Chapter 5. Experimental Implementation of SDR-based OWC Systems 100
5.1 Introduction 100
5.2 Software Defined Implementation of OWC Systems 101
5.3 Experimental Testbed for SDR-based OWC 102
5.3.1 System Configuration 102
5.3.2 Implementation of OWC System in SDR/GNU Radio Platform 104
5.3.3 Experimental Setup 107
5.3.4 Recorded Data 108
5.4 Experimental Implementation of Adaptive Switching in OWC 112
5.4.1 System Configuration and Specification 112
5.4.2 Switching Algorithm 115
5.4.3 Experimental Setup 117

5.4.4 Link Power Budget 121
5.4.5 Recorded Data 123
5.5 Summary 127
Chapter 6. Conclusions and Future Work 128
6.1 Conclusions 128
6.2 Future Works 130
References 132

List of Tables

Table 2.1.Comparison of FSO and RF communications [66, 67]. 36
Table 2.2. Radiuses of various types of particles [90], [14]. 42
Table 2.3 The comparison of APD and PIN PDs [91] [92]. 43
Table 3.1. Examples of SDR frontends. 71
Table 3.2. High-speed commercially available SDR frontends. 72
Table 3.3. Overview of SDR software capabilities and features. 73
Table 4.1. Key System parameters for the implementation of MIMO FSO system with adaptive switching in GNURadio. 89
Table 4.2. The number of Txs used as a function of L, V and LAtm under the fog condition. 92
Table 4.3. The number of Txs used as a function of L, $\sigma \mathrm{I2}$ and $\mathrm{Cn2}$ under the turbulence condition. 92
Table 5.1. Key system parameters for implementation of OWC system in GNU Radio software ecosystem. 105
Table 5.2. Key system parameters in SDR-OWC experimental set up. 107
Table 5.3. Bandwidth and jitter of the received signal corresponding to the interpolation rate and taps. 108
Table 5.4. Key system parameters of MIMO FSO with adaptive switching set up. 115
Table 5.5. Component specifications for the experimental demonstration of MIMO FSO with software defined adaptive switching. 118
Table 5.6. Link budget analysis of a combined link. 122
Table 5.7. Statistics of the system performance metrics for the B2B, clear and increasing fog density conditions of V_1, V_2 and, V_3. 126

List of Figures

Figure 1.1. Summary of original contributions. 28
Figure 2.1.Block diagram of a typical FSO system with transceivers. 33
Figure 2.2.The application of FSO in high data rate access. 34
Figure 2.3. Block diagram of a terrestrial FSO link. 38
Figure 2.4. Optical intensity: (a) internal modulation, and (b) external modulation using MZM. 39
Figure 2.5. Channel models in: (a) free space, (b) clear air with turbulence layer, and (c) a multiple scattering medium. 44
Figure 2.6. The turbulent channel consists of eddies of various sizes. 45
Figure 2.7. SD configurations of SISO, SIMO, MISO, and MIMO denoting single-input single-output, single-input multiple-output, multiple-input single-output, multiple-input multiple output, respectively. 50
Figure 2.8. Block diagram of combining implementation at the optical domain level. OTx, RxOptics, and ORx refer to the optical Tx, optical aperture, and optical Rx, respectively. 51
Figure 2.9. Block diagram of combining implementation at electrical domains with EGC technique. 52
Figure 2.10. Block diagram of combining implementation at electrical domains with SelC technique. 52
Figure 2.11. Block diagram of combining implementation at logical domains with MLC technique. 53
Figure 2.12. FSO relaying system: (a) serial configuration, and (b) parallel configuration. 54
Figure 2.13. Comparison between Rayleigh, Geometric, and Mie scattering. 56
Figure 3.1. The difference between analog, DSP, and SDR. 64
Figure 3.2. Bi-directional SDR transceiver. 65
Figure 3.3. The applications of SDR with FSO/OWC backhaul. 67
Figure 3.4. The block diagram of a traditional SDR Tx. 68
Figure 3.5. The block diagram of a traditional SDR Rx. 68
Figure 3.6. The architecture of SDN. 76
Figure 4.1. Schematic system block diagram of MIMO FSO system with adaptive switching algorithm in software defined GNURadio ecosystem. 91
Figure 4.2. System flow chart of SDR-based MIMO FSO with adaptive switching. 94
Figure 4.3. System implementation for (a) Tx with fog and turbulence, (b) channel with the additive white gaussian noise, and (c) the Rx with real-time BER estimation in GNURadio. 95

Figure 4.4. OOK waveforms at the: (a) Tx-Link A, (b) Tx-Link B, (c) optical Rx for a clear channel, and (d) Tx- Link A, (e) Tx-Link B, and (f) optical Rx for an un-clear channel. 96
Figure 4.5. BER vs. the visibility for single, MIMO and proposed FSO with adaptive switching links for: (a) 100, (b) 200, and (c) 300 m with fog. 97
Figure 4.6. BER vs. $Cn2$ for single, MIMO and proposed FSO with adaptive switching links for: (a) 100, (b) 200, and (c) 300 m with turbulence. 98
Figure 5.1. The block diagram of a proposed SDR based OWC system using USRP. 103
Figure 5.2. Implementation of FSO system in GNU Radio: (a) a hierarchical chain of blocks to generate an OOK signal which is built as a signal generator (b) an OOK signal with fog, turbulence, and geometric loss transmitted to the USRP, and (c) a BERT. 106
Figure 5.3. Real-time implementation of FSO system using SDR/GNU Radio ecosystem. 107
Figure 5.4. Received OOK-NRZ signals via USRP (lower trace, in red) and optical front end (upper trace, in yellow) with the interpolation filter length of: (a) 10, (b) 12, (c) 14, (d) 16, (e) 18, and (f) 20. 109
Figure 5.5. Eye diagrams of received OOK-NRZ via optical frontend with the interpolation filter rates of : (a) 10, (b) 12, (c) 14, (d) 16, (e) 18, and (f) 20. 109
Figure 5.6. The received OOK signals transmitted via USRP and a red laser in a 200 m link for the: (a) light, (b) medium, and (c) dense fog conditions. 111
Figure 5.7. The received OOK signals transmitted via USRP and a red laser in a 200 m link under: (a) weak, (b) moderate, and (c) strong turbulence. 111
Figure 5.8. The schematic system block diagram of an experimental implementation of MIMO FSO with SDR based adaptive switching method. 114
Figure 5.9. System flow chart of experimental GbE MIMO FSO with adaptive switching. 116
Figure 5.10. The OOT modules for the power meter and optical switch in the GNU Radio platform. 116
Figure 5.11. Screenshots of the developed python code for: (a) network performance tester for measuring the performance of the Ethernet FSO link, and (b) received data and bandwidth. 117
Figure 5.12. Experimental setup of: (a) Tx with PC connected to MC to transmit data and power meter to receive the VE laser and estimate the visibility. Optical switch connected to the PC for adaptive switching according to received CSI from the power meter. (b) Rx setup with VE laser, two collimators for received signals, coupler to combine two received signals, and MC connected to the PC. 119
Figure 5.13. Experimental setup of Channel setup when fog is injected. 120
Figure 5.14. Visibility vs.: (a) PER, (b) Jitter, and (c) data rate for 5 m SISO and MIMO FSO links under fog conditions. 123
Figure 5.15. Atmospheric loss vs.: (a) PER, (b) Jitter, and (c) data rate for 5 m SISO and MIMO FSO links under fog conditions. 124

Figure 5.16. Eye diagrams of the single FSO link: (a) under clear channel, (b) V_1, (c) V_2, and (e) V_3; MIMO link for: (d) V_2, and (f) V_3. 125

List of Abbreviations

Acronyms	Description
AA	Aperture averaging
ADC	Analogue to digital converter
AF	Amplify and forward
ANN	Artificial neural network
APD	Avalanche photodetector
ASIC	Application specific integrated circuits
B2B	Back-to-back
BER	Bit error rate
BERT	Bit error rate tester
CLI	Command line interface
CSI	Channel state information
DAC	Digital to analogue converter
DC	Direct current
DDC	Digital down converter
DF	Decode and forward
DFE	Decision feedback equalization
DSL	Digital subscriber loop
DUC	Digital up converter
EGC	Equal gain combining
FEC	Forward error correction
FPGA	Field programmable gate array
FSO	Free space optics
FTTH	Fibre to the home
GUI	Graphical user interface
I2RS	Interface to the Routing System
IF	Intermediate frequency
IIoT	Industrial internet of things
IoT	Internet of things
IM/DD	Intensity modulation/ direct detection
IR	Infrared

ISI	Inter symbol interfaces
ISM	Industrial, Scientific, and Medical
LD	Laser diode
LDPC	Low density parity check
LED	Light emitting diode
LMDS	Local multipoint distribution service
LMS	Least mean square
LNA	Low noise amplifier
LO	Local oscillator
LoS	Line of sight
MC	Media converter
MIMO	Multiple input multiple output
MISO	Multiple input single output
ML	Machine learning
mmW	Millimeter wave
MLC	Majority logic combining
MZM	Mach Zehnder modulator
NRZ	Non return to zero
Ofcom	Office of Communication
OFDM	Orthogonal frequency division multiplexing
ONF	Open network foundation
ONOS	Open networking operating system
OOK	On off keying
ORx	Optical receiver
OS	Optical switch
OTx	Optical transmitter
OWC	Optical wireless communications
PD	Photodetector
PDF	Probability density function
PER	Packet error rate
PERT	Packet error rate tester
PIN	*p*-type-intrinsic-*n*-type photodetector
PPM	Pulse position modulation
QAM	Quadrature amplitude modulation
QoS	Quality of service

RF	Radio frequency
RLS	Recursive least squares
Rx	Receiver
RxOptics	Optical aperture
SD	Spatial diversity
SDN	Software defined network
SDR	Software defined radio
SelC	Selection combining
SFP	Small form pluggable
SISO	Single input single output
SMF	Single mode fibre
Tx	Transmitter
USRP	Universal software radio peripheral
UV	Ultraviolet
UWB	Ultra-wide band
VE	Visibility estimation
VLC	Visible light communication
ZF	Zero forcing

Glossary of Symbols

A	Nominal value of $C_n^2(0)$
AF	Aperture averaging factor
A_f	Wavefront area
A_p	Cross sectional area of scattering
$\alpha_m(\lambda)$	Wavelength dependent molecular absorption coefficient
$\alpha_a(\lambda)$	Wavelength dependent aerosol absorption coefficient
β	Effective number of small-scale turbulence cells
$\beta_m(\lambda)$	Wavelength dependent molecular scattering coefficient
$\beta_a(\lambda)$	Wavelength dependent aerosol scattering coefficient
$\beta_{Rayleigh}(\lambda)$	Wavelength dependent rayleigh coefficient
C_n^2	Refractive index structure coefficient
C_T^2	Temperature structure coefficient
D_{Rx}	Optical Rx aperture diameter
D_{Tx}	Optical Tx aperture diameter
d	Circular aperture scaled by Freshnal zone
d_{s}	Optical Rx lens diameter
η	Optical to electrical conversion coefficient
γ	Extinction loss coefficient of the channel
$\Gamma(.)$	Gamma function
h	Channel gain
h_a	Atmospheric channel due to scintillation
h_t	Atmospheric channel due to path loss/scintillation
I	Irradiance vector
I_m	Irradiance received at m^{th} aperture
I_o	Signal light intensity mean
k	Wave number
$\mathrm{K_n}(.)$	Modified Bessel function of 2nd kind and order n
L	Link length
L_{Atm}	Atmospheric attenuation loss
$L_{\mathrm{Atm\ (Thres)}}$	Threshold level for atmospheric loss
L_{Cou}	Optical coupler loss

L_{Col}	Optical collimator loss
L_{fog}	Fog attenuation loss
L_{Geo}	Geometrical loss
L_{M}	Link margin
L_{misc}	Miscellaneous loss
$L_{\mathrm{LC-FC/PC}}$	LC-FC/APC connector loss
LN	Interpolation taps
L_{Op}	Optics loss
L_{OS}	Optical switch loss
L_{PE}	Pointing error loss
LR	Interpolation rate
M	Number of receiver aperture
μ_{total}	Total log-normal PDF mean
μ_x	Log-normal PDF mean
N_0	Noise spectral density
N_{P}	Number of particles per unit volume
n_0	Number of simultaneous received 0s
n_1	Number of simultaneous received 1s
OOK	On off keying
P_{Tx}	Transmit optical power
P_{Rx}	Receive optical power
$P_{\mathrm{VE-Up}}$	Upper limit of the received VE laser power
$P_{\mathrm{VE-Lo}}$	Lower limit of the received VE laser power
$P_{\mathrm{VE-Max}}$	Maximum received VE laser power
q	The size distribution pf scattering fog particles
Q	Q-factor
r_{total}	Adaptive optics received signal
R_b	Data rate
S	Transmit information bit
sps	Samples per symbol
σ_I^2	Scintillation index
σ_{lnX}^2	Large-scale irradiance fluctuations variances
σ_{lnY}^2	Small-scale irradiance fluctuations variances
σ_R^2	Rytov variance
σ_{total}^2	Total log-normal PDF variance

$\sigma^2_{I(\mathrm{Thres})}$	Threshold level for turbulence
σ_x^2	Log-normal PDF variance
t	time
θ_0	Transmitter divergence angle
V	Visibility
v	Rms wind speed

Chapter 1. Introduction

1.1 Background

Free space optical (FSO) communications, also known as laser communications, is a very well-known branch of optical wireless communications (OWC) technology mainly due to its capability of high-speed data transmission. FSO technology involves the transmission of information and utilization of a laser source enclosed with data at one point and the atmosphere as a propagation medium to another point. OWC, in various forms, has been used since pre-historic times by the ancient Greeks and Romans for a coded alphabetic system of signalling with fire beacons over a medium-range distance [1]. In the modern era, the growing interest of OWC in research, development, and deployment was first initiated by Alexander Graham Bell and his assistant Chales Sumner Tainter in 1880 [2]. The first wireless speech communication named "photophone" was invented, using sun rays to transfer voice over 200 m distance [3]. During World War II, the "Lichtsprechgerät 80/80 (literal translation: optical speaking device)" was invented by the optics company called Carl Zeiss to communicate voice signals using modulating optical beams and practical use came in by the German army.

The discovery of lasers in the 1960s elevated the technology of FSO. Several demonstrations of FSO applications were recorded throughout the early 1960s into 1970s including (*i*) a television signal transmission over a 30 mile (48 km) using a light emitting GaAs diode-based FSO link by researchers from MIT Lincolns Laboratory in 1962 [4]; (*ii*) a transmission of voice modulated He-Ne laser over 118 miles and the first TV-over-laser demonstration in 1963 by the researchers in the USA [4]; and (*iii*) A commercial laser link to control traffic was built in Japan by the Nippon Electric Company (NEC) in 1970 [4]. However, OWC/ FSO systems were not widely realized for commercial use compared to radio frequency (RF) systems. The main reasons were that the existing technologies were more than adequate to meet the demands and the impact of carrying atmospherics conditions, along with the costly optical components.

The history of wireless telecommunications massively evolved in 1934, when the first wireless phone calls were made between USA and Japan using RF technology [5]. Not much happened until the use of cellular mobile technology slowly penetrated the wireless domain through 1970s to 1980s where cellular mobile cellular access networks were deployed and the internet access was given to the military, corporate, and research laboratories in a few universities. RF technology offers a number of advantages including flexibility, availability of components, and ease of installation that have been making RF the dominant technology in wireless systems until recently [6]. In the 1990s, FSO began to gain attention as a potential alternative to traditional wired and wireless communications systems. Researchers and companies began to explore the potential of FSO for a wide range of applications, such as providing high-speed internet access to remote areas, connecting buildings in a campus environment, and creating redundant communications systems for critical infrastructure. During this period, several companies began to develop commercial FSO systems. In the 2000s, FSO technology continued to evolve and mature. Advances in laser technology, such as the development of visible light communications (VLC), made it possible to transmit data over even longer distances and to use FSO in a wider range of environments [1]. Additionally, companies and researchers began to explore the use of FSO for a wider range of applications, such as providing wireless backhaul for cellular networks and creating high-speed links for data centres [7].

Recent years have seen a significant increase in the use of FSO technology. Advancements in laser technology and modulation techniques have enabled the increase of the data rate (R_b) and the distance of the communication, making it more competitive with other wireless technologies such as millimeter wave (mmW), microwave, or fibre optics. The extraordinary amount of data flow that the optical fibre technology backbone made possible has an issue at the access network, “dubbed” the first/last mile bottleneck. This issue was foreseen back in the 1980s. Between 1990-2010, the bottleneck of first/last mile access was initially addressed by the AT&T Bell labs scientists [8]. In today’s technology, FSO appears to be the most potential optical solution for ultra-high R_b deliverability [9].

FSO capitalizes on existing technology and components (lasers, photodetectors (PD), optics) and well establishes protocols (Ethernet, SONET/SDH, ATM) to establish an optical link in a short amount of time that supports >Gbps over a distance of a few kilometers [6]. In fact, this technology has been heavily researched for NASA in inter-satellite applications [10]. Despite the fact that space FSO communication is outside the scope of this thesis and the discussion, it is worth mentioning that in the past decade, near-Earth FSO with $R_b$of up to 10 Gbps was successfully demonstrated in space between satellites [11], [12]. With the tremendous growth and maturity of optoelectronic devices, FSO has recently been utilized for ground-to-ground communications and become commercially available. Additionally, the demand for more bandwidth continues to grow, it is becoming increasingly important for communication systems to be flexible and adaptable. The growing number of new and emerging applications, such as video streaming, virtual reality, and the Internet of Things (IoT), all require large amounts of bandwidth. Therefore, relying on a single-access technology is no longer sufficient to meet the needs of end users [9]. Additionally, FSO can be used as a complementary technology to other access technologies, such as fibre optic, RF, and Millimeter-wave technology, to provide a more robust and reliable network [13]. RF and millimeter wave-based wireless networks can give data rates ranging from tens of megabits per second (point-to-multipoint) to several thousand megabits per second (point-to-point) [14]. However, due to spectrum congestion, licensing concerns, and interference from unlicensed bands, their market penetration is constrained. The license-free bands of the future show promise [15] but they have lower bandwidth and shorter ranges than the FSO. Broadband access networks to homes and businesses, as well as a high bandwidth bridge between local and wide area networks, are provided by the short-range FSO lines as an alternative to the RF links for the last or first mile [16]. Terrestrial FSO has now proven to be a viable supplementary technology for tackling contemporary communication issues, particularly the affordable bandwidth/high data rate requirements of end users. Because FSO is transparent to traffic type and data protocol, its incorporation into the current access network is significantly accelerated. However, atmospheric channel effects like as dense fog, smoke, and turbulence, as well as achieving 99.999% availability, continue to pose the greatest obstacles to long-range terrestrial FSO.

Software Defined Radio (SDR) is a technology that enables the implementation of wireless communication systems using software rather than hardware. In recent years, SDR has been applied to the field of OWC to enable more flexible and adaptable communication systems. The origins of SDR can be traced back to the late 1990s when researchers first began exploring the concept of using software to implement wireless communication systems [17]. The idea behind SDR was to create a radio system that could be easily reconfigured and adapted to different communication standards and protocols by changing the software rather than the hardware [18]. In the early 2000s, researchers began to explore the use of SDR in OWC systems. One of the key advantages of SDR in OWC is the ability to adapt the communication system to the specific characteristics of the optical channel, such as atmospheric turbulence and interference caused by other sources [19]. Additionally, SDR can enable the implementation of multiple communication standards and protocols in a single OWC system, making it more versatile and flexible. In 2015, the demonstration of the SDR-VLC system was presented in [20]. The researchers used universal software radio peripheral (USRP) and LabView software with optical frontends and successful demonstration audio streaming through an optical link of 2 m. One of the platforms demonstrated is a hybrid RF/OWC and SDR for simultaneous transmission of the radio and optical communications waveforms through to the physical layer for space applications [21]. The experimental demonstration of a real-time SDR multiple input multiple output (MIMO) VLC system with adaptivity of spatial diversity (SD) and multiplexing was reported in [22], using USRP to enhance the error performance and spectral efficiency. In recent years, SDR has become an increasingly important technology in OWC systems. With the advent of 5G and the increasing demand for high-speed and high-capacity wireless communication systems, SDR has become a key enabler for the implementation of flexible and adaptive OWC systems that can support a wide range of applications and communication standards [23], [24], [25]. In summary, the history of SDR in OWC is relatively short but it has been rapidly advancing in recent years. SDR has the potential to revolutionize the way we communicate by enabling more flexible and adaptable OWC system.

1.2 Motivation

Research in optical communications is motivated by the ever-increasing bandwidth requirements of existing and emerging communication systems (both fibre optics and optical wireless). Optical communication ensures sufficient bandwidth, which results in high data transfer rates. The enormous bandwidth available on the fibre ring networks that serve as the backbone of modern communication technology is not yet accessible to end users in the access network. This is primarily due to the bandwidth limitations of the copper wire-based technologies that connect end users to the backbone in the majority of locations. This restricts the data transfer rate/download speed available to end users. This issue is referred to as the 'access network bottleneck,' and several solutions, including fibre to the home (FTTH), Digital subscriber loop (DSL) or cable modems, power-line communication, local multipoint distribution service (LMDS), ultra-wide band (UWB), and terrestrial FSO, have been proposed to address it.

FTTH technology would be a good candidate to solve the access network bottleneck, and Asia leads the globe in FTTH deployment and penetration [26] with the UK being the highest subscriber in 2020 [27] . FTTH technology can deliver 10 Gbps to end customers, and possibly 10 Tbps with dense wavelength division multiplexing [28], [29]. However, the high cost of FTTH deployment is its biggest barrier. Also, copper-based DSL and powerline communication solutions are less appealing [9]. The LMDS is a fixed broadband, line-of-sight wireless radio access system that operates at 27.5–31.3 GHz in the US and 40.5–42.5 GHz in Europe [30]. It offers a bandwidth of several hundred Mbps, but its carrier frequencies are within licensed bands, which makes it less desirable. It also suffers severe signal attenuation and outage during rainfall [30]. Additionally, UWB, like FSO, operates unlicensed in the 3.1-10.6 GHz range [15]. The UWB can accommodate many Mbps over a short range. The technology is intriguing, but like copper wire-based options, its data rate is significantly below the backbone's multiple Gbps. Wideband technology raises issues about UWB transmissions interfering with other systems/gadgets in the same frequency spectrum [31].

Terrestrial FSO is becoming a potential supplementary technology. FSO deploys faster, is re-deployable, and requires no trenches or rights of way [32], [33]. Its capacity is similar to optical fibre and costs a fraction of FTTH deployment [32], [33]. FSO integrates well into the access network since it is traffic type and protocol transparent. Understanding the capabilities, limitations, and performance analysis of an optical wireless system based on some of the existing access network traffic types and modulation techniques would help improve its seamless integration. The major problem of FSO is atmospheric channel signal scattering, absorption, and fluctuation [34], [35], [36], [37].

Fog-induced atmospheric attenuation requires FSO systems to transmit extra optical power to compensate for the loss without exceeding regulatory safety limits or reducing link range [14]. An FSO-RF hybrid system may provide 99.999% availability in all-weather situations with an RF back-up link in fog-prone areas [38]. This hybrid technology reduces the data rate when the RF back-up link is active [14]. The hybrid system can lose data when transitioning from FSO to RF or vice versa and/or lose real-time operation owing to temporary data storage. Buffered switching prevents data loss. To avoid false triggers, the switchover switch should be rapid and smart. Additionally, as FSO is essentially a line of sight (LOS) technology that can be disrupted by obstacles such as buildings or trees and the limited mobility of FSO systems which limits their utility in certain applications such as mobile networks which poses a great design challenge.

This research investigates and proposes the cost-effective software defined implementation for an optimum switching method for a targeted bit error rate (BER), packet error rate (PER), and R_b in the presence of fog and turbulence-induced channel fading. In order to solve the issue of limited mobility and LOS characteristic, this thesis will examine and propose the adaptively reconfigurable MIMO FSO system to overcome the varying atmospheric conditions by proposing a smart and fast switching mechanism to prevent data loss. In this thesis, SD and optical combining to avoid the cost and complexity including the processing delays will be considered. To attain these goals, several research objectives have been formulated.

1.3 Aim and Objectives

The aim of this research is to investigate the performance of the flexible and reconfigurable FSO systems in order to comprehend the advantages and disadvantages including the limitations. In addition, the research aims to compare the performance of single input single output (SISO), MIMO, multiple input single output (MISO), and SDR-FSO systems. The results of the analysis will be useful to implement the real-time software defined based FSO systems experimentally and to estimate the required system architecture to reach a desired level of performance, as well as the achievable link margin and possible link range. To accomplish this, the research objectives are as outlined:

1. Review the fundamental properties of terrestrial FSO and comprehend the peculiarities of the atmospheric channel as well as the challenges put on the functioning of the system.
2. Examine the existing models used for mitigation of the atmospheric channel impacts.
3. Comprehensive simulation of the proposed FSO system for design validation.
4. Optimization of the MIMO FSO system to reduce the error rate and mitigate the atmospheric conditions.
5. Proposing a novel design for a reconfigurable FSO system that is supported by comprehensive analytical modelling and fabrication of the proposed system to implement in the real-time domain.
6. Proposing a system design to implement a real-time adaptive switching algorithm experimentally using off-the-shelf components.
7. Comparison of experimental performance analysis of existing models and the proposed models.
8. An evaluation of the system's performance based on the BER and link availability.

1.4 Original Contributions

During the course of this research, the original contributions made are best outlined with reference to Figure 1.1 and are also summarised below:

1. Investigation of the limitation of FSO system under fog and turbulence in real-time atmospheric chamber based on (on-off keying) OOK signalling technique and off-the-shelf components and demonstrated the experimental results. The link power budget and the system tolerance along with the misalignment losses are examined.
2. Developing an experimental testbed for FSO system using GNURadio to demonstrate the viability of the SDR in FSO systems as a proof of concept including (*i*) the mathematical analysis to demonstrate the functionality of the turbulence and fog, covering the regimes of light, moderate, and strong atmospheric regimes in real-time, including the BER estimator; and (*ii*) introduction of a software-based platform whereby changing the parameters at will, observing the real impact in the system performance of a practical setting.
3. Investigation of the adaptive schemes to mitigate the effect of turbulence and fog for the MIMO FSO link including (*i*) introducing the capability and implementation of SDR in OWC systems; (*ii*) simulation of the MIMO FSO using scintillation index and atmospheric loss experienced by the channel to determine the BER in real time; (*iii*) proposing an adaptive switching algorithm for MIMO FSO system using SDR based ecosystem called GNURadio; (*iv*) proposing a real-time decision-making feedback link using BER to increase/decrease the number of laser transmitter (Tx); and (*v*) introducing and employing the thresholding method to support the decision-making process.
4. Investigation of the final design and experimental demonstration including (*i*) the MIMO FSO system configuration based on adaptive switching and thresholding methods outlined in Chapters 3 and 4 respectively; (*ii*) using a power meter to estimate the visibility (i.e., channel state information (CSI)) of the FSO channel for varying fog

conditions in order to implement the thresholding method; and (*iii*) analysis of the experimental demonstration of the gigabit ethernet MIMO FSO switch software defined adaptive switching using off the shelf components such as media converter (MC), optical switch (OS), power meter, etc.

5. Investigation and analysis of the effects of FSO data rate and link availability of the gigabit ethernet MIMO FSO in a 5 m dedicated atmospheric chamber.

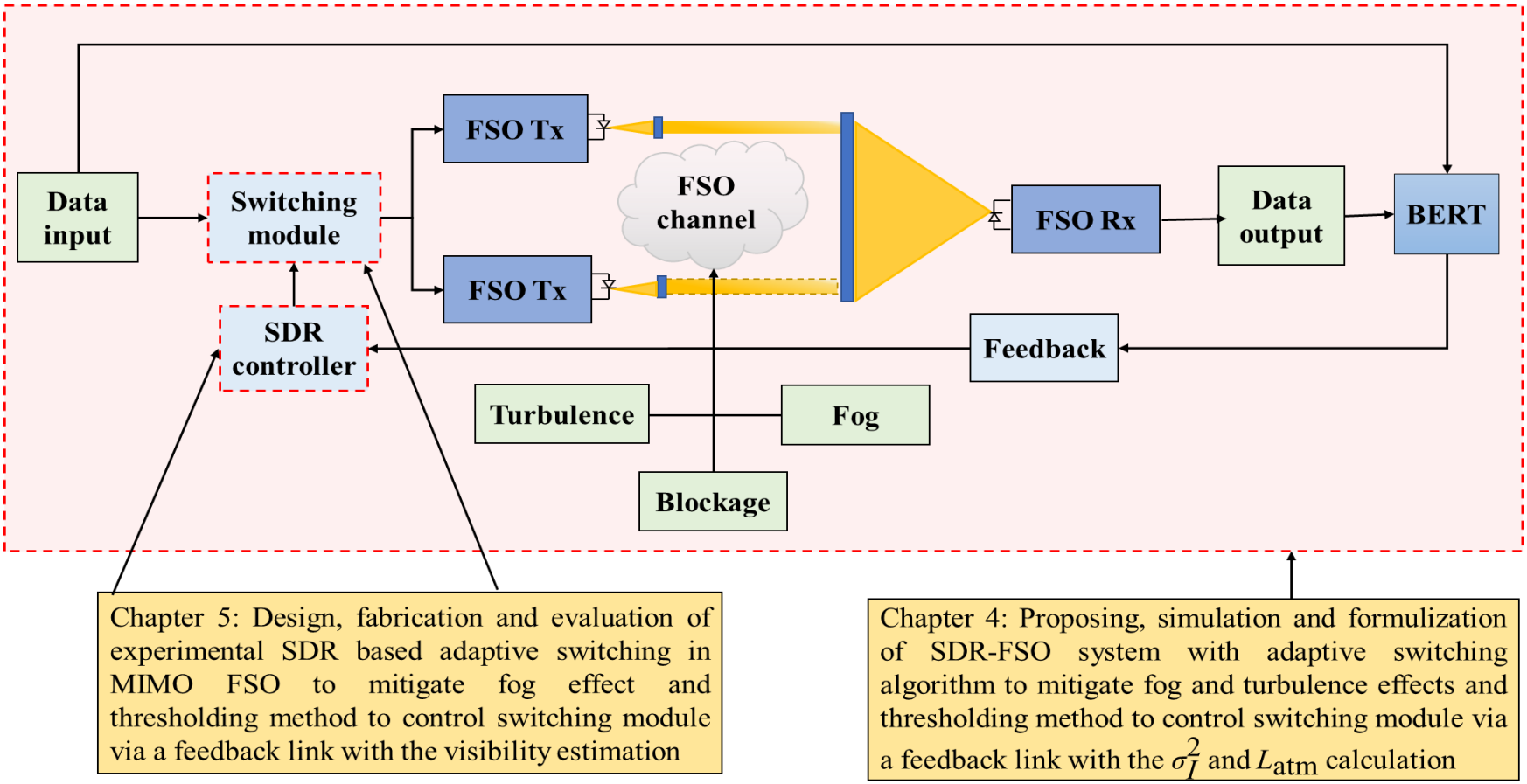

Figure 1.1. Summary of original contributions.

1.5 Thesis Structure

This thesis has been arranged into six chapters. **Chapter One** outlines a complete introduction of FSO technology and the SDR-FSO system. The background, aim, and objective of the thesis including the original contributions to knowledge are also mentioned in this chapter. In **Chapter Two**, an overview of FSO technology is discussed. The structure, the application, and the fundamental features of FSO system are discussed and explained thoroughly with a general block diagram. The functions of each distinctive part are highlighted and also presented. The limitation and bottleneck caused by the atmospheric conditions, especially fog and turbulence, along with the mitigation techniques are introduced. The link budget analysis of the traditional FSO system is also mentioned in this chapter. **Chapter Three** summarizes the background and fundamental features of SDR technology. The distinctive architecture of the SDR system is thoroughly explained and the area of applications is discussed, the commercially available frontends of the SDR technology including both hardware and software frontends are investigated and the comparison of limitations of each frontend is analysed. A brief introduction of the software defined networking system is also introduced including its structure and available frontends.

Chapter Four discusses software defined optical communications systems and various adaptive systems, such as adaptive equalization, adaptive modulation, and adaptive power allocation. A real MIMO FSO with an adaptive switching algorithm in a software defined GNURadio ecosystem is proposed to mitigate atmospheric losses. The performance of a real-time SDR/GNURadio implementation under different atmospheric conditions is evaluated and a thorough discussion on channel characterization and building real-time out-of-tree (OOT) modules for the system implementation is made. The (bit error rate tester) BERT is utilized to perform a bit-by-bit comparison with the GNURadio signal processing block. The MIMO FSO with adaptive switching technique is demonstrated to operate effectively in dense fog and validated that the switching mechanism, i.e., activating additional Txs, can only counteract turbulence up to a certain level.

Several experimental demonstrations of real-time FSO and MIMO FSO systems in software defined ecosystem GNURadio are investigated in **Chapter Five**. An implementation of the OOK signal generator and the performance of limitation due to the PC bandwidth, a real-time BER estimation of an FSO system under varying fog and turbulence conditions are first demonstrated and discussed using off-the-shelf components. In addition, the capability of the software defined FSO system in real time for very long-distance communications without the need for the required amount of physical space and the evaluation of real-time BER estimation is investigated. The implementation of a real-time MIMO FSO system with a proposed adaptive switching algorithm to validate the reconfigurability of the system is also carried out in this chapter. By employing the software defined adaptive switching method, the FSO system can operate against the severe fog regime, while the flexible configuration and easily implementable design are also provided. Finally, in **Chapter Six,** the conclusions and future recommended works are outlined.

1.6 Publications and Awards

1.6.1 Journal Papers

1. **Z. Htay**, Z. Ghassemlooy, M. M. Abadi, A. Burton, N. Mohan, and S. Zvanovec, "Performance Analysis and Software Defined Implementation of Real-Time MIMO FSO With Adaptive Switching in GNU Radio Platform," in IEEE Access, vol. 9, pp. 92168-92177, 2021, doi: 10.1109/AC- CESS.2021.3092968.
2. N. Mohan, Z. Ghassemlooy, E. Li, M. M. Abadi, S. Zvanovec, R. Hudon., and **Z. Htay**, "The BER performance of a FSO system with polar codes under weak turbulence", IET Optoelectronics, 2021. Available: 10.1049/ote2.12058.
3. **Z. Htay**, C. Guerra-Yánez, Z. Ghassemlooy, S. Zvanovec, M. M Abadi, and A. Burton, "Experimental Real-time GbE MIMO FSO under Fog Conditions with Software Defined GNU Radio Platform-based Adaptive Switching", submitted to IEEE Journal of Optical Communications and Networking (JOCN).

1.6.2 Conference Papers

1. **Z. Htay**, N. Mohan, M. M. Abadi, Z. Ghassemlooy, A. Burton, and S. Zvanovec, "Implementation and Evaluation of a 10 Gbps Real-time FSO Link," 2020 3rd West Asian Symposium on Optical and Millimeter-wave Wireless Communication (WASOWC), 2020, pp. 1-7, doi: 10.1109/WA- SOWC49739.2020.9410045.
2. **Z. Htay**, Z. Ghassemlooy, S. Zvanovec, M. M Abadi, and A. Burton, "An Experimental Testbed for Implementation and Validation of Software defined FSO under Atmospheric Conditions using USRPs", submitted to 2022 13th International Symposium on Communication Systems, Net- works and Digital Signal Processing (CSNDSP), 2022.
3. **Z. Htay**, B. R. Karanam, C. Guerra-Yánez, Z. Ghassemlooy, S. Zvanovec and M-A Khalighi, and M. M. Abadi, "Demonstration of Optical Wireless Communications System using a Software Defined Ecosystem", submitted to 2022 13th International Symposium on Communication Systems, Networks and Digital Signal Processing (CSNDSP), 2022.

1.6.3 Awards

1. Fully Paid Ph.D. Research Grant (Northumbria University, 2019).
2. European Network on Future Generation Optical Wireless Communication Technologies – Research Grant Short Term Scientific Mission-CA19111-48850 **(European Cooperation in Science & Technology, 2021).**
3. Best Poster Award, EPSRC Early career academics and postgraduate conference (PGCon) **(Edinburgh University, 2022).**
4. European Network on Future Generation Optical Wireless Communication Technologies – Research Grant Short Term Scientific Mission-CA19111-48850 **(European Cooperation in Science & Technology, 2022).**

Chapter 2. The FSO System

2.1 Introduction

A comprehensive overview of the FSO technology is thoroughly explained in this chapter including its structure, key features, and the most common application areas. Additionally, the bottleneck associated with the FSO system as well as existing challenges are outlined and discussed. The chapter also introduces mitigation methods to combat varying atmospheric conditions as well as the combining methods for MIMO FSO systems and discussed the SD technique which is critical for the following chapters.

2.2 An Overview

Fundamentally, FSO involves the transmission of data/information (i.e., digital bit streams) using the optical carrier signal through unguided channels, see Figure 2.1. FSO is essentially a LOS system, where both the Tx and the receiver (Rx) are directly aligned with no obstructions. In optical transmission systems, the optical carrier signal is either internally (i.e., intensity) , mainly used for applications below 2.5 Gbps [39], depending on the system requirement or externally (i.e., phase) modulated by the information, where the former is the most widely reported and used in the literature [13], [40]. The OOK-based intensity modulation/ direct detection (IM/DD) is the simplest and widely used scheme capable of delivering data rates up to 10 Gbps [41], [42]. Depending on the characteristics of the system and the channel conditions, i.e., laser power and the Rx sensitivity, more complex modulation schemes based multilevel-level and multi-carrier could be used to deliver higher capacity over a longer range in certain applications. However, for higher data rates (i.e., >10 Gbps) external modulation is the preferred option at the cost of increased complexity [43], [44], [13].

As for the optical source there are two options: Light emitting diodes (LEDs) and laser diodes (LDs). The LDs are mainly for the high data rates (up to 100 Tbps, using advanced modulation formats) [45] and short to long ranges (up to 70 km) and near earth laser satellite communications

FSO systems [46], [47]. The propagation medium could be a combination of sea/water, space, and atmosphere [48]. At the Rx, PDs and transimpedance amplifiers are used to regenerate the electrical signal. Note, in such systems optical components such as lens, beam splitters, optical filter, fibre, polarizers, etc, are also used both at the Tx and the Rx.

The features of FSO system, areas of applications, and thorough description of each section (i.e., the Tx, channel and Rx) will be further discussed in the following sections.

2.2.1 Application Areas

The next generation applications of the IoT demand higher reliability, improved spectral and power efficiencies to meet the service requirements as part of 5th generation (5G) and the future (6th generation) 6G wireless networks [13], [49]. It is highly desirable that the end users will have an access to high-speed data (e.g., 11 Gbps) and ultra-low latency (10 ms-1 μs) optical fibre backbone networks [50], [51]. However, not all users have direct access to fibre-based networks in urban areas and in rural areas currently as the installation cost of optical fibres are very high and time consuming [13], [44]. In addition, the limited bandwidth (3kHz-300GHz) [52] and spectrum congestion experienced in commonly used band, < 4GHz (2.4GHz ISM (Industrial, Scientific, and Medical)) in radio frequency (RF) technology are major issues in deploying them as part of the last mile/metre access networks [48], [53]. Therefore, new optical network access methods have been proposed and developed to address the aforementioned issues. In recent years, a growing interest in the use of FSO

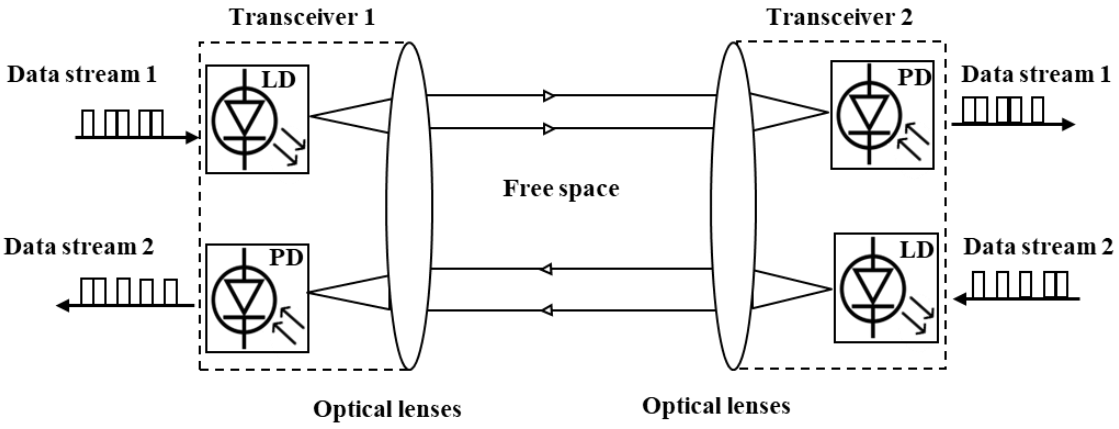

Figure 2.1.Block diagram of a typical FSO system with transceivers.

systems have been seen because of the optical fibre type ultra-high transmission capacity [54]. Moreover, it has become an excellent complement to RF based wireless technologies for future communication networks, including fifth-and-beyond-generation (5G+) and sixth-generation (6G) communication systems [55], [56], [57]. In addition to its vast license-free spectrum (up to 400 THz), FSO offers high data rates in the order of terabits/second, backbone network capability, inherent physical security, and insignificant inter-channel interference, making it a perfect choice for many applications in access and metro networks. The ability to provide high speed transmission within the short range makes FSO suitable for use to bridge the data gap between the backbone and the end users [58], [59]. The growing number of applications can be seen in Figure 2.2, which require access to the quality data services anywhere, under all conditions at all times. Among the emerging applications of FSO are the following:

- **Last-mile access -** With the most end users within a short range from the backbone, FSO is the broadband wireless solution to bridge the connectivity gap between the metropolitan networks (the end user and the fibre optic backbone) [48].

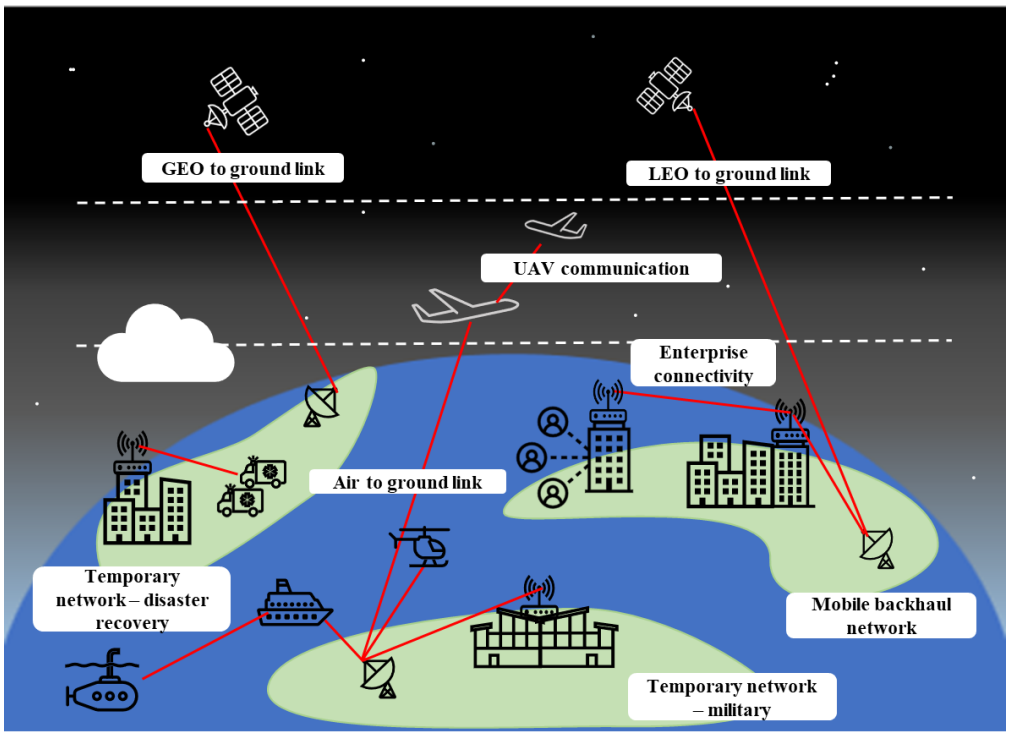

Figure 2.2.The application of FSO in high data rate access.

- **Backhaul** - Possibility to carry high speed and high data rate cellular telephone traffic via fast synchromesh networks back to the public switched telephone network using FSO [46].
- **Enterprise connectivity** - FSO systems provide high flexibility in terms of being able to redeploy and high security since it uses a LOS configuration, meaning the Txs and Rxs are in direct visual contact. This allows for the flexibility to deploy FSO systems in a wide range of environments in metropolitan areas, over water, and in challenging terrain. It is also easily installable, which makes it capable of interconnecting two buildings or other broadband and backbone networks [60].
- **Fibre backup** - In case of transmission failure through the primary optical fibre link, FSO can be used as a backup link [9].
- **Military access** - FSO is widely deployed due to its high security and undetectable characteristic. The large area connectivity and minimal planning make FSO suitable for military applications between satellites [13].
- **Space communications** - Components utilized in FSO systems can be found in an increasing number of applications of many matured high technologies which already endorse FSO space embarked systems to be more reliable and versatile [48].
- **Coherence in deep space communications** - FSO can increase spacecraft and satellite link capacities 10-100 times over RF. FSO transceivers reduce the size, weight, and power of satellite systems. Less weight and size mean a cheaper launch and less power means less drain on the energy sources of the spacecraft [61].
- **Health care and medical imaging** - Real-time access to information in FSO with such high speed in many parts of hospitals, especially around MRI scanners and in operating theatres is highly desirable compared to conventional RF-based communications [62].
- **High quality audio and video streaming** - FSO is an attractive solution for the requirement of huge bandwidth for video surveillance, high-definition cameras, and monitoring [63]. It is also widely used for live broadcasting such as sports events and emergency situations such as weather forecasts, and military coup [43].

Table 2.1. Comparison of FSO and RF communications [66, 67].

Parameter/Property	FSO	RF
Typical transmit power	mW-W	W-kW
License Free	Yes	No
Pass Through Walls	No	Yes
Data Rate	Up to 2000 THz	Up to 3 THz
Path Loss	High	High
Multipath fading	No	Yes
Security	High	Low
Device Size	Small	Large
Dominant noise	Background light	Other sources
Network architecture	Scalable	Unscalable

2.3 FSO Features

FSO communication is considered as the next leading-edge technology to solve the bandwidth bottleneck of RF systems for better spectrum management and high-speed broadband connection due to its unique features such as:

- **High data rate -** FSO system can potentially offer up to 2000 THz data bandwidth due to the optical carrier frequency range from 10^{12}-10^{16} Hz. Currently, the RF technology offers 1 to 2 Mbps for unregulated 2.4 GHz ISM bands, 20 Mbps at 5.7 GHz 4G mobile, and 875 Mbps in 60 GHz mmW technologies [64], [65]. Therefore, optical communications guarantee an increased data rate and information capacity compared with RF band-based communication systems. The comparison and key differences between RF and optical communications are given in Table. 2.1.

- **License free spectrum** - The spectrum congestion in RF technology has been a major problem in wireless technology with the increasing demand from end users and IoT devices. The Federal Communication Commission (FCC) in the US and Office of Communication (Ofcom) in the UK put a strict regulations in place to minimise this interference from the adjacent band, therefore requiring a huge amount of fees and several months of

administration [68]. On the contrary, the optical frequency bands do not require regulations and are relatively inexpensive compared to the RF license band. The absence of a license fee and the administration time delay in RF technology has begun the return on investment in FSO. Additionally, optical communication systems with wide unlicensed spectral ranges between 700 and 10,000 nm can offer protocols-free data links with data rates exceeding 2.5 Gbps per wavelength and reach up to 5 km [69].

- **Directivity/beam profile** - The beam profile, especially LDs are renowned for its narrow beam with a typical diffraction limited beam divergence of 0.01-0.1 mrad [70]. The transmit power is mainly focused within an extremely narrow beam profile due to its tight spatial confinement allowing the laser beam to operate almost independently.
- **Low cost** - In general, the cost of installation, maintenance, and license fees of FSO systems compared to the other communication technologies has major advantages [71]. FSO can also deliver the same bandwidth as optical fibre without the high cost of digging and trenching roads for fibre installation. Furthermore, its feature of license free spectrum makes the implementation of FSO much cheaper than optical fibre based and RF technologies [72].
- **Fast installation and redeployment** - The main factor of FSO system installation is the establishment of data transmission and reception between the Tx and the Rx. The speed of installation of FSO could be as low as four hours for the system to be operational whereas RF wireless technology can take up to months [73]. Moreover, it is extremely easy to be taken down and redeploy/re-implement in another location.
- **Power consumption** - Especially with the growth of internet traffic, technological advances in communication systems and equipment are causing a rapid increase in power consumption, as well as the efforts to develop more energy efficient devices [74]. Due to the FSO utilizing mainly optical lasers and LEDs, which are lighter in weight, compact, and power efficient than conventional light bulbs, it is also known for potentially being economically green compared to RF, while data communication technology is responsible for 2-10% of the global power consumption [58].

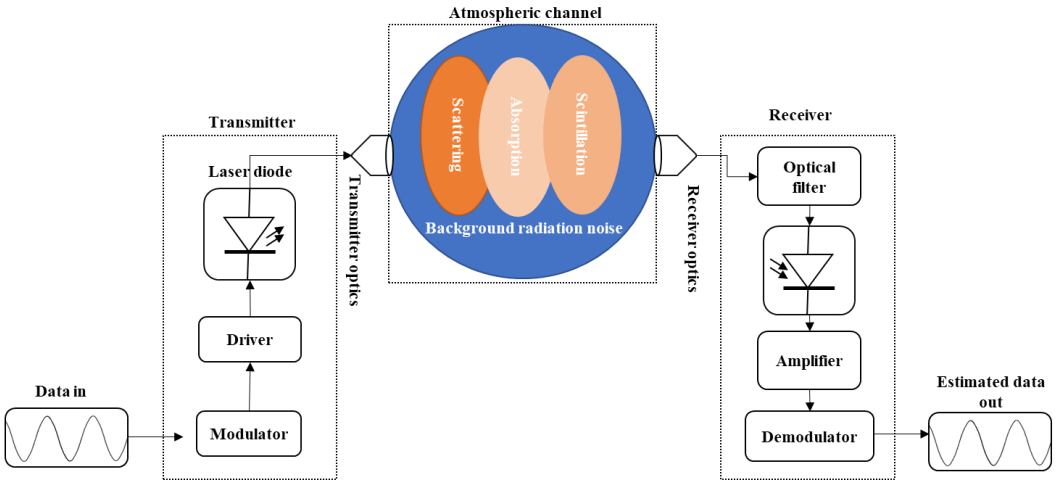

Figure 2.3. Block diagram of a terrestrial FSO link.

- **High security** - The well-confined narrow laser offer security in transmission, which is highly desirable in today's telecommunications, where the eavesdropper would need to locate the optical beam very closely to the Tx and the Rx in order to capture enough energy to access the information [75] that results in blocking [76].

2.4 FSO Structure

A typical FSO system contains three stages: (*i*) a Tx that sends optical radiation through the atmosphere in accordance with Beer-Lambert's law; (*ii*) a free space transmission channel, where turbulent eddies (cloud, rain, smoke, gases, temperature variations, fog, and aerosol) exist; and (*iii*) an Rx that processes the received signal Figure 2.3.

2.4.1 The Transmitter

In the Tx block, a modulator, an optical driver, and optics such as collimators, splitters, and fibre are typically consisted. The modulated optical signal is then transmitted through the atmosphere to the Rx. The IM/DD scheme, see Fig. 2.4 (a), is the most widely used in which the input data is modulated onto the irradiance of the optical radiation [45]. The selected modulation scheme could be a more complex multilevel phase, amplitude, and frequency scheme depending on the application and more advanced implementations. However, IM/DD is not applicable for high-speed transmission links due to the limited bandwidth of the optical sources (< 10 GHz) [77], their nonlinear properties which can

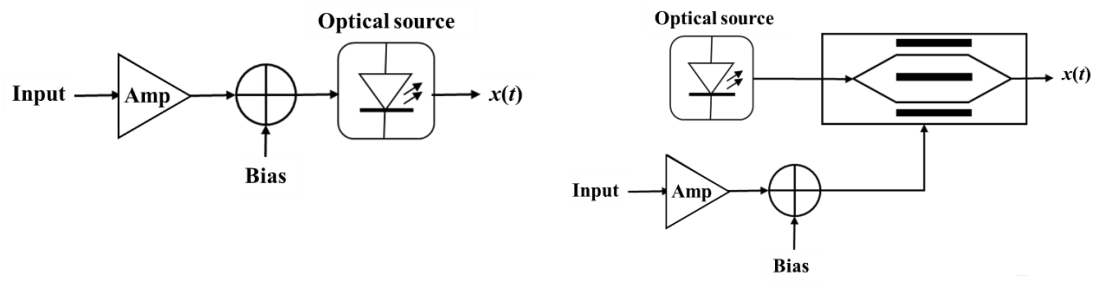

(a) (b)

Figure 2.4. Optical intensity: (a) internal modulation, and (b) external modulation using MZM.

lead to generating additional spectral sidebands that are not presented in the original signal leading to the reduced system performance, and power loss [78]. Alternatively, optical sources can be modulated by using external modulators like Mach Zehnder modulator (MZM), see Fig. 2.4 (b). Considering that the source and external modulator are both linear, the free space optical link only acts as an attenuator and is transparent to the RF signal. In such systems, complex and advanced modulation formats such as quadrature amplitude modulation (QAM), orthogonal frequency division multiplexing (OFDM), orbital angular momentum multiplexing can be used [79], [80], [81]. The mmW signals approaching 100 GHz could be transmitted using external modulators but at the cost of power efficiency and linearization [82]. However, LDs are linear at low power levels but become progressively nonlinear at higher power levels, thus resulting in harmonic intermodulation and distortions [83].

The driver is utilized to regulate the current flow of the LD, whereas optics are used to collect, collimate, and direct the optical beam toward the Rx aperture. Both LEDs and LDs can be used in FSO systems, where collimated LED-based links can potentially be used in indoor applications. The wavelength bands used in OWC are [13]:

1. 200-280 nm – Ultraviolet (UV) band also called deep UV band and is mainly used for military communications [43].
2. 390-750 nm – Visible band also known as VLC, which can be used in several applications including wireless local area networks, personal area networks, and vehicular networks [44].
3. 750 – 1600 nm – Near Infrared (IR) bands are commonly referred to as FSO systems. High-speed, protocol-transparent links that typically use lasers as Txs [43].

4. 0.780–1.4 μm – Near infrared (IR-A) are commonly used in optical fibre communications
5. 1.4–3 μm – Short-wavelength infrared (IR-B) is the dominant spectral region for long-distance telecommunications (especially the 1530-1560 nm range), including optical fibre and free-space optics.
6. 3–5 μm – Mid-wavelength infrared (IR-C).
7. 8–15 μm – Long-wavelength infrared (IR-C).
8. 15–1000 μm – far infrared.

The majority of FSO systems are usually designed to operate in spectral windows between 780 - 850 nm, and 1520 - 1600 nm with a typical attenuation of < 0.2 dB/km [84]. Due to the wide utilization of 850 and 1550 nm transmission windows in optical fibre networks, the devices and components are readily available [85], [46], [13]. Today's service provider networks and transmission equipment widely use 850 nm Txs and detector components that are reliable, high-performing, and affordable. Highly sensitive silicon avalanche photo diode (APD) detectors and sophisticated vertical cavity surface emitting lasers can be used in this window [86], [46]. Moreover, the 1550 nm band is well suited for free space transmission with semiconductor laser technology and amplifiers being used in commercial systems.

2.4.2 The Channel

In FSO, the main drawback of the LOS configuration is that the link performance can be affected by flying objects such as birds, low clouds, and atmospheric conditions (i.e., fog, turbulence, rain, snow, smoke, sandstorm, etc.) [36]. The atmospheric condition affects the transmitted laser beam in terms of absorption, scattering, and fluctuation due to the interaction of photons with aerosol particles of different types and shapes [87]. Typically, the laser beams are highly directional with a high degree of spatial coherence (close to zero) [88]. However, the beam spot/ footprint becomes larger, which increases with transmission distance L as it propagates through the atmospheric channel experiencing beam spreading. Since the PD has a finite physical size and the beam spot is larger than the PD aperture, the system can potentially experience a link failure.

The beam spot is given as [85]:

$$\text{Beam footprint (m)} = \theta_0(\text{mrad}) \times L\ (\text{km}). \tag{2.1}$$

An additional loss due to misalignment between the Tx and the Rx, an increase in components losses due to aging, and other unknown factors are categorized as **miscellaneous loss** L_{Misc}. Another feature of interest is the **atmospheric attenuation loss** L_{Atm}. This is due to the inhomogeneous phenomena of temperature, which causes changes in the refractive index of the atmosphere, creating eddies or cells of varying sizes from ~ 0.1cm to ~ 10 m changing with different temperatures [89]. The air packets/eddies act like mirrors, which deviate and fluctuate the laser beam from its main transmission path. The optical beam propagating the turbulent channel experiences random variation/fading in its irradiance (i.e., scintillation) and phase. One of the most important impairments to consider in an FSO system is the attenuation due to fog/ **fog loss** L_{Fog}.

When a light signal transverse the atmosphere, some of the photons are absorbed by molecular elements such as water, vapor, carbon dioxide, fog, and smoke particles, which results in reduced power and beam spreading (i.e., dispersion). Consequently, the interaction between aerosols and photons can be highly dynamic in terms of the wavelength range of interest and magnitude of atmospheric scattering. This is because most aerosols are created at the earth's surface (e.g., desert dust particles, human-made industrial particulates, maritime droplets, etc.), the boundary layer (a layer up to 2 km above the earth's surface) contains the highest concentration of aerosols. Above the boundary layer, the concentration of aerosols decreases rapidly. Due to atmospheric activities and the mixing action of winds, aerosol concentration becomes spatially uniform and less dependent on geographic location at higher elevations. The primary interaction between aerosols and a propagating beam is scattering [47]. Mie scattering theory is used to describe aerosol scattering as the aerosol particle sizes are comparable to wavelengths of interest in optical communications and will be discussed thoroughly in the next section. The different types of atmospheric constituents' sizes and concentrations of the different types of atmospheric constituents are listed in Table 2.2.

Table 2.2. Radiuses of various types of particles [90], [14].

Type	**Radii (μm)**	**Concentration (cm^{-3})**
Air molecules	10^{-4}	10^{19}
Aerosol	10^{-2} to 1	10 to 10^{3}
Fog	1 to 10	10 to 100
Cloud	1 to 10	100 to 300
Raindrops	10^{2} to 10^{4}	10^{-5} to 10^{-2}
Snow	10^{3} to 5×10^{3}	N/A
Hail	5×10^{3} to 5×10^{4}	N/A

The Beer-Lambert law describes the scattering coefficient of the channel as [9]:

$$\beta_a(\lambda) = -\frac{\log\left(\frac{P_{\mathrm{Rx}}}{P_{\mathrm{Tx}}}\right)}{L}, \tag{2.2}$$

where P_{Rx} is the power received for the channel condition under evaluation and P_{Tx} is the transmit power. The modelling of the fluctuation and scattering of an optical source under fog and a turbulent atmosphere will be further explained in the next section.

2.4.3 The Receiver

Typically, the Rx consists of an optics, optical bandpass filter, PD, amplifier, and post-detection processor/circuit. Note that a larger aperture PD is more desirable to collect multiple uncorrelated optical radiations, which is known as aperture averaging (AA). However, a wider aperture also leads to higher background noise. The optical bandpass filter minimizes the background light, thus improved signal to noise ratio (SNR). The most commonly used PDs in laser communication systems are *p*-type-intrinsic-*n*-type (PIN) PD and APD, see Table 2.3. The filtering, amplification, and signal processing are done in the post-detection processor stage to guarantee reliable data recovery.

2.5 Atmospheric Conditions

FSO link availability is significantly important under all channel conditions [48]. For example, fog and turbulence significantly affect the performance of the link by changing the optical wavefront's amplitude (power) and phase as it passes through the free space channel.

2.5.1 Turbulence

Due to local temperature variations that leads to the fluctuation in the refractive index of air, random changes in the optical phase of the light beams occurs and it is also known as turbulence [93]. Other well-known impacts of turbulence include the sparkling of stars due to fluctuations in the irradiance of stars and the shimmering of the horizon on a hot day due to random variations in the optical phase that result in worse image quality [70]. Atmospheric turbulence also depends on the atmospheric pressure/altitude, wind speed, and changes in the index of refraction due to temperature inhomogeneity, which results in [94], [95], [96]:

Table 2.3. The comparison of APD and PIN PDs [91] [92].

Features	**PIN**	**APD**
Sensitivity	Low	High
Cost	Low	High
SNR	Poor	Good
Conversion efficiency	0.5 to 1 A/W	0.5 to 100 A/W
Modulation bandwidth	Tens of MHz to tens of GHz	Hundreds of MHz to tens of GHz
Photocurrent gain	1	10^2 - 10^4
Special circuitry required	None	Temperature compensation circuitry
Linearity	High	Low
Bias voltage (V) for Si	45 -100	220
Capacitance (pF) for Si	1.2 - 3	1.3 - 2

a) Beam steering – The propagating direction of the beam deviates from its original path causing the beam to drift away from the Rx.

b) Beam spreading – Leads to received power loss due to the increased beam divergence due to scattering.

c) Beam scintillation – Depends on the radius of the particles (fog, aerosol) encountered during the propagation process causing the variation in the spatial power density at the Rx side.

d) Refraction and reflection – Due to the bouncing of the optical beam in its regular pattern off the surface of an object or as the beam passes at an angle from one medium to another one of different density.

e) Spatial coherence degradation – The phase coherence between the beam phase fronts experiences loss due to turbulence [97].

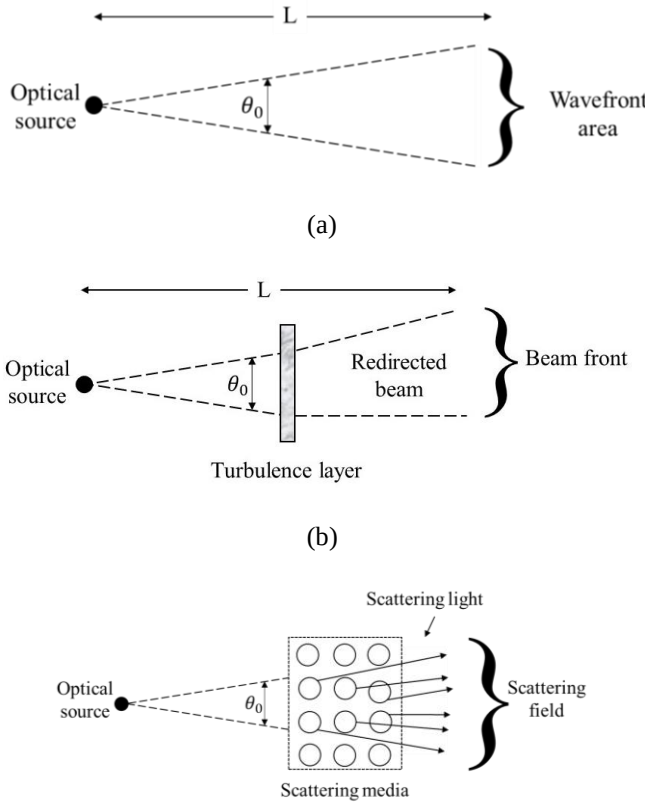

Figure 2.5. Channel models in: (a) free space, (b) clear air with turbulence layer, and (c) a multiple scattering medium.

f) Image dancing - Due to changes in the laser's arrival angle, the received beam's focus shifts randomly in the image plane [36].

These aforementioned conditions also depend on the beam itself as shown in Figure 2.5. Figure 2.5 (a) shows a wavefront area, $A_f = \frac{\pi(\theta_0 L)^2}{4}$ at the distance of L, and a corresponding field intensity inside the beam of transmitted power $\frac{P_{\mathrm{Tx}}}{A_f}$ watts/area in free space, i.e., clear channel. Figure 2.5 (b) shows channel eddies and temperature variation as turbulence. When the beam front is smaller than the dimension of the turbulence (shown as a flat plane), the beam can be attenuated by clear air but is undistorted, except for the possibility of beam redirection [98]. Figure 2.5 (c) shows the diffracted beam passing through the atmospheric medium where the channel can be considered as a dense collection of liquid particles that cause beam absorption and multiple scattering. In addition, due to the optical source not being collimated the scattered radiation will be received from different directions i.e., beam spreading [98]. Considering that the turbulent eddies are fixed or frozen at t = 0, the lens-like eddies are shown in Figure 2.6.

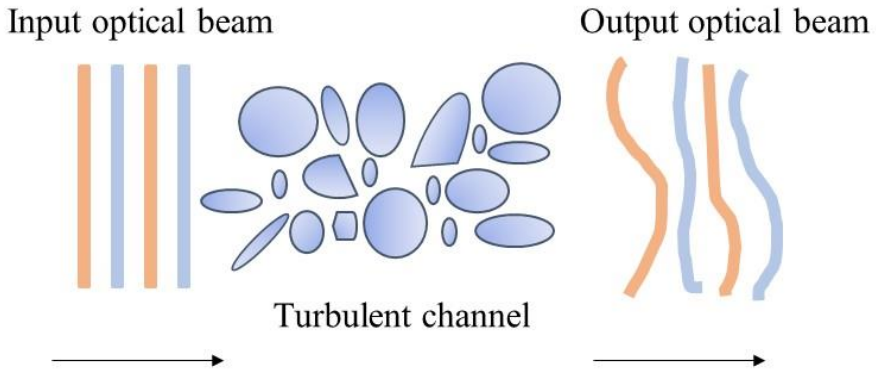

Figure 2.6. The turbulent channel consists of eddies of various sizes.

Turbulence is a slow varying fading channel with temporal coherence ranging from 1 to 10 ms. [97]. The channel state models the random attenuation experienced by the propagating laser beam in the atmospheric channel due to scintillation h_t and atmospheric attenuation/path loss h_a given by the channel gain $h = h_a h_t$ .The path loss due to atmospheric conditions over a distance L is given by $h_a = e^{-\gamma L}$, where γ is the extinction loss coefficient of the channel in reciprocal distance units.

The intensity of the optical I of a wave propagating under turbulence suffers from a random fading effect with the normalized variance or the scintillation index, given by [99]:

$$\sigma_I^2 = \frac{\langle I^2 \rangle - \langle I \rangle^2}{\langle I \rangle^2}, \tag{2.3}$$

where $\langle . \rangle$ denotes the ensemble average equivalent to long-time averaging with the assumption of an ergodic process. Assuming plane wave propagation, σ_I^2 is given by [100]:

$$\sigma_I^2(D) = \exp\left[\frac{0.49\,\sigma_R^2}{\left(1 + 0.653d^2 + 1.11\sigma_R^{\frac{12}{5}}\right)^{\frac{7}{6}}} + \frac{0.51\,\sigma_R^2\left(1 + 0.69\,\sigma_R^{\frac{12}{5}}\right)^{-\frac{5}{6}}}{(1 + 0.9d^2 + 0.621\,d^2\sigma_R^2)^{\frac{12}{5}}}\right] - 1, \tag{2.4}$$

where $d = \frac{D}{2}\sqrt{\frac{k}{L}}$ is the circular aperture scaled by the Fresnel zone provided, k is the wavenumber. σ_R^2 is Rytov variance showing the strength of the turbulence is expressed by:

$$\sigma_R^2 = 1.23 C_n^2 k^{\frac{7}{6}} L^{\frac{11}{6}}, \tag{2.5}$$

where $k = \frac{2\pi}{\lambda}$ is the wave number with λ the wavelength, and L is the link distance. In this way, weak, moderate, and strong turbulence conditions are characterized by $\sigma_R^2 < 1$, $\sigma_R^2 \approx 1$, and $\sigma_R^2 \gg 1$, respectively. C_n^2 stands for refractive index structure coefficient, and the most commonly used among several available C_n^2 profile model is the Hufnagle-Valley model described by [101]:

$$C_n^2(h) = 0.00594\left(\frac{v}{27}\right)^2 (10^{-5}h)^{10} \exp\left(\frac{h}{1000}\right) + 2.7 \times 10^{-6} \exp\left(-\frac{h}{1500}\right) + A \exp\left(-\frac{h}{1000}\right), \tag{2.6}$$

where h is the altitude in meters (m), v and A is the rms wind speed in meters per second (m/sec), and a nominal value of C_n^2 (0) at the ground respectively. For FSO links near the ground, C_n^2 can be taken approximately to be 1.7×10^{-14} $m^{-2/3}$ during daytime and 8.4×10^{-15} $m^{-2/3}$ at night. In general, C_n^2 varies from 10^{-13} m−2/3 for strong turbulence to 10^{-17} $m^{-2/3}$ for weak turbulence

with 10^{-15} $m^{-2/3}$ [102]. A similar parameter for temperature variation related to C_n^2 can be described as temperature structure parameter and can be defined as [103]:

$$C_n^2 = \left[79 \times 10^{-6} \frac{P}{T^2}\right] C_T^2 . \tag{2.7}$$

Where P is the atmospheric structure in millibar and T is the average temperature in Kelvin. Generally, the weak turbulence regime can be modeled using Log-normal distribution if $\sigma_R^2 < 0.3$. The probability distribution function (PDF) of the normalized irradiance with mean μ_x and variance σ_x^2 is given as [104]:

$$f_I(I) = \frac{1}{2I} \frac{1}{\sqrt{2\pi\sigma_x^2}} \exp\left(- \frac{\left(\ln\left(\frac{I}{I_0}\right) - 2\mu_x\right)^2}{8\sigma_x^2} \right), \tag{2.8}$$

where I_0 is the signal light intensity without turbulence. Assuming the weak turbulence, σ_I^2 and σ_x^2 are related as follows [105]:

$$\sigma_I^2 = \exp(4\sigma_x^2) - 1 \cong 4\sigma_x^2. \tag{2.9}$$

Different expressions for the variance of the Log-normal distribution are introduced depending on the light propagation model. It can be assumed that for the weak turbulence and plane wave propagation, $\sigma_I^2 = \sigma_R^2$. For moderate to strong turbulence (where $\sigma_R^2 \approx 1$ for moderate and $\sigma_R^2 > 1$ for strong turbulence) the received optical signal intensity *I*, the PDF of Gamma-Gamma distribution can be used and is given by [106]:

$$f_I(I) = \frac{2(\alpha\beta)^{\frac{\alpha+\beta}{2}} I^{\frac{\alpha+\beta}{2}-2}}{\Gamma(\alpha)\Gamma(\beta) I_0^{\frac{\alpha+\beta}{2}}} K_{\alpha-\beta}\left(2\sqrt{\alpha\beta\frac{I}{I_0}}\right), \tag{2.10}$$

where α and β represent small and large-scale eddies of the scattering cells respectively [107], [108]. $K_n(x)$ is the modified Bessel function of the second kind and order α and $\Gamma(\alpha)$ is the Gamma function. α and β that characterize the optical irradiance fluctuations PDF are related to the σ_I^2 and the atmospheric conditions, and can be expressed as [105]:

$$\alpha = \frac{1}{\exp\left(\sigma_{\ln X}^2\right)} - 1, \tag{2.11. a}$$

$$\beta = \frac{1}{\exp\left(\sigma_{\ln Y}^2\right)} - 1. \tag{2.11. b}$$

If $\sigma_{\ln X}^2$ and $\sigma_{\ln Y}^2$ is denoted as the variances of large- and small-scale log-irradiance, respectively, the scintillation index is given by:

$$\sigma_I^2 = \frac{1}{\alpha} + \frac{1}{\beta} + \frac{1}{\alpha\beta} = \exp\left(\sigma_{\ln X}^2 + \sigma_{\ln Y}^2\right) - 1. \tag{2.12}$$

For the plane wave propagation model, the close-form expressions for $\sigma_{\ln X}^2$ and $\sigma_{\ln Y}^2$ parameters can be described as [105]:

$$\sigma_{\ln X}^2 = \frac{0.49\sigma_R^2}{\left(1 + 0.65d^2 + 1.11\sigma_R^{\frac{12}{5}}\right)^{\frac{7}{6}}} \tag{2.13. a}$$

$$\sigma_{\ln X}^2 = \frac{0.51\sigma_R^2 \left(1 + 0.69\sigma_R^{\frac{12}{5}}\right)^{-\frac{5}{6}}}{1 + 0.9d^2 + 0.62\, d^2\sigma_R^{\frac{12}{5}}} \tag{2.13. b}$$

where $d = \left(\frac{k\, {d_s}^2}{4L}\right)^{0.5}$ and d_s is the aperture diameter.

2.5.2 Mitigation Techniques

In turbulence channels, the performance of the traditional SISO FSO link is extremely poor and cannot satisfy the typical BER target. Several mitigation techniques have been proposed in the literature to improve the propagating optical signal to reduce the effect including the use of the **AA** technique, error control coding, adaptive optics, spatial and time diversities, and maximum likelihood sequence detection [109]. **AA** is a widely used technique, used to reduce the variation of optical intensity according to the aperture diameter (d_s). In this method, the Rx aperture needs to be larger than the spatial coherence distance ρ_0 of the atmospheric turbulence to receive several uncorrelated signals, which is defined as [110]:

$$\rho_0 = (1.46k^2 C_n^2 L)^{-\frac{3}{5}}. \tag{2.14}$$

This is particularly useful to determine the size of the Rx aperture and the separation distance of detectors in a multiple Rx system. The fading effect can be mitigated significantly by utilizing the AA technique and the parameter that is typically used to quantify the fading reduction is the AA factor, given by [100], [106], [111]:

$$AF = \frac{\sigma_I^2(d_s)}{\sigma_I^2(0)} = \left[1 + 1.6682 \left(\frac{d_s}{d_0}\right)^2\right]^{-\frac{7}{6}}, \tag{2.15}$$

where $\sigma_I^2(d_s)$ and $\sigma_I^2(0)$ can be defined as the scintillation index of the Rx with and without d_s, respectively.

Adaptive optics is used to correct the distortion of the incoming wavefront by reversing the wavefront deformation effect of the atmospheric turbulence. The simplest method of adaptive optics is a tip-tilt correction, where correction of the wavefront takes place in two dimensions [112]. However, the cost and the design complexity are major bottlenecks. The adaptive optics combining technique is also utilized as a linear combining method in SD techniques at the Rxs and will be further discussed in the next section.

Error correction coding is introduced mainly to combat fading due to random fluctuations of intensity in a turbulence channel, as well as to deal with burst errors due to the temporal coherence time of turbulence being far greater than the typical symbol duration. Among several coding techniques, polar codes are the only one that have been proven to reach the Shannon limit with low complexity [113]. In [114], the utilization of low density parity check (LDPC) codes in an FSO system was discussed, and reported that LDPC OFDM and MIMO concept improved the BER under a strong turbulent channel. However, the polar codes have been proven to obtain higher coding gains (>20 dB) than LDPC codes in FSO systems in [115]. The use of turbo codes for optical subcarrier phase shift keying and optical pulse position modulation (PPM) FSO systems were reported in [116]. The investigation and design of an OFDM VLC system with a Viterbi decoder was reported in [117] showing that convolutional encoding and Viterbi algorithm offered improved performance. On the

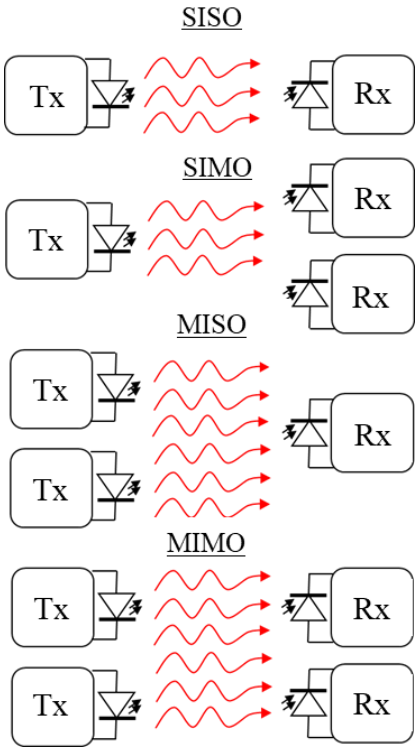

Figure 2.7. SD configurations of SISO, SIMO, MISO, and MIMO denoting single-input single-output, single-input multiple-output, multiple-input single-output, multiple-input multiple output, respectively.

contrary, polar codes are selected into the standard of 5G channel coding due to their unique advantages. Adaptive coding with different code rates using polar codes to improve the system performance was reported in [118]. However, invoking error control coding could introduce huge processing delays and efficiency degradation in view of the number of redundant bits that will be required [119].

The SD technique is particularly critical to adopt under strong turbulence, where SISO links cannot tolerate [120]. The technique significantly reduce the possibility for blocking of the laser beam with no concerns on the transmit power density limitation (usually expressed in terms of milliwatts per square centimetre) and the allowable safe laser power levels [102]. Figure 2.7 illustrates a simple block diagram of the general SD schemes of SISO, SIMO, MISO, and MIMO.

2.5.3 Combining Methods

2.5.3.1 Adaptive optics combining

Adaptive optics is applied at the Rx side, where the outputs of optical apertures are combined optically prior to photodetection and is mainly used in this research, see Figure 2.8. Generally, the

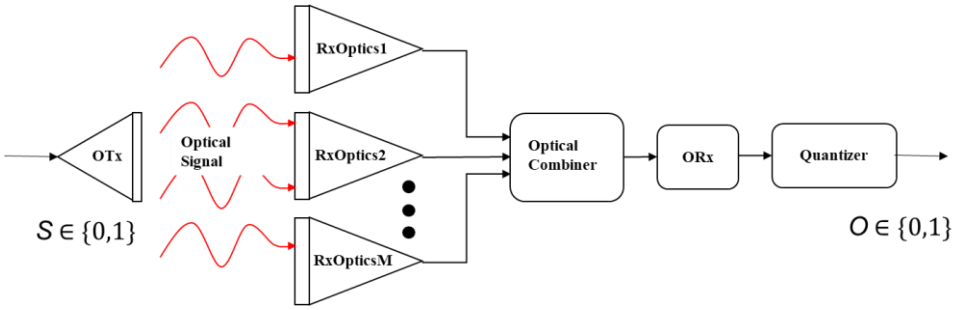

Figure 2.8. Block diagram of combining implementation at the optical domain level. OTx, RxOptics, and ORx refer to the optical Tx, optical aperture, and optical Rx, respectively.

adaptive optics technique is characterized by an equivalent SISO system with the total received signal given as [121]:

$$r_{\text{total}} = S\eta I_{\text{total}} + n_0, \tag{2.16}$$

where total irradiance received $I_{total} = \frac{1}{M}\sum_{m=1}^{M} I_m$, $S = \in [1,0]$ represents the information bit, η is the optical-to-electrical conversion coefficient, M is the number of receiver aperture, and n_0 represents the number of simultaneously received 0s [122].

The simplified closed form of BER for the weak turbulence regime can be described as:

$$\text{BER} = \frac{1}{\sqrt{\pi}}\sum_{i=1}^{p} \omega_i \, Q\left(\eta I_0 \frac{\exp\left[2\mu_{\text{total}} + z_i\sqrt{8\sigma_{\text{total}}^2}\right]}{\sqrt{2N_0}}\right), \tag{2.18}$$

where p is the order of approximation, ω_i is the weight factor for the pth-order approximation, and z_i is the zero of the pth-order Hermite polynomial. For values of, z_i and ω_i refer to mathematical handbooks such as [123]. σ_{total}^2 and μ_{total} are the total variance and mean which can be described as [121]:

$$\sigma_{\text{total}}^2 = \ln\left[1 + e^{\sigma_x^2} - \frac{1}{M}\right], \tag{2.19.a}$$

$$\mu_{\text{total}} = 0.5\left(\sigma_x^2 + \sigma_{\text{total}}^2\right). \tag{2.19.b}$$

Using Wilkinson's method for uncorrelated random variables [124]. There are other available linear combining techniques such as (*i*) equal gain combining (EGC); (*ii*) majority-logic combining (MLC); and (*iii*) selection combining (SelC).

2.5.3.2 *Equal gain combining (EGC)*

In EGC method, the outputs of the optical apertures are detected at the photodetection stage and combined in electrical domain before being applied to the quantizer module as shown in Figure 2.9.

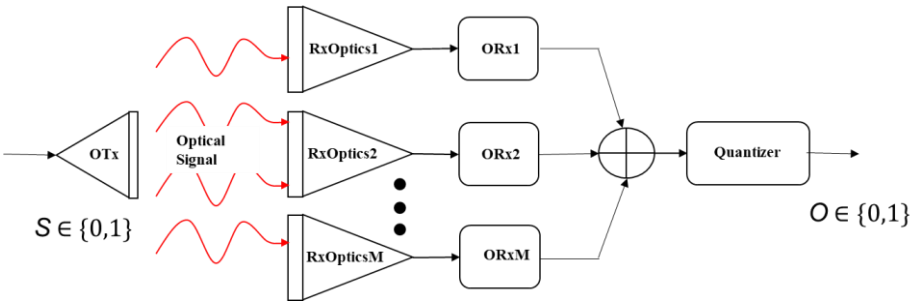

Figure 2.9. Block diagram of combining implementation at electrical domains with EGC technique.

The BER is given by:

$$\text{BER} = \frac{1}{\sqrt{\pi}} \sum_{i=1}^{p} \omega_i \, Q\left(\eta I_0 \frac{\exp\left[-2\widehat{\sigma_x^2} + z_i\sqrt{8\sigma_x^2}\right]}{\sqrt{2N_0}}\right), \tag{2.21}$$

where $\widehat{\sigma_x^2} = \frac{\sigma_x^2}{M}$ [102].

2.5.3.3 *Selection combining (SelC)*

In SC method, the received signal from the PD that experiences the highest intensity or SNR level is chosen for the processing at the Rx, see Figure 2.10. The signal intensity of each received signal is compared via signal level comparator prior to the quantizer.

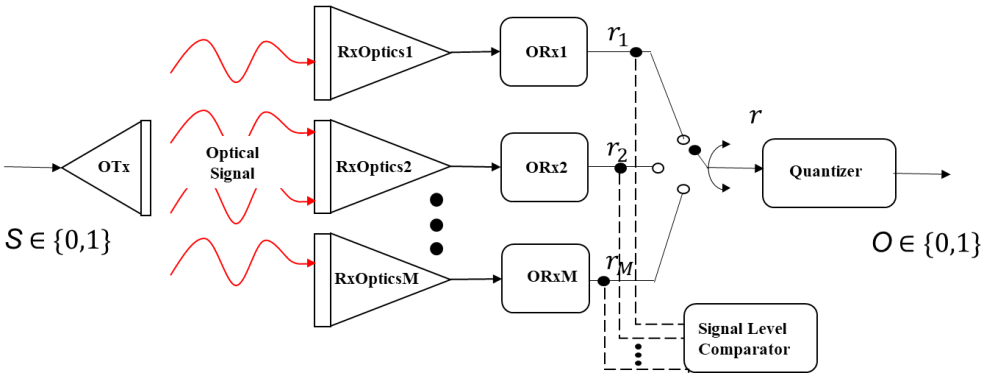

Figure 2.10. Block diagram of combining implementation at electrical domains with SelC technique.

The BER of SelC technique is given as [125], [107]:

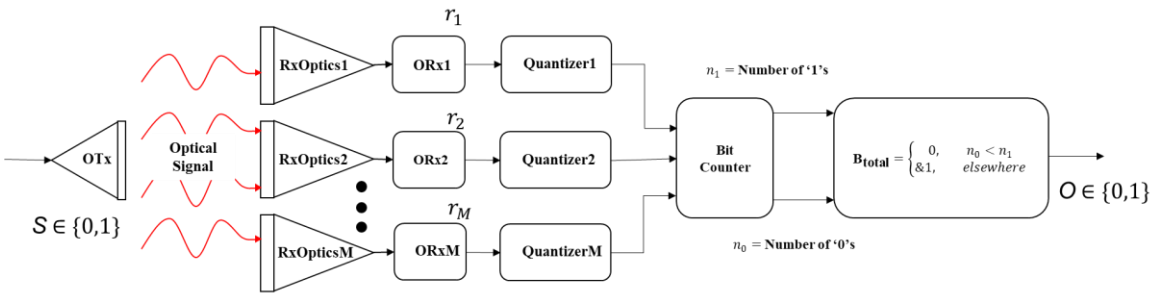

Figure 2.11. Block diagram of combining implementation at logical domains with MLC technique.

$$\text{BER} = \frac{M}{\sqrt{\pi}} \sum_{i=1}^{p} \omega_i \, Q(-\sqrt{2}z_i)^{M-1} Q\left(\eta I_0 \frac{\exp\left[-2-\sigma_x^2+z_i\sqrt{8\sigma_x^2}\right]}{\sqrt{2MN_0}}\right), \tag{2.23}$$

2.5.3.4 Majority-logic combining

In SelC where the strongest signal from M received signals is selected to be processed at the Rx, hence, neglecting (M-1) of M observations. Unlike SelC, in the MLC technique, all N observations are used and very similar to the process of the matched filter in frequency domain to the incoming signal. The output bits at each branch are monitored and the final output bit B_{total} stream based on the received number of 1s (n_1) and 0s (n_0) as shown in Figure 2.11.

For this technique, the probability of error is given by [126]:

$$BER = \begin{cases} \sum_{i=N+1}^{M} \binom{M}{i} P_b^i P_c^{M-i} + \frac{1}{2}\binom{M}{N} P_b^N P_c^N, M = 2N \\ \sum_{i=N}^{M} \binom{M}{i} P_b^i P_c^{M-i}, M = 2N-1 \end{cases}, \tag{2.24}$$

where P_b denotes the probability of error of each received branch that can be obtained by replacing I_0 to $\frac{I_0}{M}$ in Eqn. (2.21), $P_c = 1 - P_b$ and N >2, which is an integer number. However, considering that $P_c \cong 1$ and with higher SNRs where $P_b \ll 1$ and assuming that all channels are independent and identically distributed. Eqn. (2.24) can be rewritten as:

$$BER = \begin{cases} \sum_{i=N+1}^{M} \binom{M}{i} P_b^i + \frac{1}{2}\binom{M}{N} P_b^N, M = 2N \\ \sum_{i=N}^{M} \binom{M}{i} P_b^i, M = 2N-1 \end{cases}. \tag{2.25}$$

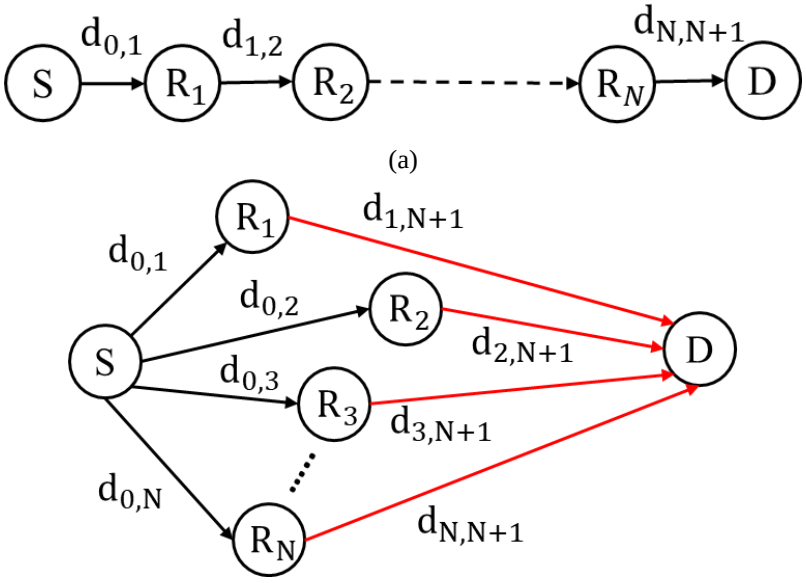

Figure 2.12. FSO relaying system: (a) serial configuration, and (b) parallel configuration.

Another concept of cooperative diversity is a **relay-assisted** transmission system. By creating a virtual multiple aperture system which is also useful to combat the turbulence fading effect, the relay assisted systems can be a promising candidate as one of the long-distance transmission solutions. The system is designed to overcome the traditional FSO systems such as limited transmission distance and susceptibility to atmospheric turbulence. Instead of using multiple apertures, a single antenna is capable of achieving a huge diversity gain to realize the advantages of MIMO techniques. There are

two possible configurations in relay-assisted transmission: serial (i.e., multi-hop transmission), and parallel configurations (i.e., cooperative diversity), described in Figure 2.12. The relay-assisted FSO transmission can be categorized into amplify and forward (AF) and decode and forward (DF) modes where the system with a high SNR radio such that the received signal strength is sufficiently higher than the noise or atmospheric fading [127]. In case of low SNR, relays will be forwarding the replicas of the noise/errors of the information they received [128].

In a relay-assisted AF FSO system, a relay is placed between the Tx and the Rx to amplify and retransmit the signal, allowing for longer transmission distances and higher data rates. The transmitted signal travels through the air to the relay. The relay receives the light signal and amplifies

it using an optical amplifier, such as an erbium-doped fibre amplifier [129]. The amplified signal is then retransmitted to the Rx. The primary downside of the AF technique is that the relay node amplifies the received signal, which also amplifies any noise present in the signal. This can lead to a degradation of the overall SNR. Moreover, the AF scheme can make the network more vulnerable to attacks, as the relay nodes amplify and forward the signal without necessarily checking its authenticity [130].

In DF relaying, the relay node receives a signal from the source node, decodes the signal to obtain the original data, and then forwards the decided data to the destination node only if the received SNR is greater than a predetermined decoding threshold. This is necessary to prevent error propagation. However, the main disadvantage of DF relaying is that it has a high decoding delay. Since the relay must decode the signal before forwarding it, there is a delay (typically >1 ms) [131] between the time the signal is received by the relay and the time it is forwarded to the destination node. This can limit the applicability of decode-and-forward relaying in certain real-time applications.

2.5.4 Fog and Visibility

Generally, the performance of FSO is mostly attenuated by the fog condition. The presence of aerosols and particles triggers the absorption and scattering of the propagating optical signals. The aerosol is made up of tiny particles of various shapes ranging from spherical to irregular shapes suspended in the atmosphere. The attenuation coefficient is the sum of the absorption and the scattering coefficients from aerosols and molecular components. Note, weather attenuation as a function of wavelength λ which can be expressed as [132]:

$$\gamma(\lambda) = \alpha_m(\lambda) + \alpha_a(\lambda) + \beta_m(\lambda) + \beta_a(\lambda), \tag{2.26}$$

where, $\alpha_m(\lambda)$ and $\alpha_a(\lambda)$ are the molecular and aerosol absorption coefficients, respectively, and $\beta_m(\lambda)$ is the molecular scattering coefficient. The last term represents the aerosol scattering coefficient due to fog attenuation. The absorption takes place while photons propagate in a channel and interacts with molecules [96]. The absorption coefficient depends on the type of gas molecules and their concentration [98]. Absorption is wavelength dependant leading to the atmosphere having

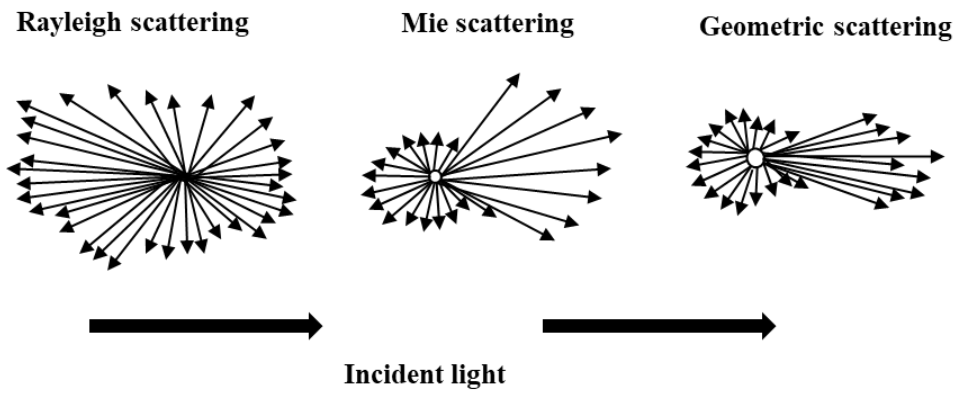

Figure 2.13. Comparison between Rayleigh, Geometric, and Mie scattering.

transparent zones which is a range of wavelengths with minimal absorption and also known as transmission windows. The wavelength selected in FSO systems is basically chosen to coincide with the atmospheric transmission windows [37]. Therefore, the attenuation coefficient is dominated by scattering as $\gamma(\lambda) \cong \beta_a(\lambda)$. On the other hand, the scattering effect depends on the size of the particles (fog, aerosol), particularly radius (r). The scattering process can be classified by the size parameter, $x_0 = 2\pi r/\lambda$. If $x_0 \ll 1$, it can be described as Rayleigh scattering whereas $x_0 \approx 1$ is Mie scattering. If $x_0 \gg 1$, the scattering process can be explained using the diffraction theory. The comparison of each scattering process is shown in Figure 2.13.

2.5.4.1 Rayleigh scattering

A closed-form expression of Rayleigh scattering is given by [133] :

$$\beta_{Rayleigh}(\lambda) = 0.827 N_p A_p^3 \lambda^{-4}, \tag{2.27}$$

where N_p is the number of particles per unit volume along the propagation path and A_p is the cross-sectional area of scattering. The proportionality of the Rayleigh scattering suggests that the shorter wavelengths get scattered more; this effect is what is responsible for the blue color of the sky during the day.

2.5.4.2 Mie scattering

Mie scattering occurs when the particle size is comparable to the beam size and as the fog particle size compares very much with the wavelength band of interest in FSO (0.5 m – 2 μm), this makes

fog the major photon scatterer and Mie scattering the dominant scattering process in terrestrial FSO systems. The particles encountered in the atmosphere have complex shapes and orientations and applying the theory of Mie scattering to these atmospheric particles is therefore very complicated.

Henceforth, the description of attenuation due to scattering will be based on the reported empirical formula. These empirical equations are often expressed in terms of the visibility range V in km. It is measured with an instrument called the transmissometer and a commonly used empirical model for Mie scattering is given by [132]:

$$\beta_a(\lambda) = \frac{3.91}{V}\left(\frac{\lambda}{550\,nm}\right)^{-q}, \tag{2.28}$$

where q is the size distribution of scattering fog particles for which the two well-known models of the Kim model which can be defined as [134]:

$$q = \begin{cases} 1.6 & V > 50 \text{ km} \\ 1.3 & 6 \text{ km} < V < 50 \text{ km} \\ 0.16V + 0.34 & 1 \text{ km} < V < 6 \text{ km} \\ V - 0.5 & 0.5 \text{ km} < V < 1 \text{ km} \\ 0 & V < 0.5 \text{ km} \end{cases}. \tag{2.29}$$

To estimate the fog attenuation, where $\beta_a(\lambda)$ is wavelength dependant for V < 0.5 km and the Kruse model can be given as:

$$q = \begin{cases} 1.6 & V > 50 \text{ km} \\ 1.3 & 6 \text{ km} < V < 50 \text{ km} \\ 0.585V^{\frac{1}{3}} & 0 < V < 6 \text{ km} \end{cases}. \tag{2.30}$$

Depending on the visibility (V), fog can be defined as thick (V<0.1 km), medium (0.1<V<1), or thin (V>1), and the atmospheric loss (L_{Atm}) can be calculated as [135]:

$$L_{\text{Atm}}\left(\frac{dB}{km}\right) = 4.343\beta_a(\lambda). \tag{2.31}$$

2.5.5 Mitigation Techniques

In order to improve the FSO performance in fog conditions, various types of mitigation techniques, such as multiple beam transmission/transmitter diversity, i.e., MIMO or MISO, employing relay transmission, and hybrid RF/FSO are some of the physical layer mitigation techniques. Additionally, in case of thick fog, high-power lasers with special mitigation techniques can potentially offer better link availability. According to the IEC 60825-1 standard lasers are divided into four groups [98], [137]. Among the classification of Class 1 to Class 4 lasers with Class 1 being the least powerful and Class 4 being the most powerful, Class 1 lasers are mostly desirable in OWC systems due to their safety under all conditions. This is defined by the accessible emission limit metric which depends on the wavelength of the laser source, the geometry of the emitter, and the intensity of the source [138]. Generally, the two wavelengths mostly used for the FSO system are 850 and 1550 nm due to their low molecular absorption and readily availability of the Tx and Rx components at these wavelengths [128].

In fog attenuation, the use of SD to correct the system power according to the density of the fog helps in overcoming the effect of molecular absorption. Employing multiple Txs for parallel transmission where multiple copies of the information signal are transmitted to increase the transmitted power or by means of optical or electrical amplification could be considered. The system could perform better as MIMO or MISO configuration, not only for the purpose of intensifying the transmitted power but also could be used for power allocation in which a pair of Tx and Rx can be placed where the signal propagates in a different channel. In MIMO system considering that two pairs of Txs (Tx1 and Tx2) and Rxs (Rx1 and Rx2) are utilized for parallel transmission, Tx1 and Rx1 could be placed as a default link whereas Tx2 and Rx2 could be implemented in a different channel. The received signals can be optically or electrically combined afterward to be post processed by using the combining methods mentioned in Section 2.5.3. The same concept could be applied to MISO system where each Txs can be implemented in different channels and pointing toward the Rx from different angles. In this case, it is important to synchronize the two propagating signals to avoid system degradation.

Error correction and relay-assisted techniques can also be utilized to ease the fog attenuation which is mentioned in Section 2.5.2 as mitigation techniques for turbulence. In a dense fog regime, an RF back up link can be implemented as a complementary technology to have a hybrid FSO/RF system that has the capability of delivering 99.999% availability in all weather conditions [38]. A hybrid FSO/RF scheme uses the FSO link as a default transmission option, while RF is used as a backup when the channel conditions change due to weather conditions (i.e., fog, turbulence). RF transmissions will need to be switched to FSO once weather conditions change (rain, snow, or a clear channel) [139], [140]. In FSO, the scattering effects due to fog/smoke defocus the optical signal degrading the BER, hence, the system performance. On the other hand, RF links are more sensitive to rain scattering. Since the probability of the occurrence of fog and rain simultaneously is very low [141], the RF link can be utilized as a backup link to FSO in fog conditions. Hybrid systems, however, result in reduced data rates whenever the RF back-up link is active [126]. There are some challenges associated with hybrid systems, including data loss during switching from FSO to RF or vice versa and real-time performance loss due to temporary data storage. It is required to use buffers to prevent data loss during switching.

2.6 Link Budget Analysis

Link budget analysis is needed to estimate the system power limitations. It outlines all the losses encountered by the propagating beam, i.e., L_{Geo}, L_{Misc}, optical losses due to the imperfections in the lenses, and losses due to component aging. Usually, the beam is collimated to reduce L_{Geo} which is given by [13]:

$$L_{\mathrm{Geo}}(\mathrm{dB}) = -20\log_{10}\left(\frac{D_{\mathrm{Rx}}}{D_{\mathrm{Tx}} + L\theta_0}\right), \tag{2.33}$$

where, D_{Rx} and D_{Tx} are the size of the Rx and Tx aperture, respectively. It is noticeable that a very narrow beam divergence is desirable in terrestrial FSO systems. However, wide beam divergence angle sources are also preferred for short-range FSO links to mitigate the misaligning issue and eliminate the necessity for active tracking systems at the expense of increased L_{Geo}. Another

additional loss due to optics L_{Op}, imperfect lenses and other optical components can be obtained from the component manufacturer [9]. Although the glass windows allow the optical signals to pass through, they also contributed to the overall power loss. This is due to the absorption loss of ~5% per mm of glass thickness, scattering loss of > 0.1, and reflection loss of 0.1-8% [142]. L_{Misc} also includes the coupling losses due to fibre and optics coupling. Considering that the Tx is directly pointed at the Rx, L_{Misc} would be 0 dB, which is not an issue for short FSO links (<1km).

The received optical power in dBm is given as:

$$P_R = P_T - L_{\mathrm{Geo}} - L_{\mathrm{Op}} - L_{\mathrm{Misc}} - L_{\mathrm{Atm}} - L_{\mathrm{M}}, \tag{2.34}$$

where L_{M} is the link margin that takes care of all possible future losses once the system is installed. Note, the link budget analysis could be used to determine the achievable link range, for given values of Rx sensitivity and link margin.

2.7 Summary

This chapter describes the fundamentals and introduction of the FSO system. The chapter also discusses the key features and structure of FSO systems including the areas where FSO is suitable to integrate to solve the bottleneck as last mile last meter access has been discussed. Turbulence and fog, which contribute the most to loss in FSO channels, are highlighted, and the challenges imposed by the atmospheric channel to an optical beam passing through it is also covered. Mitigation techniques to overcome the turbulent and fog channel along with the Rx diversity techniques and combining techniques are all equally mentioned, and the importance of link budget and link margin is also discussed.

Chapter 3. Software Defined Systems

3.1 Introduction

In communication networks, wireless technology has become immensely popular and influential in the past few decades [143]. The number of new standards on this technology replacing the old ones keeps increasing over time, thus resulting in a surplus. In addition, the high cost and the time taken to create new features and functionalities in response to the changing standards and applications introduce further challenges that need addressing. One option to avoid the paperwork would be to go down the path of reconfigurability in the hardware domain, which also contributes to the sustainability agenda in information and communications technology. The software defined systems concept is an emerging field and a potential pragmatic solution that could be adopted in systems including wireless communications to dynamically changes device sub-systems in response to environmental changes and the user's requirements. Software defined ecosystems can be implemented and evaluated in a flexible and reconfigurable manner by removing hardware limitations. In this chapter, the widely used methods and ecosystems of SDR and commercially available frontends will be discussed thoroughly. Another useful architecture as a networking approach known as a software defined network (SDN) for network management issues in communications systems will also be briefly explained in this chapter.

Generally, radio systems can be classified into five categories depending on their capability and flexibility. These are (*i*) hardware radio – that can be modified through physical intervention only [144]; (*ii*) software-controlled radio – Which has a limitation in changeable functions using the software [145]; (*iii*) SDR - which uses the software for coding, modulation, decoding, and demodulation of radio signals including filters, mixer, etc. [146]; (*iv*) ideal software radio - Which allows the user to remove the RF front-end processing completely, where the antennas are directly connected to the data converter [147], [148]; and (*iv*) lastly, the ultimate software radio which is

expected to be a fully programmable radio that supports a wide range of frequencies (i.e., below 10 kHz to several GHz) and multiple on-the-air frontends [147], [148].

Among several software defined systems, SDR is a promising option that allows the user to implement other frontends that used analogue signals as a part of the system. The term SDR has been around for about 30 years and is still a common topic of discussion carrying more than its share of misconceptions such as SDR: (*i*) is strictly and mainly used for the military purpose [149]; (*ii*) is a software version of a traditional radio [150]; and (*iii*) can operate on any frequency bands [151]. SDR is a radio in which most or all the physical layer functions are defined in the software domain. In another word, a communication technology entity, where hardware is enriched by utilizing the software. Initially, SDR was considered as two main concepts: (a) reuse of hardware components; and (b) a flexible control. In this chapter, SDR is mainly used to provide the freedom of choosing the frontends and for the variety of user interfaces.

3.2 Software Defined Radio (SDR)

The origins of SDR can be traced back to the early days of radio communication. The idea of using software to control the behaviour of a radio system was first proposed in the 1920s and 1930s by a number of pioneering engineers and scientists [152]. However, it wasn't until the late 20th century that the technology and computer processing power necessary to make SDR a reality began to be developed [153]. One of the early pioneers of SDR is Joe Mitola, who first coined the term "software radio" in 1991 while working as a researcher at the European Space Research and Technology Centre. Mitola introduced the concept of software radio in his PhD thesis, where he proposed a novel approach for the design of radio systems that separates the radio hardware and the radio software, and to make radios more adaptable and upgradeable [152], [151]. He defined SDR as a radio system whose behaviour is defined in software rather than being hard coded in hardware and proposed the concept of cognitive radio. In the following years, many researchers and companies began to work on SDR technologies, and the concept started to gain more attention. The U.S. Department of Defence has been actively funding SDR research since the early 2000s with the goal

of developing software-controlled radios that can operate across multiple frequency bands, protocols, and standards [153], [17]. The military was interested in SDR because it allows for a more flexible, efficient, and cost-effective way of managing its communication systems. SDR technology has become more prevalent in recent years, particularly in the area of mobile communications [154].

The development and deployment of 5G and 6G wireless communication systems are expected to rely heavily on SDR technology. SDR is a versatile and adaptable technology that enables the software implementation of numerous communication protocols and standards, making it a suitable choice for 5G and beyond systems that will support a wide range of services and applications. SDR can be utilized in future wireless communications technology to develop advanced beamforming techniques that increase system range and capacity, as well as advanced modulation algorithms that boost data rate. SDR can also be utilized to implement cognitive radio functions, increasing the efficiency and usage of existing spectrum resources [155]. Furthermore, SDR can be utilized to construct flexible and reconfigurable radios in the 5G and 6G environments that can adapt to changing conditions and requirements [156].

It is pretty well known that the traditional analogue radios are being replaced by digital radio, i.e., digital signal processing (DSP) radios due to its characteristics of offering a cleaner signal with, less interference from distances, varying weather conditions, or other devices [154]. Due to the economic and performance realities of DSP-based radios, nearly all consumer and military radios use them including cable TV Rxs LAN Rxs, smart phones, global positioning system devices, etc. However, in the legacy of analogue radio, components such as inductors, capacitors, and resistors manufactured with specified tolerances and their distributed values over an allowed range are still being used in DSP radios which leads to a lack of configurability and fixed parameters. On the contrary, SDR radios are low cost, high performance, and DSP engines. The processing engine can be application specific integrated circuits (ASIC), field programmable gate arrays (FPGA), general purpose microprocessors, or specialized co-processors [157]. The difference between the three possible radio options is described in Figure 3.1. SDRs are more than simply radios with flexible digital signal processing. Using SDR, traditional radio hardware such as mixers, modulators, demodulators, and

analogue circuits are replaced by digital techniques. SDR is quickly becoming the go-to solution for a wide variety of wireless applications due to the possibility of wireless applications that are not possible with traditional analogue systems. SDR Rxs could also be reconfigured on the fly to receive signals from various types of Txs and vice versa from the Tx side.

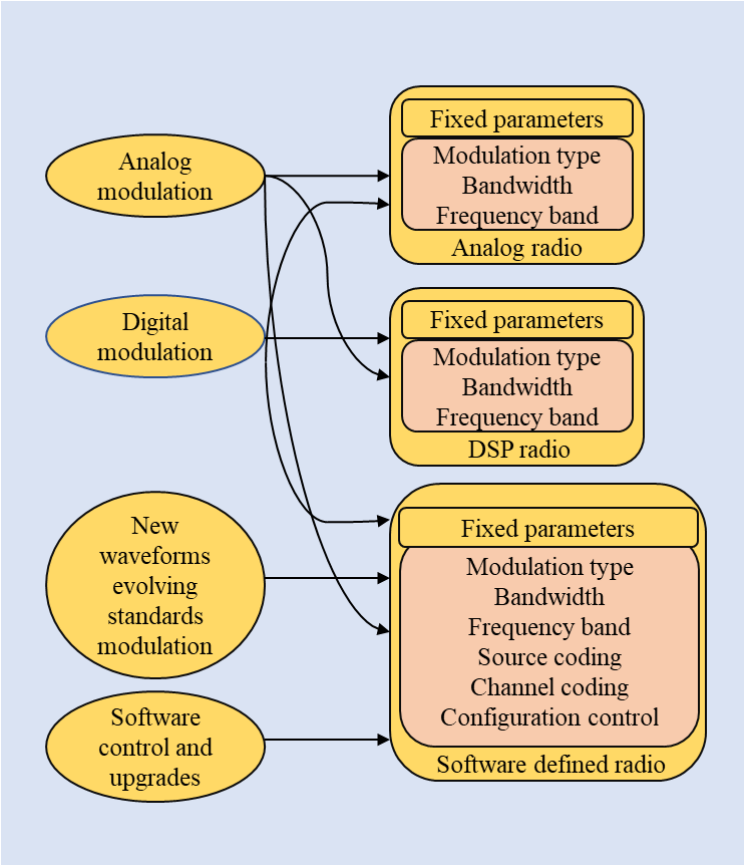

Figure 3.1. The difference between analog, DSP, and SDR.

An analogue to digital (ADC) and digital to analogue converters (DAC) are used to connect SDR to the air interface of analogue circuitries and antennas, where it often performs some of the essential signal processing tasks [158]. Therefore, several radios may be synthesized using the SDR's software by reprogramming the DSP section of the physical layer. The radio system's air interface components and higher-level data processing layers can also be modified in the software domain. The DSP part of the radio handles the signal processing and signal conditioning required to modulate and demodulate the sampled data baseband waveforms. The result of this process is an extremely adaptable radio that can support a wide range of signalling technologies. A simple block diagram of a radio transceiver is shown in Figure 3.2, illustrating the bidirectional signal flow between various

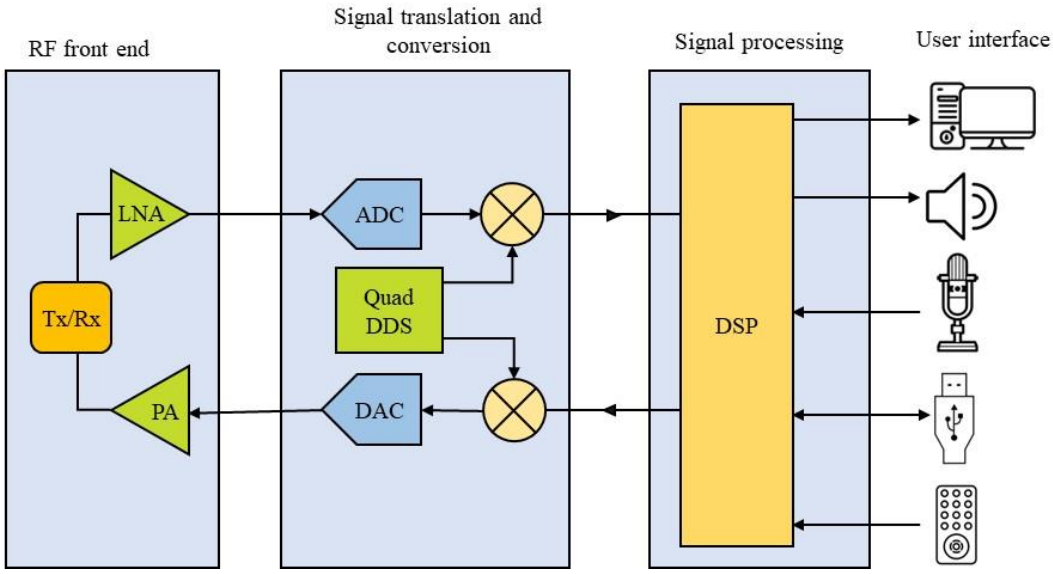

Figure 3.2. Bi-directional SDR transceiver.

signal processing blocks. Bringing the DSP functionalities closer to the antenna is a major focus of the design work in DSP-based radio. DSP is used to perform the tasks traditionally carried out by analog hardware components such as mixers, modulators, demodulators, filters, voltage-controlled amplifiers, etc. The SDR-based radio designs are usually more cost-effective to manufacture and offer superior general performance as well as less sensitivity to aging and environmental factors [159].

3.2.1 Areas of Applications

An important advantage of SDR is the ability to provide implementation by means of software that can be installed on personal computers or embedded devices. Figure 3.3 shows the applications of SDR in different areas, with an FSO/OWC link as the backhaul to provide flexible and high-speed services to the end users. The design paradigm opens a wide range of applications in different fields since it is possible to produce devices that can transmit and receive different radio protocols based solely on software. Several applications of SDR as outlined follows:

- **Radio Astronomy** - In this application, there is a need for very sensitive Rxs to detect faint radio signals from astronomical objects such as stars, galaxies, and quasars. The SDRs, radio

astronomers are able to easily tune their Rxs at different frequencies, which is essential for tracking down specific objects of interest [144].

- **Military application** - Here, SDR can be used in a number of applications including electronic warfare, signal intelligence, and military applications [154].
- **Hospital environments** - In hospital settings, where many wired and wireless devices need to coexist in constrained areas, such as operating rooms and intensive care units, SDR opens up a number of possible applications. There are several possible applications, including an integrated platform for wireless medical devices to facilitate seamless interoperability, cognitive radio for body area networks, and wireless sensor networks for monitoring medical environments [160], [149].
- **Commercial wireless applications** - SDR can be utilized for wireless network testing, spectrum monitoring, interference detection, and avoidance. They are also used in some commercial wireless networks, such as those used for Wi-Fi and cellular phone service.
- **Time-sensitive industrial internet of things (IIoT) applications** - SDR-based solutions can provide low latency in end-to-end IoT applications. Therefore, SDR can be used in IIoT applications that require low latency and time synchronization, such as Human-Machine-Interaction, sensor data collection, and automated guided vehicle systems [161].
- **Combination of SDR and SDN technology -** Can facilitate the implementation of complex time-sensitive networking for use in IIoT applications. This technology enables resource and security orchestration and helps to overcome congestion and other latency-related issues. In addition, SDN can be used to reconfigure a network based on established criteria in real-time [162].
- **Satellite applications:** SDR can support the reduction of size, time, and cost in the development of small satellite communication systems SDR due to its capability to address different communication needs, such as changing frequencies, modulation schemes, and data rates. SDR can be applied to small satellites to increase data throughput while down- or up-linking by changing communications parameters, and it can be used for several missions by

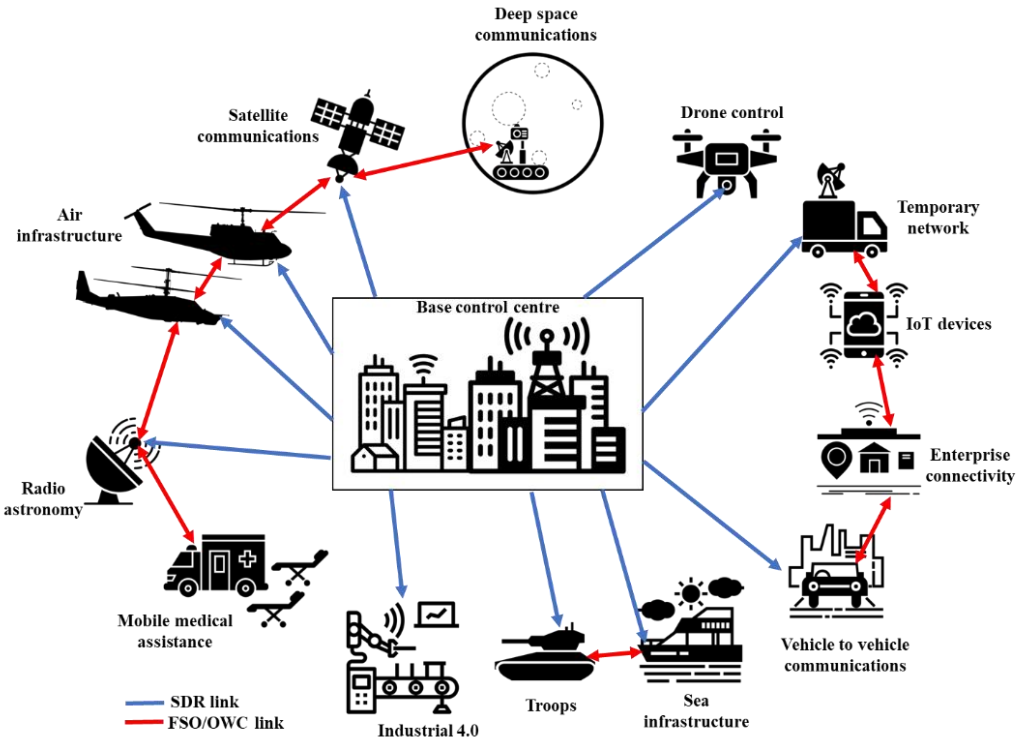

Figure 3.3. The applications of SDR with FSO/OWC backhaul.

updating the software. SDR can also support Earth monitoring and communication services [163].

3.2.2 Structure of SDR

This section discusses and explains the differences in the implementation of Txs and Rxs for traditional and SDR systems as well as the process of software defined transmission.

3.2.2.1 The SDR Tx

In SDR-based systems, Rxs are more prominent than Txs. SDR transmit functions are based on superheterodyne or direct conversion [158]. It is common for a DSP or baseband ASIC to generate modulated baseband data, which is then sent either directly to a pair of baseband DACs cosine and sine waveform (I and Q) for direct RF modulation or to a digital processor, which converts it into a suitable digital intermediate frequency (IF) within the digital upconverter (DUC) section, as depicted in Figure 3.4. In the DUC, the interpolation filter is responsible for increasing the sample rate of the baseband signal in order to match the operating frequencies of the subsequent components [164]. In the Rx architecture, it fulfils the opposite function of the decimator, followed by shifting the samples

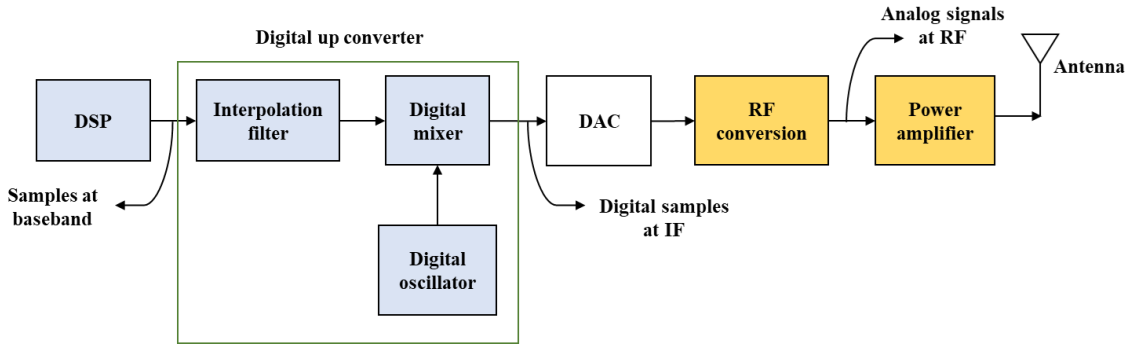

Figure 3.4. The block diagram of a traditional SDR Tx.

to the IF range using a combination of a digital mixer and a local oscillator (LO), with the LO controlling the shift. Next, the RF converter raises the frequency prior to amplification and transmission via the antenna.

3.2.2.2 The SDR Rx

SDR Rxs, see Fig. 3.5, are known to be low cost than SDR Txs/transceivers, which typically cost ~ 300 USD [159]. The RF tuner converts the RF signal to IF which replaces the RF amplifier, mixer, and IF amplifier as in a traditional analog Rx. The ADC module converts the analog IF into digital samples before digital down conversion (DDC) to translate it back to digital baseband samples (i.e., I and Q data). DDC consists of a digital mixer, LO, and FIR low pass filter, which limits the signal bandwidth [165]. For the implementation of each part, DDC includes several adders, multipliers, and shift registers. The digital baseband samples are applied to the DSP chip, which is programmed to perform demodulation, decoding, and any other necessary tasks. This digitally implemented design is the SDR. It is common for FPGA to be substituted for DSPs for rapid signal processing. With a software-based baseband processing chain based on DSP/FPGA, it will be possible to correct real-

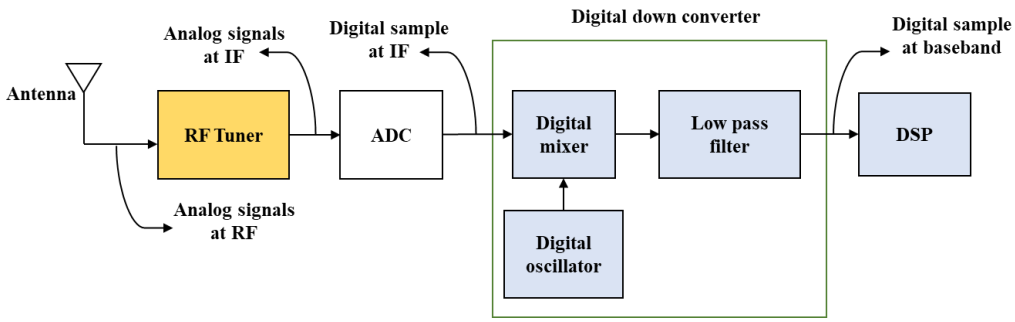

Figure 3.5. The block diagram of a traditional SDR Rx.

time baseband and RF-related impairments in the I/Q data by using sophisticated algorithms [166]. Often, SDR Rxs use methods such as direct current offset correction, I/Q gain, and phase imbalance correction, as well as time, frequency, and channel impairment correction.

3.2.3 SDR Frontends

SDR frontend refers to the hardware components that act as an interface between an SDR and the antenna. This allows SDR to receive and transmit RF signals. Frontends play a significant role in the performance and functionality of an SDR system, and a range of options are available on the market to meet the number of requirements and applications. When selecting an SDR frontend, considering its operating frequency range is crucial. While some frontends are only able to support a specific band of frequencies, others can accommodate a much wider range of frequencies, i.e., of 30 MHz - 1 GHz, and up to 6 GHz or even higher [149]. Therefore, selecting a frontend that can support the required frequency range for a specific application is important [167]. When selecting an SDR frontend, it is important to consider its level of sensitivity and input signal dynamic range [154]. The type of modulation supported by an SDR frontend is another important consideration. SDR frontends supporting multiple modulation formats are highly desirable [167], [168].

In addition to these primary aspects, there are also a variety of other factors that can be important when choosing an SDR frontend, depending on the application's specific requirements including the gain, power, and noise [167]. Low-noise amplifiers (LNAs) are a form of SDR frontend that is frequently employed, which are used in situations where sensitivity is critical. However, as with any active devices, LNAs will also introduce both noise and distortions, which will impact the signal-to-noise-and-interference ratio [158], [159], [169]. Mixers are another type of SDR frontends, which are often utilized in conjunction with LOs to down-covert the frequency of the incoming signal for the SDR to process. Mixers can be constructed to accommodate a broad spectrum of frequencies and can be utilized to either upconvert or down convert signals according to the application requirements [169]. Filters, baluns, and RF switches are also considered as SDR frontends. While filters are used to pass or block signals within a given frequency range, baluns are used to match the impedance of

the antenna to the SDR. RF switches are used to switch between several antennas or RF sources, which are particularly useful in applications where multiple antennas are needed [169].

Several experimental works have been reported using SDR for 5G and beyond communication networks, especially for multi-antenna applications. Using PXIe-7976R FPGA for data processing, the design and implementation of an eight antenna module system for smartphone applications were reported in [170]. In [171], the design of an SDR testbed to record live cellular signals from multisite was presented using USRP boards. More experimental testbeds using USRPs for different applications were discussed in [156], [172], [168], and [173]. Highly flexible and powerful SDR platforms to accommodate 5G wireless networks have also been reported in the literature [174-176]. Most of the SDR applications in specific areas required dedicated hardware and software which will be discussed in the next section.

3.2.3.1 Commercially available SDR Hardware

The SDR technology is used in a variety of commercially accessible products including standalone SDR hardware platforms, development kits, software tools, and end-user devices like wireless routers and smartphones. There are many commercial SDR frontends as shown in Table 3.1, including basic, low-cost dongles that plug into a computer's USB port, and more advanced versions.

Among the numerous frontends, the most extensively used devices with Xilinx FPGA Processors are USRPs from Ettus and national instruments (NI) research. Some of the high-speed SDR frontends are used in wireless communications for testing as well as research and development. High-speed SDR frontends typically necessitate the use of specialized software and hardware and are more costly. Table 3.2 shows the most used and commercially available high-speed SDR frontends. These hardware platforms are intended for use by developers and researchers, and they offer a wide range of capabilities and features, such as support for a wide range of frequencies, high-speed data transfer, and the ability to be readily incorporated into custom systems.

Table 3.1. Examples of SDR frontends.

SDR frontend	Frequency range	Processor/chip	Sensitivity - dBm	Input signal dynamic range - dB	Maximum input power - +dBm
RTL-SDR dongle [177]	24 MHz to 1.75 GHz	Realtek RTL2832U	-90 to -20	60 to 80	10
HackRF One [178]	1 MHz to 6 GHz	Samsung S5L8960X	-100 to -50	70 to 90	20
LimeSDR [179]	100 kHz to 3.8 GHz	Lime Microsystems LMS7002M RFIC	-120 to -40	70 to 90	10
Red Pitaya [180]	10 MHz to 6 GHz	Xilinx Zynq-7010 SoC	-120 to -60	60 to 80	10
Airspy R2 [181]	24 MHz to 1.75 GHz	Rafael Micro R820T2	-130 to -120	80 to 110	10
BladeRF[182]	300 MHz to 3.8 GHz	Xilinx XC6SLX9 FPGA	-120 to -90	70 to 90	10
KiwiSDR [183]	10 kHz to 30 MHz	NXP LPC4330 microcontroller	-120 to -100	70 to 90	10
PlutoSDR 250 [184]	325 MHz to 3.8 GHz	Analog Devices AD9363	-130 to -120	70 to 90	10
SoftRock RXTX 89 [185]	Varies by model	Varies by model	-120 to -100	60 to 80	10
SDRplay RSPduo 214 [186]	10 MHz to 2 GHz	Dual tuner architecture	-120 to -100	70 to 90	20
FunCube Dongle Pro+ [187]	64 MHz to 1.7 GHz	Amanero USB 2.0	-120 to -100	70 to 90	10
USRP [188]	Varies by model	Varies by model	Varies by model	Varies by model	Varies by model

Table 3.2. High-speed commercially available SDR frontends.

SDR frontend	Frequency range	Processor/chip	Sensitivity dBm	Input signal dynamic range -dB	Maximum input power-+dBm
USRP X310 [189]	300 MHz to 3.8 GHz	Xilinx Kintex-7 FPGA	-120 to -100	70 to 90	10
USRP N320[190]	70 MHz to 6 GHz	Xilinx Kintex-7 FPGA	-130 to -120	80 to 100	10
AD9371[191]	70 MHz to 6 GHz	AD9371 RFIC	-115 to -100	80 to 100	14
LMS8001[192]	300 MHz to 3.8 GHz	LMS8001 RFIC	-110 to -90	70 to 90	14
PlutoSDR[184]	325 MHz to 3.8 GHz	Analog Devices AD9363	-130 to -120	70 to 90	10
SoftRock RXTX Ensemble[185]	Varies by model	Varies by model	-120 to -100	60 to 80	Varies by model
SDRplay RSPduo[186]	10 MHz to 2 GHz	Dual tuner architecture	-120 to -100	70 to 90	20

3.2.3.2 Commercially available SDR software

SDR software allows users to process and manipulate radio signals using a computer, rather than relying on specialized hardware. Several things can be performed using SDR software, depending on the specific capabilities and features of the software. Typically, SDR software can be used to execute the following tasks:

- Listening and tuning in to a wide range of radio frequencies.
- Visualization and analyzation of radio signals - Using tools for spectrum analysers, oscilloscopes, and signal strength meters to evaluate the signals.
- Signal processing and analysis - Using tools and algorithms for filtering, demodulation, decoding, and error correction.
- Design, implementation, and deployment - SDR software, such as GNURadio, contains tools for creating, constructing, and deploying custom radio communication systems. Building

specific radio waveforms, modulated and demodulated signals, and developing custom communication protocols are examples of such activities.

- Radio signal transmission and reception - Offered in some SDR software such as LimeSDR. This can involve duties such as designing and setting up a radio transceiver, as well as transmitting and receiving data or audio signals.

The most widely and commonly used SDR ecosystems can be seen in Table 3.3, along with a brief overview of their capabilities and features. Moreover, LabView is also an easy, efficient, and widely used software to pair with the frontends. However, it is a costly with an annual licensing fee. The application of SDR is not limited to RF, and it can be used in optical communication and optical frontends. Software defined controlled optical systems will be discussed in Chapter 4.

Table 3.3. Overview of SDR software capabilities and features.

SDR Software	**Capability**	**Platform**
GNU Radio [193]	Open-source software for designing, building, and deploying radio communication systems.	Linux, MacOS, Windows
SDR# (SDRSharp) [194]	Windows-based software for listening to and tuning in to a wide range of radio frequencies.	Windows
Gqrx [195]	Open-source software for listening to and visualizing a wide range of radio frequencies.	Linux, MacOS, Windows
HDSDR [196]	Windows-based software for listening to and tuning in to a wide range of radio frequencies, as well as performing various types of signal processing and analysis.	Windows
SDR Console [197]	Windows-based software for listening to and tuning in to a wide range of radio frequencies, as well as performing various types of signal processing and analysis	Windows
SDR-J [198]	Open-source software for listening to and visualizing a wide range of radio frequencies, as well as performing various types of signal processing and analysis	Windows, Linux, MacOS
LimeSDR [179]	Open-source software for using LimeSDR hardware to transmit and receive radio signals across a wide range of frequencies	Linux, MacOS, Windows

3.3 Software Defined Networking

SDN is a network management technique that allows for dynamically programmable network configuration, and it plays a major role in network layer flexibility as much as SDR does in the physical layer. In traditional networking, the control and data planes are often tightly connected, with the control plane selecting how data should be carried via the network and the data plane delivering the data. In contrast, SDN allows for improved network flexibility and control by detaching the control plane from the data plane. The control plane is isolated from the data plane and implemented in software in an SDN architecture, thus allowing effortless programming and flexibility. Separation of the control plane and the data plane allows for greater network control and centralized management of the network.

One of the primary advantages of SDN is the ability to make changes to network configuration rapidly and easily. Adjustments to the network configuration in traditional networks can be time-consuming and complex, as they frequently necessitate manual changes to individual devices. Changes to the network can be made centrally and automatically distributed to all relevant devices with SDN, thus reducing the time and effort needed to make changes and enhance network efficiency. SDN also enables the use of more advanced networking technologies, such as network virtualization and automation. Network virtualization facilitates the establishment of virtual networks on top of physical network infrastructure, allowing the creation of several isolated network environments on a single physical infrastructure. This can be beneficial for a variety of applications, such as building separate networks for various departments within an organization or allowing the use of multiple networking technologies within the same network.

Another important element of SDN is automation, which enables for the automation of numerous networking processes like provisioning, configuration, and monitoring. This can considerably minimize the complexity and cost of network management by reducing the need for manual intervention and assisting in ensuring that the network is correctly setup and working optimally.

3.3.1 Application Areas

SDN represents a fundamental shift in the way networks are conceived, built, and managed. The design of SDN offers the potential to alter the way networks are utilized in a variety of scenarios by separating the control plan from the data plan and allowing greater flexibility and control over the network which opens several advantages of applications in various areas. Several areas in which SDN has been applied are:

- **Data centre networking** - To increase the efficiency and adaptability of data centre networking by enabling network virtualization and automation. Network virtualization enables the establishment of virtual networks on top of physical network infrastructure, hence permitting the development of several isolated network environments on a single physical infrastructure. Using automation to automate provisioning, setup, and monitoring reduces the complexity and expense of administering a data centre network [199].
- **IoT** - To improve the performance and flexibility of IoT networks and can significantly improve the performance of IoT networks, resulting in reduced latencies and improved resource utilization [200].
- **Cloud computing** - SDN significantly improved the performance of cloud computing networks due to its capability to reprogram and be easily partitionable and virtualizable. Additionally, the simplified data plane allows the cost of thee forwarding elements to be cost-effective [201].
- **Satellite terrestrial network** - SDN-enabled management and deployment architecture of integrated satellite-terrestrial network reduces the complexity of managing infrastructures and networks, lowers maintaining and deployment costs, enables optimal resource allocation, and boosts overall system network performance [202].
- **5G wireless and network**: Advanced features in 5G such as massive MIMO, digital beam forming techniques, elastic optical networking, and other techniques cannot be handled without distributed software management which can be controlled from a few centralized locations in the network [203].

3.3.2 Structure of SDN

The architecture of SDN can be briefly explained in three main parts including application, control, and data plane as shown in Figure 3.6. Generally, forward decisions and the configuration of the forwarding devices such as switches and routers are handled by a centralized controller. The controller uses a southbound interface to communicate with these devices and a northbound interface to communicate with applications or higher-level controllers and receives instruction from the controllers. The application plane is the layer of the SDN architecture that communicates with and receives instructions from applications or higher-level controllers. It is responsible for expressing the needs and requirements of the applications to the SDN controller, which uses this data to make forwarding decisions and design the network's forwarding plane.

Typically, the application plane is accessed via a northbound API to interface with the SDN controller and request specific configurations and actions. This may include requests to create or destroy virtual networks, allocate resources, or configure Quality of Service (QoS) settings for certain traffic flows, routing, and security. The application plane is a vital component of the SDN architecture because it allows the network to be more closely aligned with the requirements of the applications that use it. This can result in enhanced network performance and more effective resource

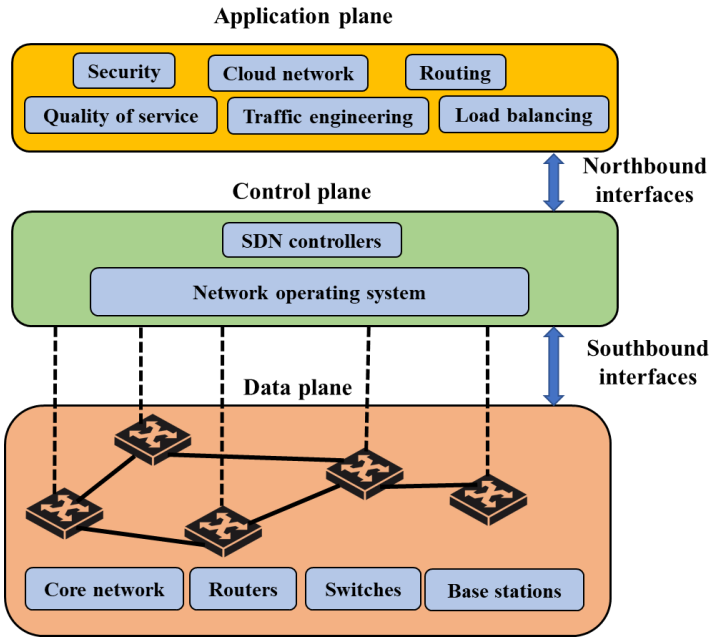

Figure 3.6. The architecture of SDN.

utilization [204]. The control plan is a logical component that makes forwarding decisions and configures the data plan (also known as the forwarding plan) of a network device such as a router or switch. The control plan is responsible for establishing the optimal network routing for traffic and configuring the data plan to forward traffic accordingly. It accomplishes this by connecting with other control plans and network devices, gathering information about the network architecture and available resources, and utilizing this information to determine the optimal path for traffic [205]. The control and data plans communicate via a southbound interface, which is commonly implemented using a protocol such as OpenFlow [206]. This separation of the control and data plans makes the control plan more adaptable and easier to update, as it may be modified without requiring hardware modifications. It also enables the data plan to concentrate on effectively forwarding traffic while the control plan handles the more difficult responsibilities of establishing the optimal traffic routing and configuring the data plan accordingly [204].

The data plan is implemented in hardware whereas the control plane is written in software it operates at a high speed, forwarding traffic based on the rules and configurations set by the control plan. The data plan (also known as the forwarding plan) is the logical component of a network device that forwards traffic according to the rules and forwarding table specified by the control plan. The data plan is usually implemented in hardware, such as a network device's ASICs. In addition to providing responsibilities such as packet filtering and QoS activities, it is responsible for forwarding traffic at high speeds and with low latency.

3.3.3 SDN Frontends

In SDN, the frontend usually refers to the interfaces that is used to interact with the SDN controllers to implement the SDN architecture. There are several types of frontends that can interact with an SDN controller including:

- **Native frontends -** These are specific to a particular SDN controller or an SDN architecture. Examples include OpenFlow for the OpenFlow protocol and the open network foundation (ONF) 's Interface to the Routing System (I2RS) for I2RS [207].

- Frontends that are not tied to a specific SDN controller or protocol can be used to interact with multiple types of SDN controllers and protocols. Examples include the ONF's I2RS and the Network Configuration Protocol [208].
- **Application programming interfaces (APIs)** - Frontends that allow applications to programmatically interact with an SDN controller. Examples include the OpenFlow Java API and the OpenDaylight REST API [209], [210].
- **Graphical user interfaces (GUIs)** - Frontends that provide a visual interface for interacting with an SDN controller. Examples include the OpenDaylight GUI and the open networking operating system (ONOS) GUI [210], [211].
- **Command line interfaces (CLIs)** - Frontends that allow users to interact with an SDN controller using commands entered at a command prompt. Examples include the OpenFlow CLI and the ONOS CLI [209], [212].

3.3.4 SDN Software

SDN software refers to the programs and protocols that are used to enable the separation of the control and data plane of network devices. Some examples of software used in SDN include:

- **SDN controllers** - Central components of an SDN architecture that are responsible for making forwarding decisions and configuring the data plane of network devices. Examples include the OpenDaylight controller and the ONOS controller [213].
- **Southbound interfaces** - Protocols that are used to communicate between the SDN controller and the data plane of network devices. Examples include OpenFlow and the Generic Network Virtualization Encapsulation protocol [214].
- **Management and orchestration software** - Programs and tools that are used to manage and operate an SDN network. Examples include the OpenStack cloud management platform and the ONF's Resource and Services Management platform [207].

- **Applications** - Programs that can be used to leverage the capabilities of an SDN network to solve specific problems or perform specific tasks. Examples include network function virtualization and network slicing [206].
- **Virtualization software** - Programs that are used to virtualize network functions and resources in an SDN environment. Examples include Open vSwitch and the ONF's Virtual Tenant Network Manager [206].
- **Network operating systems (NOSs)** - Operating systems that are optimized for use in SDN networks and that provide support for SDN controllers and protocols. Examples include the ONF's Atrium NOS and the Open Network Linux NOS [206].

In contrast, SDN hardware in terms of physical network devices usually includes switches, routers, and appliances that are used to build a network. Especially the control plan and data plan are typically implemented in hardware such as in the ASICs of a network device. Moreover, these two technologies can also be integrated together for the optimization of network performance in the 5G standard as proposed in [162]. The integration of SDR and SDN to enhance the cross-layer performance of mobile and ad hoc networks was also reported in [215].

3.4 Summary

In this chapter, the overview, the fundamental architecture of the SDR system, and the concept behind a typical SDR system were thoroughly discussed. The process of a traditional SDR Tx and Rx is explained deeply with the benefits and areas of SDR applications, The capability, flexibility, and adaptability in terms of signals that can be processed as well as the operating frequencies and modulation schemes that can be used, including the SDR frontends (hardware and software) are also described in this chapter. The details and specifications of the SDR frontends which vary depending on the specific device are mentioned, along with the commercially available SDR software and the areas of applications are mentioned. Moreover, a brief introduction of SDN and a traditional architecture was also discussed in this chapter.

Chapter 4. Software Defined Optical Wireless Communication

4.1 Introduction

As OWC technologies have significantly gained interest over the past two decades focusing on point-to-point links and novel modulation techniques, the field now has moved recently towards higher layer design and analysis of multi-cell/multiuser systems. This has led to novel schemes for resource allocation among devices and overlapping access points. Moreover, the received signal in FSO communication is highly vulnerable to atmospheric effects such as fog, smoke, snow, rain, and vibration caused by the building sway [43], [216], [13], which can lead to severe power loss, channel fading, and distortion. In order to overcome these concerns, several techniques were proposed in Chapter 2, including the MIMO system. However, most MIMO FSO systems currently demonstrate the fixed MIMO technology with integrated DSP techniques, static channel condition estimation, and offline signal processing. As the channel condition is not constant and is changing constantly with time, spectral efficiency would be required to optimize adaptively in practical outdoor scenarios. For example, in the case of MIMO FSO using spatial multiplexing , link interruption can occur if any sub/extra channel condition deteriorates [217], [218]. In order to compensate for the loss caused by varying atmospheric conditions, MIMO FSO would benefit from a degree of flexibility and adaptability in real-time. Moreover, adaptive systems can be efficiently used to adjust the transmit power, modulation scheme, or frequency bands to maintain a strong and reliable communication link in the presence of fading and/or interference. In MIMO FSO and VLC systems, an adaptive switching technique can be used to adjust the transmit power and other parameters to minimize the energy consumption, which can be important for battery powered systems. Adaptive OWC systems can also be used in satellite communications to provide high-speed links between ground stations and satellite payloads. These systems are particularly useful in scenarios where the satellites are in the lower Earth orbits since the relatively low distance to the ground allows for higher data rates and lower latency

than would be possible with traditional satellite communications. Moreover, this chapter discusses the software defined OWC systems with different adaptive algorithms and a thorough evaluation of a theoretical and simulation-based software defined MIMO FSO system with an adaptive switching technique.

4.2 SDR-based OWC

There are several technologies available to make FSO systems adaptive such as software defined techniques, dynamic resource allocation, and machine learning (ML). The dynamic resource allocation technique requires feedback and can only manipulate some parameters of the systems [219], whereas the ML -based scheme relies on predicted information from the previous data or performance to learn and adapt to the changing conditions [220]. The software defined technique in OWC systems have shown some promising results. Software defined optical system using LEDs and USRPs was reported in [221] and evaluated the performance in terms of the SNR in both LOS and non-LOS scenarios. In [222], SDR for laser beam modulation in an OWC system was discussed, and validated the flexibility and re-adjustable capability of SDR without interfering with the electronics of the system. A bi-directional system with adaptive modulation, where modulation selection is based on noise, interference, and environmental impacts was shown in the experimental demonstration of a VLC system was examined in [223]. In [224], experimental evaluation and performance analysis of an indoor VLC system with adaptive software defined equalization using USRPs and LabView was reported. The implementation of a VLC system using the SDR approach, low-cost and commercial off-the-shelf devices, and LabVIEW to experimentally demonstrate audio streaming over a 1 m distance was reported in [225]. LiFi systems in the range of visible, IR, and UV bands over a 20 m linkspan using LimeSDR USB and GNU Radio for research and development purposes to perform data transmission between two optical transceivers were also commercially reported [226]. Validation of the IR optical front ends with a bandwidth of 10 MHz for USRPs for transmission of an audio signal was reported in [227]. In [24], the advantages of implementing FSO systems based on the SDR technique were evaluated and the flexibility of the system adapting to

varying weather conditions to increase link availability and reliability was discussed. Theoretical and experimental analysis of a software defined adaptive modulation MIMO VLC was reported in [228]. It is noticeable that the software defined technique has several advantages and can offer a real time reconfigurable smart system in adaptive OWC systems. Several advantages of SDR-OWC system includes:

- **Adaptivity and reconfigurability** - Easily reconfigurable and adaptable to changing environmental or network circumstances. As a result, software defined optical systems are well-suited for applications requiring a dynamic or flexible operation, such as in the military or emergency applications [229].
- **Enabling the use of advanced modulation and coding schemes** - The use of SDR enables the development of complex coding and modulation schemes that may not be possible with standard hardware-defined systems [230].
- Integration with other communication systems [162].
- **Cost-effective** - SDR-OWC system can be implemented using off-the-shelf components and does not require costly custom hardware [221].
- **Enabling the use of ML algorithms** - For example, GNURadio has an ability to implement an artificial neural network (ANN), which can be used to process the transmit and receive signal on the fly [231].

4.3 An Adaptive SDR

For a time-varying optical wireless channel, self-adaptive systems are a very attractive option that can support to choose the best method constantly. Several things to bear in mind, when it comes to real-time adaptive systems are that (*i*) it requires system performance feedback (e.g., BER, SNR, received power, etc.); (*ii*) the need for a certain level or levels of threshold depending on the system to make a decision on transmission parameters; and (*iii*) real-time monitoring and measurement of the channel conditions utilizing software defined technique to keep the system as affordable to implement as possible [232]. It is noticeable that software defined technique has several advantages

and can offer a real-time reconfigurable smart system in adaptive OWC systems as discussed in section 4.2. There are several adaptive algorithms that may be used in OWC systems including adaptive power control, adaptive equalization, switching algorithm, modulation, and coding schemes, frequency selection, antenna beamforming, network coding, and ML algorithms [233]. The adaptive power control technique can be adopted to control the transmit power of the system in order to maintain a reliable link in the presence of fading due to atmospheric attenuation or interference [234]. Adaptive modulation can provide the adjustment of the type of modulation and coding used for data transmission to optimize the system performance by maintaining the data rate and error control in different scenarios [235]. Frequency selection controls the frequency band used to transmit data to avoid interference and to take advantage of favourable propagation conditions [236]. Adaptive network coding can be used to encode and transmit data in a way that can improve the reliability and capacity of the communications system while ML algorithms can be used to adaptively change the algorithms for the purpose of error correction in a varying environment [237].

4.4 SDR-based Adaptive Equalization for OWC Systems

Equalization is a technique used in communication systems to improve the performance of the system in the presence of channel impairments such as intersymbol interference and noise. The channel impairments arise from different sources such as multipath fading, dispersion, and attenuation. These impairments can cause significant distortion in the received signal, making it difficult for the Rx to detect the transmitted data correctly [238]. The equalization can be used to estimate the impulse response of the channel and then use this estimate to cancel out the effects of the channel on the transmitted signal [239]. There are different types of equalization:

- Linear equalization: Linear equalization methods are based on the linear filtering of the received signal. These methods include zero-forcing (ZF), least mean squares (LMS), minimum mean-squared error, Recursive least squares (RLS), and decision feedback equalization (DFE) [240], [241].

- Non-linear equalization: Non-linear equalization methods are based on the non-linear filtering of the received signal. These methods include DFE and maximum likelihood sequence estimation [242], [241].

LMS is a typical and widely used algorithm that works by reducing the mean squared error between the received and transmitted data. The LMS algorithm has low computational complexity and is simple to implement, making it a most used choice for many applications [243], [46]. Another prominent technique is the RLS algorithm, which is computationally costly but has faster convergence and higher steady-state performance than the LMS algorithm [244]. In addition to the algorithm selection, a number of other variables can influence the performance of an adaptive equalization system. The choice of an equalizer structure is crucial, as it can have a significant effect on the performance of the system. The transversal filter, the decision feedback equalizer, and the maximum likelihood sequence estimator are typical equalizer structures [245]. The training sequence, which is a known sequence of data transmitted at the beginning of the communication to allow the equalizer to learn the characteristics of the channel, is another important factor. The duration and organization of the training sequence can have a substantial effect on the convergence and performance of the equalization system [245]. There are also several other considerations that can affect the performance of an adaptive equalization system, such as the SNR and the bandwidth of the channel, and the dispersion of the optical source. All of these variables can impact the convergence and performance of the equalizer, so they must be considered when designing and implementing an equalization system [246].

Several reported literature has proven that the equalization technique in OWC has been a successful and effective implementation such as: in [247], an underwater OWC system using 32-QAM single carrier signals using a frequency domain equalizer combined with a time-domain decision feedback noise predictor, employed at the Rx was reported. The reported system achieved a data rate of 3.48 Gbps, which is 17.2% higher than that of the OFDM scheme. The performance analysis of a joint temporal and spatial ANN, a joint DFE, and the ZF DFE equalizer decoder at the Rx for MIMO VLC system was reported and experimentally demonstrated that the joint ANN

equalization technique performs best with the capability if separating the channels with a data rate of ~27 Mbps [248]. The improvements in data rate and system performance using pre-equalization techniques in OFDM-VLC systems were reported and experimentally demonstrated in [249], [250], [251], and [252].

Since the implementation of equalization techniques in OWC systems shows a promising improvement in system performance, the capability of adaptive equalization to reflect the time-varying channel properties can be appreciable by actively modifying the equalizer's parameters [253]. As most of the communication systems OWC systems also can experience a dynamic change in the channel conditions This is where adaptive equalization comes in. Additionally, adaptive equalization techniques can improve the robustness of the system by adjusting the equalizer coefficients to adopt the changing channel conditions and interference levels. In [224], experimental evaluation and performance analysis of an indoor VLC system with adaptive software defined equalization using USRPs and LabView was reported. The work reported validated the flexibility of the LabView software platform and the ability to improve the measured data simply by changing the software side of the testing prototype. A channel feedforward software defined equalizer for VLC adopting multistate QAM is also reported in [254]. In this report, three equalization techniques: LMS, normalized LMS, and QR decomposition based RLS techniques are tested to provide the best QoS. An experimental demonstration of a software defined channel equalizer for a VLC system is evaluated in [255]. The demonstration of a VLC system using WARP boards with the transmission of OFDM frames utilizing an LED and RF at 2.4 GHz is reported in [256]. In summary, adaptive equalization in OWC systems is used to improve performance by actively adjusting the characteristics of the equalizer to match the time-varying properties of the channel and an efficient technique to maintain the link availability and reliability [257].

4.4.1 SDR-based Adaptive Modulation for OWC Systems

Generally, adaptive modulation algorithms are used to improve the transmission efficiency of the system by means of changing the modulation schemes dynamically according to the requirement of the system based on the channel conditions [233]. While maintaining a certain level of error performance, it allows the system to adapt to changing channel conditions in real-time. Usually, adopting this kind of technique can result in improved system performance compared to systems that use a fixed modulation scheme [258]. For instance, if the channel conditions are optimal, the system can utilize a higher-order modulation scheme (e.g., quadrature amplitude modulation) to achieve a higher data rate. If the channel conditions are poor, however, the system can switch to a lower-order modulation scheme (such as OOK) to reduce the error rate [259]. The necessity for real-time monitoring and measurement of channel conditions is one of the primary challenges of implementing software defined adaptive modulation. To accurately estimate the channel conditions and select the appropriate modulation format, it is necessary to employ sophisticated signal processing techniques or a thresholding technique [260]. The thresholding technique can be determined in such a way that if the system performs with BER of 10^{-9}, considering that, the system uses 64 QAM format, at BER of $10^{-6,}$ the system can adaptively change to lower level QAM to maintain the system performance. Meaning that the threshold level is at 10^{-6} and the CSI (in this case BER) is known from the feedback link [261].

Additionally, implementing adaptive modulation algorithms requires hardware for DSP that is fast and effective[235]. This requires the utilization of sophisticated DSP architectures and algorithms to facilitate the rapid and efficient processing of signals [262]. Despite these challenges, software defined adaptive modulation has numerous advantages. It can significantly enhance the performance and efficiency of optical communication systems, as well as reduce the transmission complexity of the system and expense [263].

In [230], an application of a real-time adaptive modulation scheme for an underwater acoustic communication system was evaluated using the received SNR as feedback to select the transmission parameters. The investigation of the relay effects on bandwidth efficiency by utilizing adaptive

modulation was reported in [264]. In this work, CSI was considered to be known at the Tx and the Tx adjusts the modulation formats according to the CSI. An experimental demonstration and investigation of a VLC system based on a software defined adaptive modulation system using LabView and USRPs for transmission of multistate QAM was carried out in [232]. The adaptive hybrid RF-FSO with LDPC encoded transmission and RF feedback line was reported in [265]. It is shown that the spectral efficiency performance was significantly improved and the deep fades in the order 35 dB and above can be tolerated. Additionally, a real-time software defined adaptive MIMO VLC system with different modulation formats and configurations was proposed and demonstrated in [266].

4.4.2 SDR-based Adaptive Power Control OWC Systems

Adaptive power control in optical systems uses software algorithms to adjust the power of an optical signal in response to changing conditions in the transmission environment [267]. This technique can be effectively utilized in FSO systems, particularly under fog and turbulence conditions as it can significantly degrade the performance of the FSO systems by scattering and absorbing the laser beam[268]. In order to mitigate such conditions, it is important to implement an effective power control strategy. Software defined adaptive power control can be used to adjust the transmitted power in order to maintain a reliable link between the Tx and Rx [269]. This allows the system to be more flexible and adaptable, as the software can be easily updated or modified to reflect changes in the system or the surrounding environment [269].

One way to implement software defined adaptive power control is to use feedback control, where the power of the signal is adjusted based on the measured performance of the system. For example, if the signal quality degrades due to increased noise or interference, the power of the signal can be increased to compensate [270]. Another approach is to use feedforward control, where the power of the signal is adjusted based on predicted conditions in the transmission environment [271]. This can be done using algorithms that estimate the impact of various factors, such as temperature or humidity, on the performance of the system.

In addition to these approaches, other factors can influence the power control strategy in FSO systems operating in fog. The laser beam divergence angle, which determines the beam size at the Rx, can affect transmission range and power requirements. Using a laser with a smaller beam divergence angle may allow for longer data transmissions or more data over the same distance with less power. The type of modulation used to encode the laser beam can also affect the power control technique in foggy FSO systems. Different modulation schemes have different noise and interference sensitivity, which affects transmitted power and system performance.

There are several approaches that can be used to improve the performance of the FSO systems in fog conditions as discussed in chapter 2. Moreover, MIMO FSO systems can also effectively mitigate the varying fog conditions using SD techniques by transmitting the same data over multipath and reducing the chances of a single path being blocked by fog. Adaptive algorithms can be used in MIMO architecture more effectively due to the independence and higher level of flexibility the software defined techniques can offer, such as allocating power and the amount of transmitted power in different channels.

4.5 SDR-based MIMO FSO System with Adaptive Switching

In section 4.4, the adaptive OWC with different algorithms such as adaptive equalization, modulation, power control, and power allocation has been discussed. Similar to the adaptive power allocation system, to overcome the unavoidable atmospheric conditions, the implementation and investigation of a software defined adaptive switching algorithm in MIMO FSO system using GNURadio for real-time evaluation is proposed and discussed in this section. The decision-making method and thresholding technique to perform the adaptive switching and channel modelling in GNURadio are also evaluated.

4.5.1 System Design Configuration

The link availability as a function of transmission distance is a crucial factor in FSO systems, which can vary depending on the applications and geographic regions. The vast majority of FSO

systems are employed in the enterprise market (i.e., the last mile access networks), where link availability must meet the five-nine requirements (i.e., 99.999 %) [272], [273]. The proposed system with OOT modules facilitates the implementation of *N* number of Txs and Rxs. As a proof of concept, a 4 × 2 MIMO FSO system is considered and described in Figure 4.1. In this simulation, the design employs two sets of Txs and Rxs for parallel transmission of two different signals to improve link reliability. A dedicated switching algorithm is proposed to turn on the Tx(s) based on the channel conditions. Each Tx and Rx can operate independently or in a unified cluster. Fog and turbulence-induced attenuation and geometric losses are taken into account when determining the link's reliability. The key system parameters considered are listed in Table 4.1.

The Tx unit is comprised of four Txs (Tx-A1, Tx-A2, Tx-B1, and Tx-B2) grouped into two clusters of two Txs, with each cluster transmitting different OOK data streams i.e., $d_a(t)$ and $d_b(t)$.

Table 4.1. Key System parameters for the implementation of MIMO FSO system with adaptive switching in GNURadio.

Parameter	**Value**
Link length L	100, 200, 300 m
Number of bits	3.6×10^{10} bits
Transmit power P_{Tx}	10 dBm
Rx lens diameter D_{Rx}	50 mm
Tx lens diameter D_{Tx}	5 mm
Tx beam divergence θ_0	0.01°
Optical wavelength λ	850 nm
Effective focal length at Rx	~50 mm
Responsivity of PD at 830 nm	0.4 A/W
Rx operating wavelength range	300-1100 nm
Rx bandwidth	30 kHz-1.2 GHz
Noise equivalent power	60 pW/√Hz
PD	PIN
Channel temporal correlation	10 ms
Txs correlation length (for 100, 200 and 300 m)	~1, ~1.3, ~1.6 cm
Tx separation distance d_{Tx}	~7.5 cm
Rx separation distance d_{Rx}	~2.5 cm

Note that at the Tx unit within the Tx switch module, threshold levels of Tx-A and Tx-B are included for fog and atmospheric-induced loss and intensity fluctuations, respectively, to determine the operation mode using Log-normal and Gamma-Gamma turbulence models [274], [275]. Under normal weather conditions, Tx-A1 and Tx-B1 transmit two independent data streams. In fog or turbulence, however, additional Txs (Tx-A2 and Tx-B2) can be used if the following conditions, i.e., $L_{\text{Atm (input)}} \geq L_{\text{Atm (Thres)}}$ or $\sigma^2_{I(\text{input})} \geq \sigma^2_{I(\text{Thres})}$ are met. This is to ensure that the link's availability is maintained to the maximum extent possible at the expense of increased transmit power P_{Tx}. Using optical lenses, the intensity modulated optical beams are launched into the free space channel. On the Rx side, the received optical beams are focused by optical collimators onto two optical Rxs (Rx-A and Rx-B), which are composed of PD and trans-impedance amplifiers. The electrical signal that has been regenerated is then applied to moving average filters, samplers, and threshold detectors (slicers) to recover the estimated sequence of the transmitted data stream. The BERT is then employed to determine the real-time BER by comparing the received and transmitted data streams. Note that (*i*) the used parameters and link characteristics in terms of the channel loss (V, σ_I^2, and C_n^2) are monitored using SDR/GNU Radio, and (*ii*) the extracted link characteristics and the received OOK signal are generated in the GNU Radio software domain. In this research, it is assumed that the signals transmitted and received are uncorrelated [276]. The separation space between Txs and Rxs is numerically calculated which must exceed the correlation length:

$$d_c \approx \sqrt{\lambda l}\,. \tag{4.1}$$

The correlation coefficient as a function of the separation distance d between the Txs is given by [277]:

$$\rho = \exp\left(\frac{d}{d_c}\right). \tag{4.2}$$

Using equations (2.3), (2.4), and (2.5) σ_I^2 is determined for C_n^2 of 10^{-17} to 10^{-11}, and using (2.28), (2.29) and (2.30), L_{Atm} is estimated for a range of V from 20 km to 1 km, which are then adopted in the system simulation to evaluate the link performance in terms of the BER and therefore to

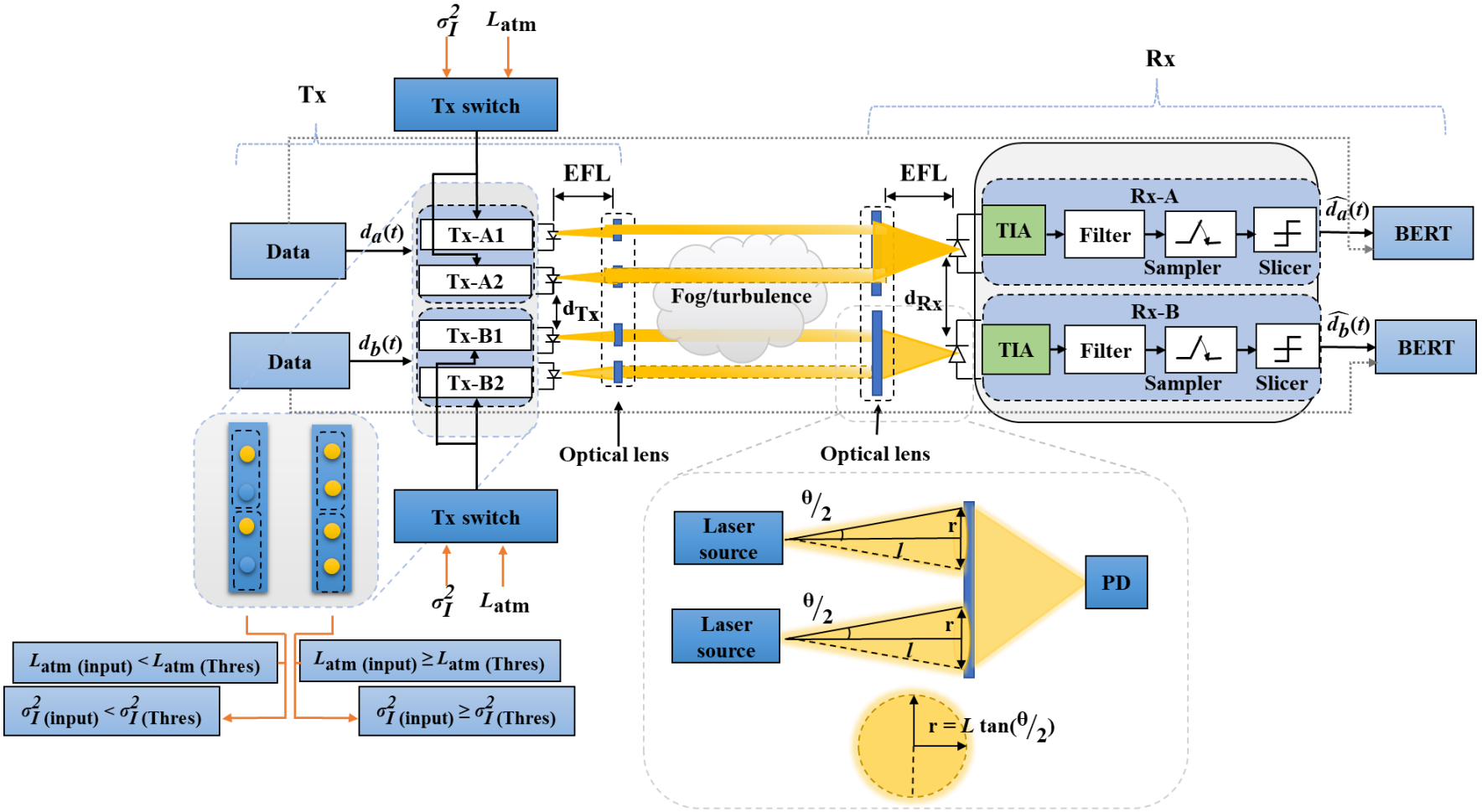

Figure 4.1. Schematic system block diagram of MIMO FSO system with adaptive switching algorithm in software defined GNURadio ecosystem.

Table 4.2. The number of Txs used as a function of L, V and L_{Atm} under the fog condition.

Link length *L* (m)	**Visibility *V* (km)**	**Atmospheric loss L_{Atm} (dB)**	**Txs used**
100	20	0.048	Tx-A1, Tx-B1
	2	0.48	Tx-A1, Tx-B1, Tx-A2, Tx-B2
	1	0.96	Tx-A1, Tx-B1, Tx-A2, Tx-B2
200	20	0.096	Tx-A1, Tx-B1
	5	0.41	Tx-A1, Tx-B1, Tx-A2, Tx-B2
	1	2.7	Tx-A1, Tx-B1, Tx-A2, Tx-B2
300	20	0.14	Tx-A1, Tx-B1
	8	0.36	Tx-A1, Tx-B1, Tx-A2, Tx-B2
	1	4.1	Tx-A1, Tx-B1, Tx-A2, Tx-B2

Table 4.3. The number of Txs used as a function of L, σ_I^2 and C_n^2 under the turbulence condition.

Link length *L* (m)	**Scintillation index σ_I^2**	**Refractive index structure parameter C_n^2 ($\mathrm{m}^{-2/3}$)**	**Txs used**
100	5.9×10-9	10^{-20}	Tx-A1, Tx-B1
	0.589	10^{-12}	Tx-A1, Tx-B1, Tx-A2, Tx-B2
	> 1	10^{-11}	Tx-A1, Tx-B1, Tx-A2, Tx-B2
200	2.01×10-8	10^{-20}	Tx-A1, Tx-B1
	0.21	10^{-13}	Tx-A1, Tx-B1, Tx-A2, Tx-B2
	>1	10^{-12}	Tx-A1, Tx-B1, Tx-A2, Tx-B2
300	4.4×10-8	10^{-20}	Tx-A1, Tx-B1
	0.414	10^{-13}	Tx-A1, Tx-B1, Tx-A2, Tx-B2
	>1	10^{-12}	Tx-A1, Tx-B1, Tx-A2, Tx-B2

determine $L_{\mathrm{Atm(Thres)}}$ and $\sigma^2_{I(\mathrm{Thres})}$, where the BER range is ~10^{-5} to ~10^{-3}. Based on the numerical evaluation of L_{Atm} for a given *V* and *L*, the link status is studied and a set of Txs to be used is carried out and outlined in Table 4.2 while Table 4.3 outlines the number of Txs used under turbulence for the link spans of 100, 200, and 300 m in the MIMO FSO system. Note, σ_I^2 and C_n^2 are predicted to reach a forward error correction (FEC) BER of 3.8×10^{-3}, the upper limit.

4.5.2 Implementation of SDR-based MIMO FSO with Adaptive Switching

In this simulation, the information on CSI (i.e., σ_I^2 and L_{Atm}) is already available at the Tx unit or provided via a feedback path. Using the flow chart shown in Figure 4.2, simulation to determine the BER as a function of *V* for single FSO, MIMO FSO, and proposed MIMO FSO links with a range of 100, 200, and 300 m under turbulence and fog conditions. To investigate the performance of the software defined adaptive switching MIMO FSO system, the SDR-based Tx, Rx, and channel have been implemented in GNURadio, along with a general-purpose processor-based real-time signal processing framework. The GNURadio is also capable of functioning as a simulation environment without the need for actual hardware. Note that GNURadio applications are typically written in Python as a package and combined with DSP blocks integrated within GNU Radio and implemented in C++ to perform crucial signal processing tasks [193] . Figure 4.3 depicts the implementation of the MIMO FSO system in the GNU Radio domain, which consists of a Tx, a channel, and an Rx. At the Tx, a sequence of pseudo-random binary data in the OOK format is applied to the throttle module, which is used to prevent CPU congestion following real-time simulation. Throttles outputs are applied to (*i*) virtual sink modules and (*ii*) MIMO-Tx modules which output is applied to virtual sink modules. In addition, the MIMO- Tx is provided with the outputs of the virtual sources, which represent feedback data on atmospheric loss $L_{\mathrm{Atm\ (input)}}$ in dB and $\sigma^2_{I(\mathrm{input})}$ of the channel. Since GNU Radio provides a graphical user interface (GUI) to generate and configure signal processing flow graphs, sample time waveforms were generated at the outputs of the MIMO-Tx (links A and B) and the optical Rx as shown in Figure 4.4(a-f). Figure 4.4(a-c) depicts the received signal under a clear channel, where only a single Tx (TxA1 and TxB1) is active at any time given. Additional Txs

are activated to ensure link availability based on the channel condition, provided $L_{\text{Atm}} \geq L_{\text{Atm (Thres)}}$ of 0.3 and $\sigma_I^2 \geq \sigma_{I(\text{Thres})}^2$ of 0.02, thus meeting the FEC BER limits of 3.8 ×10^{-3}. Figure 4.3(d-e) depict the simulated time waveforms in this instance.

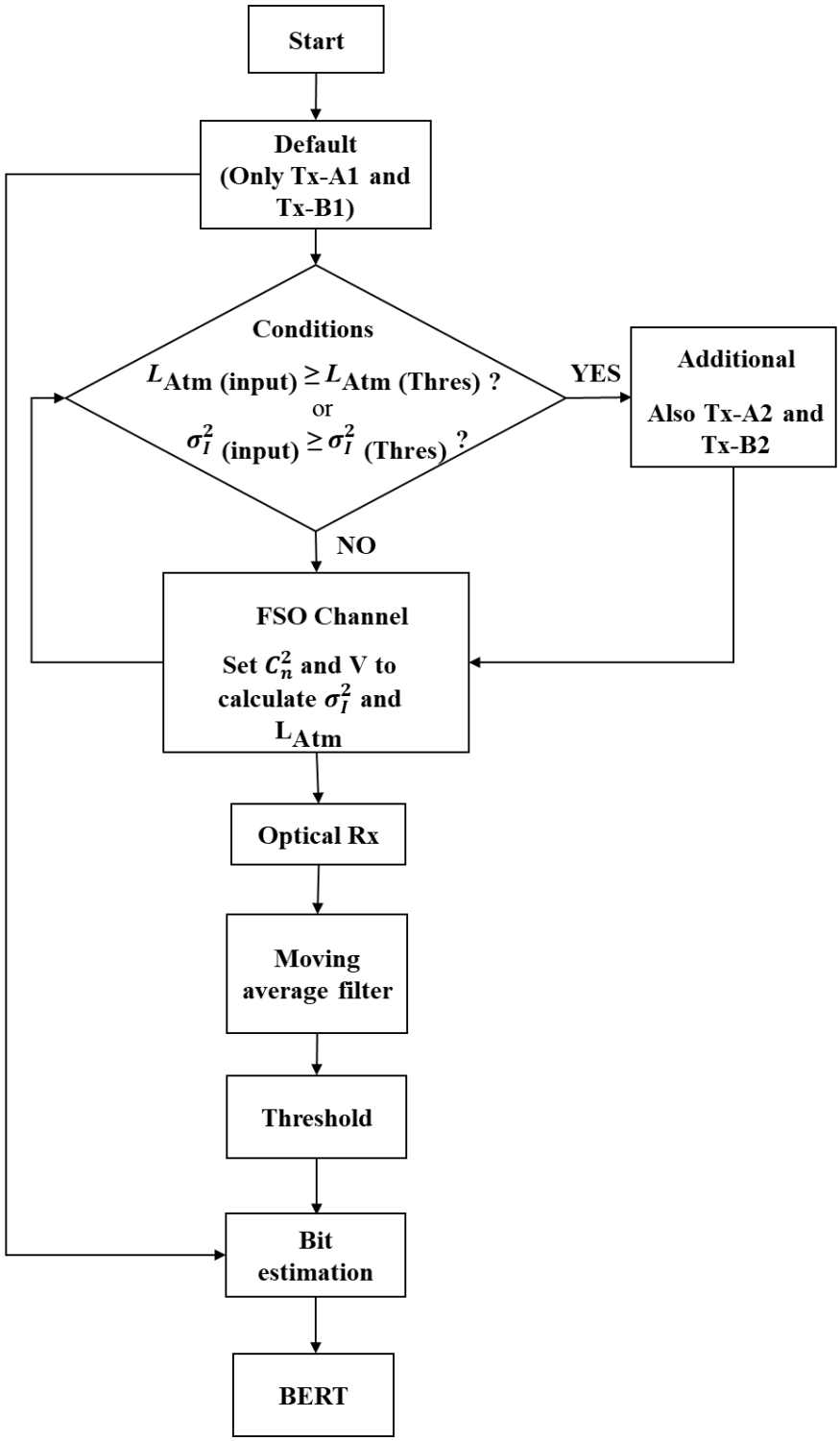

Figure 4.2. System flow chart of SDR-based MIMO FSO with adaptive switching.

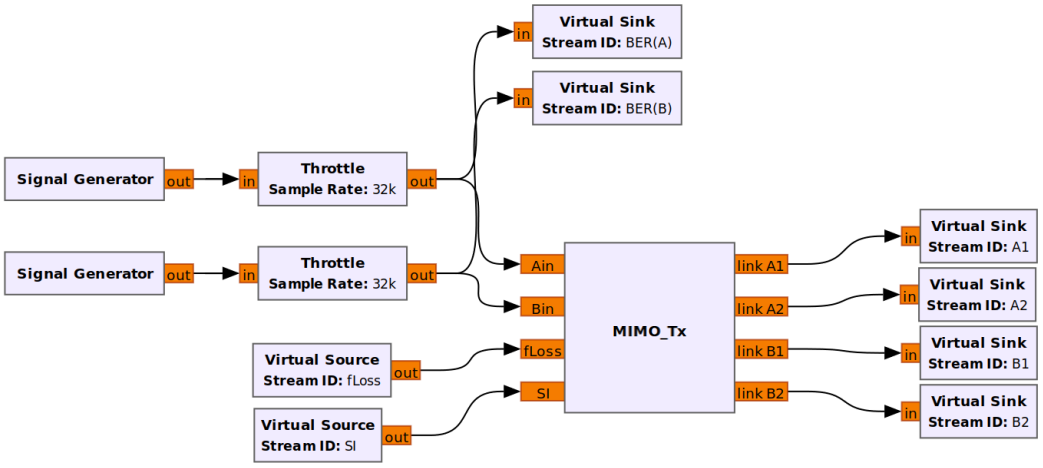

(a)

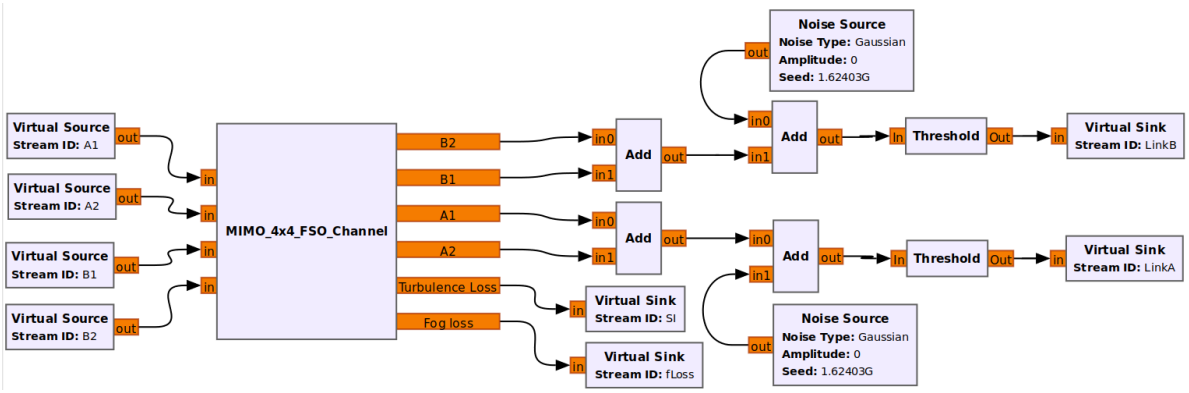

(b)

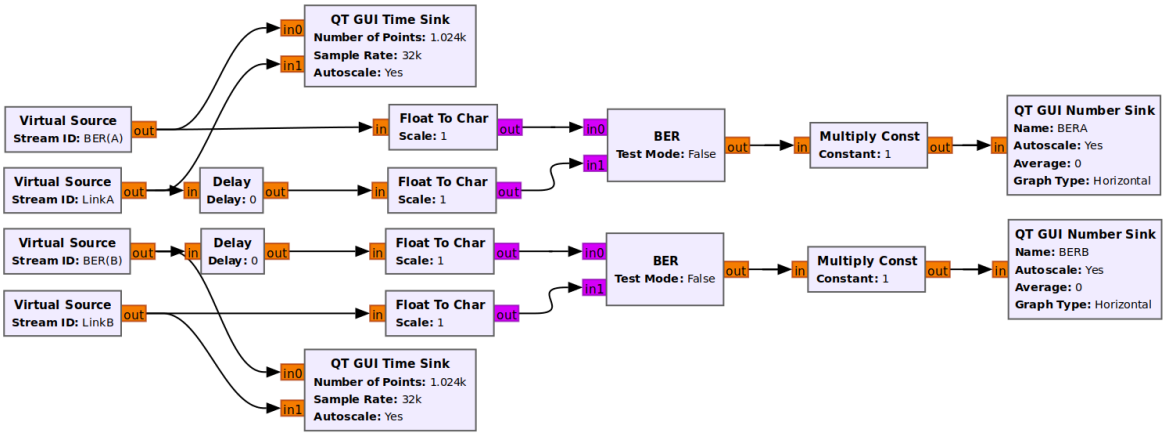

(c)

Figure 4.3. System implementation for (a) Tx with fog and turbulence, (b) channel with the additive white gaussian noise, and (c) the Rx with real-time BER estimation in GNURadio.

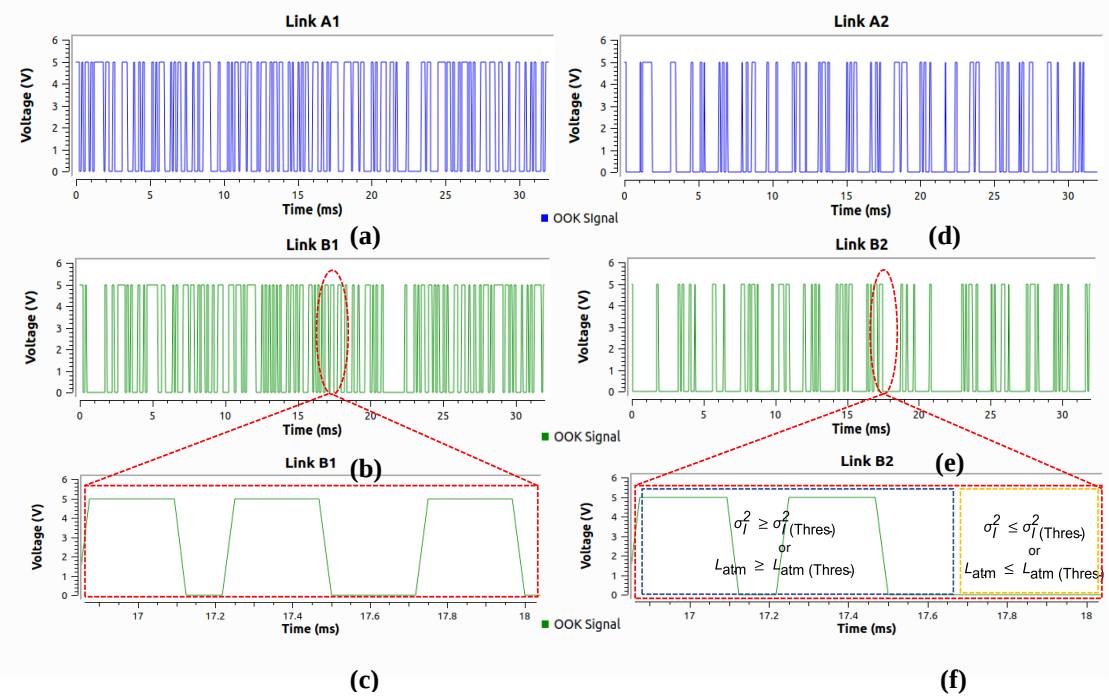

Figure 4.4. OOK waveforms at the: (a) Tx-Link A, (b) Tx-Link B, (c) optical Rx for a clear channel, and (d) Tx- Link A, (e) Tx-Link B, and (f) optical Rx for an un-clear channel.

4.5.3 Recorded Data

The investigation of the implementation of MIMO FSO in GNU Radio is carried out using the system parameters in Table. 4.1 using the OOT DSP blocks, which are built from scratch. The designed and built OOT not only satisfies the objective to monitor the system performance in real-time, also satisfies the purpose of reconfiguring without the need to change the hardware platform. Moreover, it also offers an easy experimental implementation on the fly due to direct communication with the SDR platform which will be demonstrated and discussed thoroughly in Chapter 5. For a clear channel with V of 20 km, the required P_{Tx} is considered to be 10 dBm with 0 dB channel loss and the additional losses including L_{Geo} are assumed to be low. Following the simulation procedure in Section 4.4.2, the system performance in terms of BER for the link range of 100, 200, and 300 m links under the fog conditions are depicted in Figure 5. For a 100 m link, MIMO outperforms the single FSO link for V<18 km and especially at lower values of V as expected. For the FSO link with the proposed adaptive switching algorithm, the BER pattern follows the single FSO link, up to a distance of 3 km, after which the BER drops to the MIMO FSO link level with a BER of 10^{-9} which

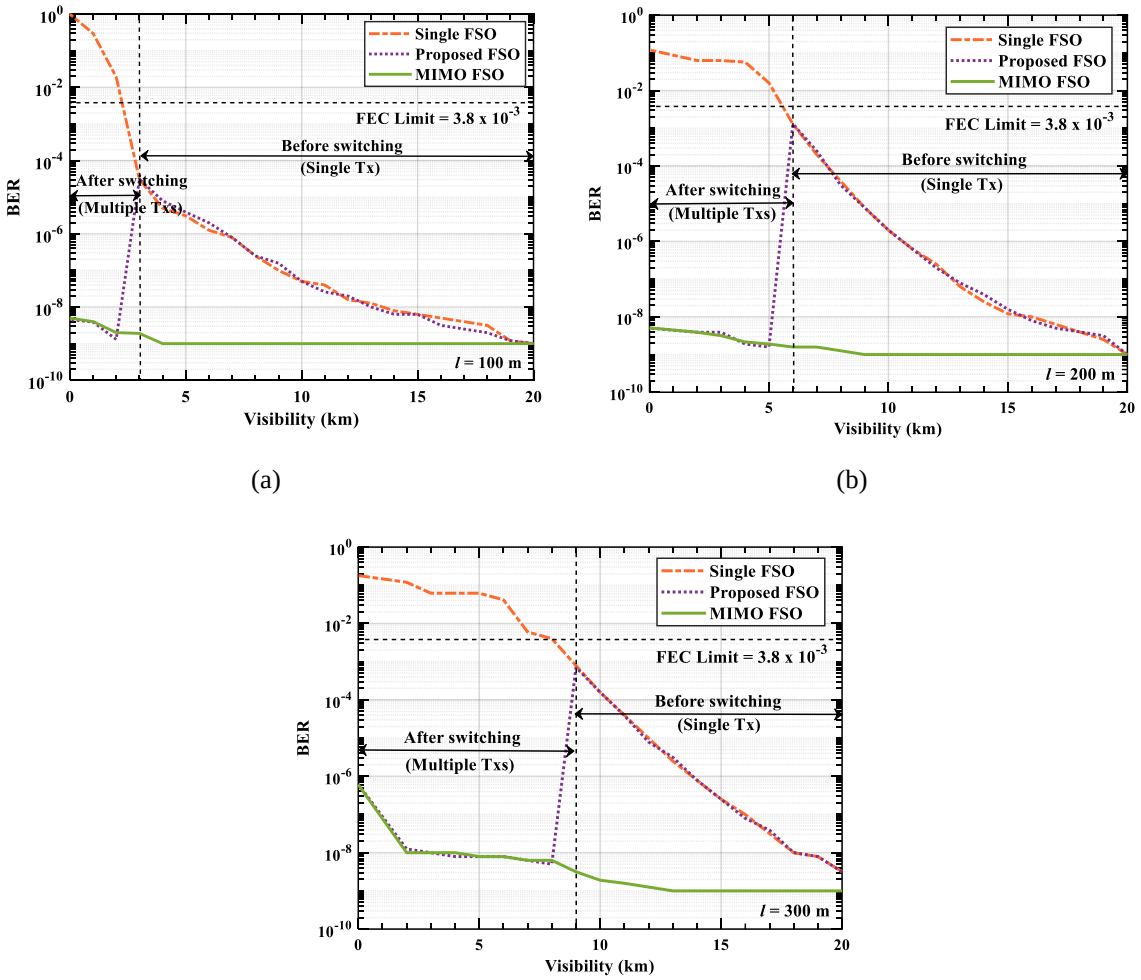

Figure 4.5. BER vs. the visibility for single, MIMO and proposed FSO with adaptive switching links for: (a) 100, (b) 200, and (c) 300 m with fog.

is due to turning on the additional Txs as explained before. The same pattern is observed for 200 and 300 m links as depicted in Figure 4.5(b) and (c) except when the switching takes place at V of 6 and 9 km where the BER values are at 1.3×10^{-3} and 7.4×10^{-4}, respectively. Also observed are (i) the BER plot for the MIMO FSO link, which is almost constant (i.e., 10^{-9}) at $V > 5$ and 10 km in Figures 4.5(b) and (c). Additionally, compared to D_{Rx}, the beam spot sizes of 17.5 and 34.9 mm in 100 and 200 m, respectively, are smaller. Therefore, L_{Geo} is neglected. Due to the beam spot size of 52.4 mm, an extra 1.2 dB L_{Geo} of is introduced in the 300 m link. For all three systems, the estimated BER exceeds the FEC limit for $\sigma_I^2 < 0.02$, hence, $\sigma_{I(Thres)}^2$ was set at ≤ 0.02. The systems were then simulated under weak to moderate turbulence (i.e., $10^{-11} < C_n^2 < 10^{-17}$) to determine the BER

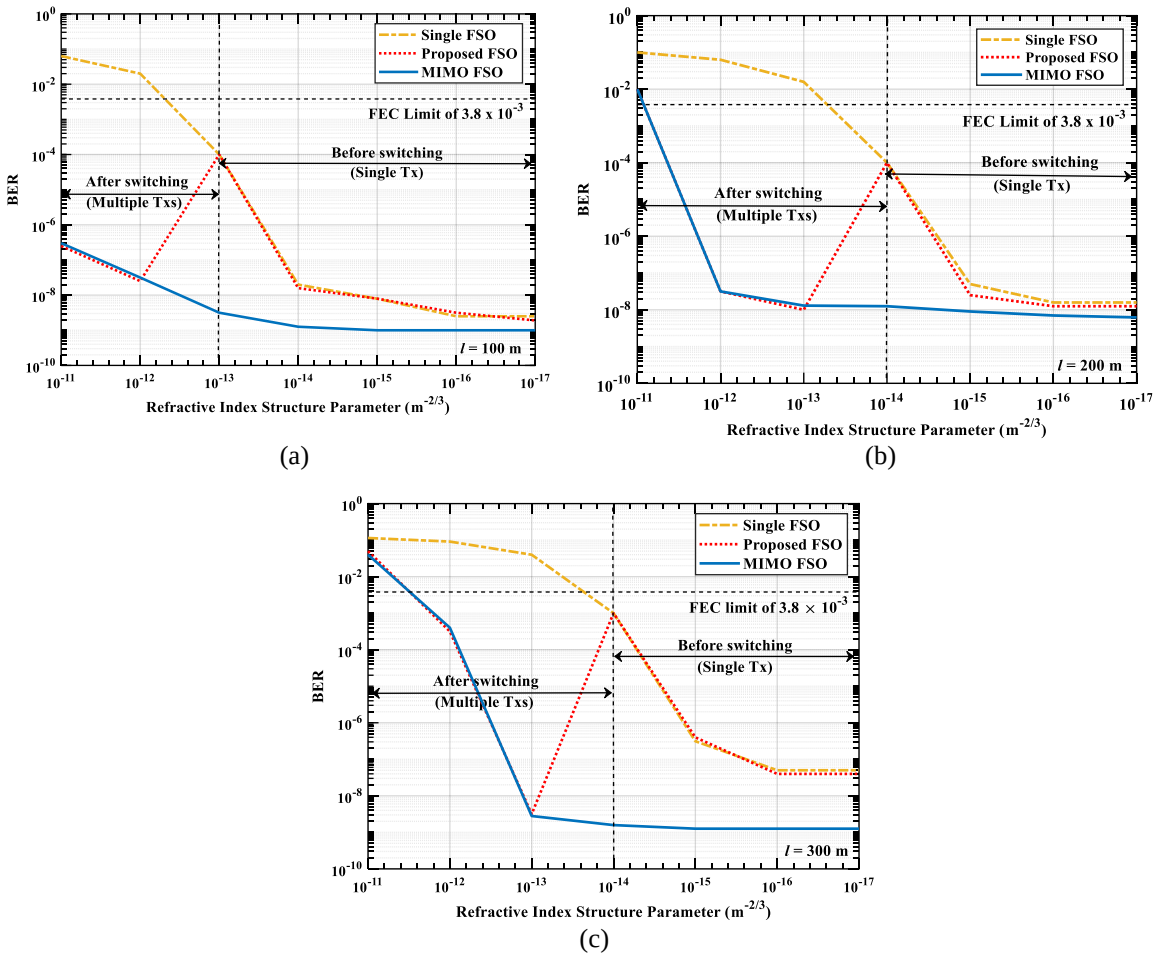

Figure 4.6. BER vs. C_n^2 for single, MIMO and proposed FSO with adaptive switching links for: (a) 100, (b) 200, and (c) 300 m with turbulence.

performance for all three systems and link spans of 100, 200, and 300 m as depicted in Figures 4.6. In these plots, the same pattern is observed as in Figure 4.5 where the BER of the 100 m link adaptive switching the FSO link followed the single FSO link plot for C_n^2 of 10^{-13}m$^{-2/3}$, beyond which the BER significantly improves, reaching the level of MIMO FSO link at C_n^2 of 10^{-12} from 10^{-4} to 2.5 × 10^{-8}, see Figure 4.6(a). This improvement in BER performance is due to the addition of Tx-A2 and Tx-B2. In Figure 4.6(b), the BER plot for the proposed link changes direction at $C_n^2 < 10^{-14}$ decreasing to 10^{-8} at $C_n^2 < 10^{-13}$ and then increasing with C_n^2. In Figure 4.6 (c), the BER transitions from 10^{-3} to 2×10^{-9} at C_n^2 of 10^{-14} to 10^{-13} for the proposed system. Note that, (*i*) the BER floor level for both MIMO FSO and proposed FSO links is ~ 10^{-9} for $C_n^2 > 10^{-13}$ and (*ii*) the 200 and 300 m long MIMO FSO link performance degrades more under effects (i.e., $C_n^2 > 10^{-13}$).

4.6 Summary

In this chapter, the software defined optical communications systems and different adaptive systems, including adaptive equalization, adaptive modulation, and adaptive power allocation are discussed Moreover, the adaptive switching algorithm is proposed to mitigate the atmospheric loss and implemented using software defined GNURadio ecosystem. The demonstration of a real-time SDR/GNURadio implementation was carried out and its performance under various atmospheric conditions. A bit-by-bit comparison is performed with the GNURadio signal processing block, and BERT is utilized. It was discovered that the proposed switching mechanism effectively mitigated fog and turbulence-induced attenuation. The MIMO FSO with adaptive switching technique is proven to operate effectively in dense fog while it experienced a peak turnover degradation after switching in 200 and 300 m in moderate turbulence conditions. Therefore, it can be concluded that the switching mechanism, i.e., activating additional Txs can only overcome the effect of turbulence of a certain level.

Chapter 5. Experimental Implementation of SDR-based OWC Systems

5.1 Introduction

Due to the obvious proliferation of mobile computing devices such as smartphones, tablets, and laptops, as well as recently introduced wearable linked gadgets, it is anticipated that more than 70 percent of the world's population would have access to mobile connectivity by the year 2023 [278]. It is anticipated that the 5th and 6th generation wireless networks, as well as future generations, would be able to satisfy these tremendous demands for connectivity [279]. It is very well known that OWC technology offers enhanced safety, higher data transfer rates, virtually limitless bandwidth that is unregulated on a global scale, generates no electromagnetic interference, and is not affected by the RF-induced interference generated by other communication devices [280]. Therefore, as a result of these reasons, the OWC technology is capable of being supplied as a complimentary system to the well-established and dominant RF wireless technologies in particular focused application areas [280].

However, evaluating the FSO link in a real-time setting is a difficult and time-consuming task, and the results are largely dependent on the weather conditions [48]. Most of the reported literature primarily showcased FSO systems with fog and turbulence under controlled environments. Especially, generating light-to-dense fog and weak turbulence to evaluate the system in experimental laboratories can be found in recently reported research. However, the generation of medium-to-strong turbulence with a scintillation index of > 0.35 is quite challenging, and the real time FSO system analysis under such condition has not been reported in the literature. Due to the aforementioned issues practical evaluation of FSO systems has become a daunting task. It is worth mentioning that OWC systems can benefit from the facility and flexibility of SDR. In this chapter,

the practical implementation of OWC systems using the SDR platform, specifically GNU Radio software is outlined and discussed in detail.

5.2 Software Defined Implementation of OWC Systems

The flexibility and capability to adopt modulation, coding and synchronization utilized in conventional RF systems are provided by the SDR platform [281], [168]. SDR is a well-known technology that enables signal processing to be implemented all the way through the physical and data link layers. Additionally, SDR offers system reconfigurability and flexibility by allowing changes to only be made in the software domain rather than in the hardware platform, which is costly, time-consuming, and resources-wise not sustainable [282]. In [19], the performance analysis and SDR implementation of a MIMO FSO system with adaptive switching was reported. The authors demonstrated that the proposed system is capable of operating efficiently under severe fog conditions with a BER value in the range of 10^{-8} to 10^{-7} over transmission link spans of 100, 200, and 300 m using the OOK modulation format. A bi-directional system with adaptive modulation, where modulations selection was based on the noise, interference, and environmental impacts, for a VLC system, was investigated and achieved a 2 Mbps communication link using $k=2^1$-2^3 of k-pulse amplitude modulation and k-pulse PPM techniques [223]. An experimental implementation of a software defined VLC system for short-range transmission using a USRP and the visual programming language of LabVIEW for a fully standard compliant implementation of all the PHY I modes (data rate up to ~266 kbps) in the IEEE 802.15.7 standard with OOK and variable PPM was demonstrated over a 2 m link in [225]. It is important to note that LabVIEW SDR is a stable and highly modular platform, which can be readily modified, adjusted, or transferred. In [227], the FSO system using IR optical front ends using QAM with a bandwidth of 10 MHz and using USRPs for an audio car entertainment system was successfully presented.

In contrast to the hardware reconfiguration in the traditional approach, the software defined ecosystem offers a method that is relatively simple, cost-effective, and highly flexible in terms of designing dynamic, efficiently re-deployable, and highly secure components for wireless and wired

communication networks [147]. In SDR technology, most of the physical layer functionality can be realized in the mutable software platform. This makes it possible to decrease the cost of the hardware by introducing new wireless functionalities without the need for new components, which is highly desirable for service providers, product developers, and end users [282]. In addition, SDR makes it possible to easily implement a range of wired and wireless RF and optical systems. It does this by utilizing off-the-shelf components and adopting a common platform architecture. Some examples of these components include wireless open-access research platform boards and USRPs. To put this into perspective, some research works have been published on the development of software defined optical communications systems. For example, a software defined underwater VLC testbed was demonstrated using green laser as the Tx with PPM formatted signal and PD and USRP as the Rx achieving 4 Mbps with the BER of 5.5×10^{-3}. The demodulation of the signal and the BER estimation was carried out using MATLAB [283]. The design and implementation of SDR-based VLC transceivers were reported using binary pulse shift keying modulation technique, achieving the BER of 9.7×10^{-5} at 2.5 Mbps and a distance of 160 cm [284]. Additionally, SDR based VLC system was demonstrated to determine the parameters (the transmit speed, BER, and highest attainable distance) to develop a real VLC system was described in [285]. Th work was centred on evaluating a QAM system, using LabVIEW and USRPs, as well as two different types of Txs, namely, a Skoda Octavia III tail-light, achieving 28 Mbps, and a Phillips interior light, achieving 2 Mbps for a maximum distance of 325 m.

5.3 Experimental Testbed for SDR-based OWC

In Chapter 3, the implementation of adaptive systems utilizing the SDR ecosystem has been mentioned. The basic concept outlined in this chapter for practical validation is like the proposed technique in the previous chapter in order to overcome the hardware limitation and to provide reconfigurability of the OWC systems as a proof of concept.

5.3.1 System Configuration

An experimental testbed for the FSO system utilizing GNU Radio, an open-source SDR platform is developed, and testing and measurements in real-time under fog and turbulence conditions are conducted. To illustrate the practicality of SDR in FSO systems, a proof-of-concept testbed is developed and measurements are performed for a 199.5 m connection span in the GNU Radio domain and a 50 cm link span in an actual experimental setup under atmospheric conditions. Note that the operational speed (i.e., the bandwidth) of the link was not the primary objective, which depends on the types of devices used in the experimental setup (PC, USRP, optical and electrical, etc.). The objective was to develop a software-based platform that would allow us to observe the immediate effects of parameter changes on the performance of the system. Additionally, by evaluating the performance of the system we have demonstrated that the availability is compromised under severe turbulence conditions.

Figure 5.1 depicts a schematic diagram of the experimental setup. The Tx unit is comprised of a PC with GNU Radio, which creates an OOK non return to zero (NRZ) signal and drives the N200/210 USRP with Xilinx® Spartan® 3A-DSP XC3SD1800A and a low frequency transmitter (LFTx) daughterboard via an Ethernet cable. USRP's output is utilized to modulate the intensity of a red laser via a current driver for transmission over a 50 cm-long free space channel. An optical Rx (a PDA100A2 Thorlabs PD) is utilized to regenerate the electrical signal at the Rx device. Note that,

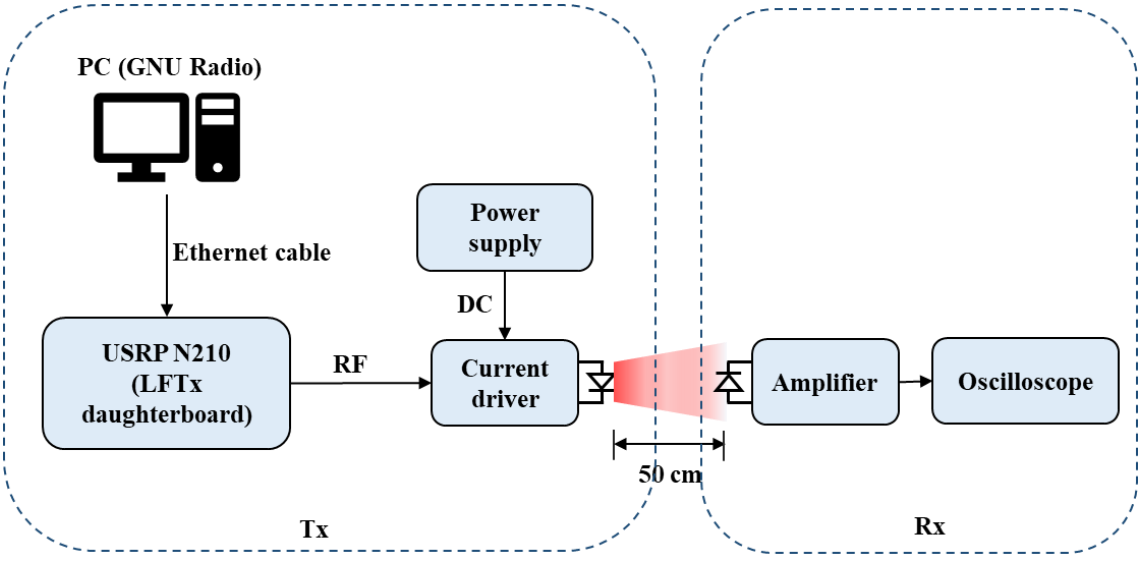

Figure 5.1. The block diagram of a proposed SDR based OWC system using USRP.

raising the light intensity can increase the link distance. On the software side, however, we have set the link distance for fog and turbulence to be 199.5 m, resulting in a total link length of 200 m for both software and physical instances.

5.3.2 Implementation of OWC System in SDR/GNU Radio Platform

To investigate the FSO system implemented in the SDR platform, the OOT modules for the generation of the OOK signal, and simulation of fog and turbulence-induced attenuations as well as the geometric loss are designed. The channel parameters can be changed and observed in real-time, see Figure 5.2, in GNU Radio. The generation of the OOK NRZ signal in GNU Radio is depicted in Figure 5.2(a). The built-in modules used are described as the following:

i. **Random uniform source:** This generates pseudo-random binary numbers included in [min, max).

ii. **Int to float:** In this block, the conversion of a stream of integers into a float data type is implemented. The interpolation filter only takes float and complex data types, which necessitates the completion of this step.

iii. **Interpolation filter:** This is a finite impulse response filter, which up-samples the input to a higher rate by inserting (L–1) zeros between samples and uses the method of the zero-order hold [286]. The number of taps is given by:

$$LN = sps \times LR, \quad (1)$$

where *sps* is the number of samples per symbol, and *LR* represents the interpolation rate.

iv. **UHD** (USRP Hardware Driver) **USRP sink:** This is the main connection between the GNU Radio environment and the USRP. The unique Internet protocol address of USRP in the experimental setup is required in this module.

The hierarchical chain of blocks to generate the OOK signal is built as a signal generator module shown in Figure 5.2(a). The fog/smoke loss block for the estimation of the fog induced attenuation in terms of the link visibility *V*; the turbulence effect on the propagating optical beam (i.e., intensity and phase fluctuations) and geometric loss modules built from scratch and are based on equations

Table 5.1. Key system parameters for implementation of OWC system in GNU Radio software ecosystem.

Parameter	**Value**
Optical wavelength λ	850 nm
Tx lens diameter D_{Tx}	5 mm
Tx beam divergence θ	0.01°
Link length L	199.5 m
Rx lens diameter D_{Rx}	50 mm
Channel temporal correlation	10 ms

provided in chapter 2. The evaluation of the system performance is carried out in terms of the BER over a transmission link span of 200 m. The key system parameters for GNU Radio are given in Table 5.1. Figure 5.2(b) and (c) show, the architecture of the implemented OWC system with atmospheric conditions and BER comparisons respectively. In Figure 5.2(b), the output of the pseudo random sequence generator module in OOK format is applied to (*i*) the fog loss block; and (*ii*) the virtual sink block in order to store the transmitted signal for the BER estimation. The output of the fog loss module is then applied with customizable parameters to the turbulence and geometric loss modules. The signal is subsequently sent to the virtual sink, the QT GUI time sink, and the UHD modules. Ethernet cable connects the USRP Sink block (i.e., UHD) with a unique Internet Protocol address to the USRP. In GNU Radio, a time sink module is used to see the simulated signal. Figure 5.2(c) depicts the system's BER estimation. The transmitted and received signal streams, i.e., virtual sources (BER-Tx and BER-Rx), are connected to the BER module, and the number sink is used to examine the estimated value in real-time. Note that the float to char module is utilized to alter the Data type. We estimate the BER in GNU Radio in real time, demonstrate the impact of atmospheric variables, and present experimentally collected received signals.

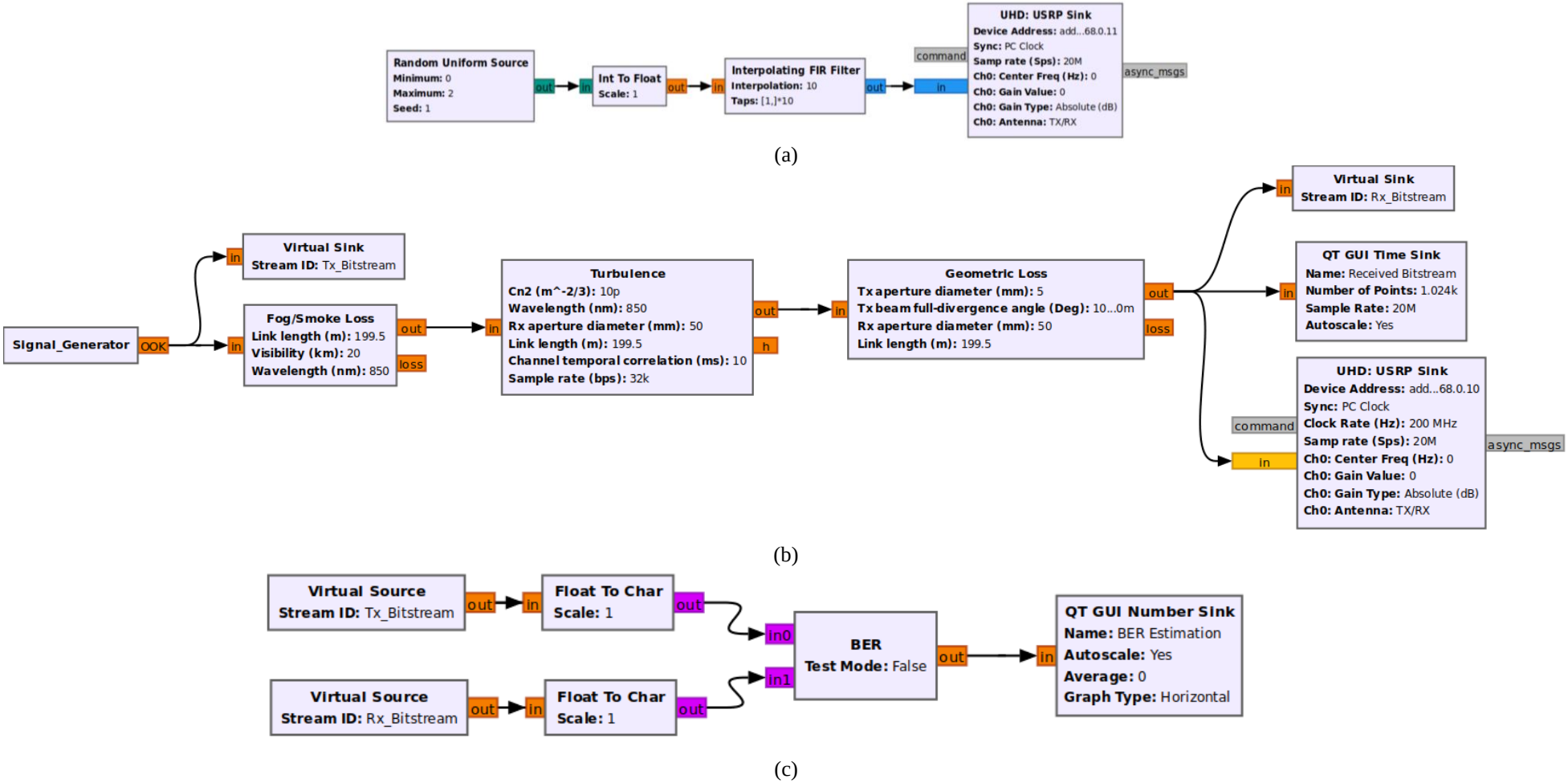

Figure 5.2. Implementation of FSO system in GNU Radio: (a)a hierarchical chain of blocks to generate an OOK signal which is built as a signal generator (b) an OOK signal with fog, turbulence, and geometric loss transmitted to the USRP, and (c) a BERT.

5.3.3 Experimental Setup

As indicated in Figure 5.3, an experimental testbed to evaluate the implementation of the proposed system in the SDR and GNU Radio environments is demonstrated. Note that all important system parameters are listed in Table 5.2. The goal is to monitor and control the system without modifying the hardware platform and by updating only the software platform. As shown in Figure 5.3, several tests, and measurements on the implementation of GNU Radio blocks using USRPs as the Tx and an

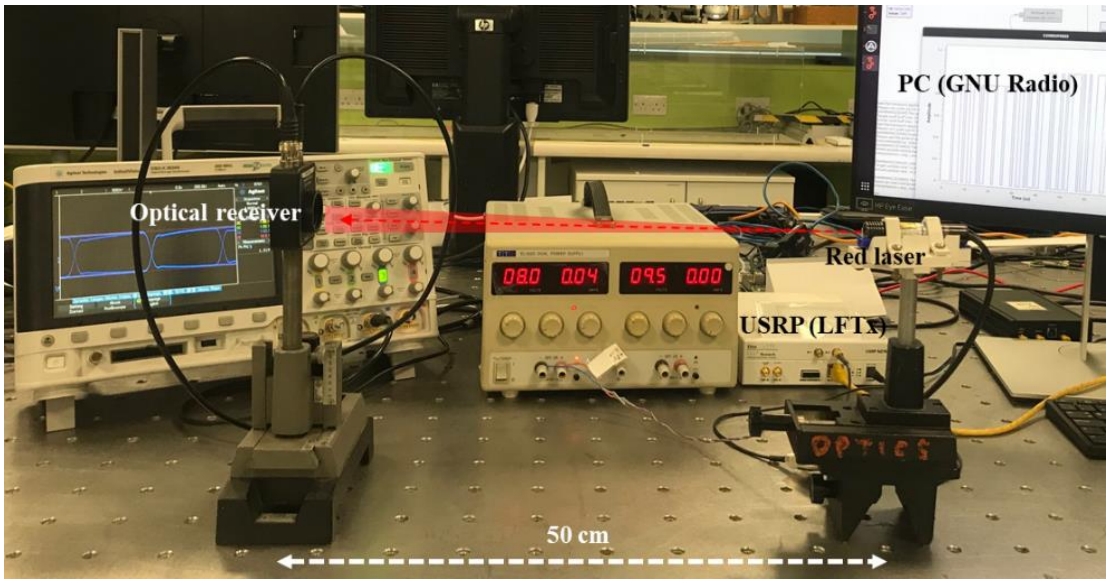

Figure 5.3. Real-time implementation of FSO system using SDR/GNU Radio ecosystem.

Table 5.2. Key system parameters in SDR-OWC experimental set up.

Parameter	**Value**
LFTx daughterboard bandwidth	0-30 MHz
Optical transmit power P_{Tx}	4.5 dBm
Tx beam divergence θ	<0.03°
Optical wavelength λ	670 nm
Link length L	50 cm
Optical Rx	PDA100A2 – Si Switchable gain detector
PD active region	75.4 mm2
Responsivity of PD at 960 nm	0.72 A/W
Rx operating wavelength range	320-1100 nm
Rx bandwidth	11 MHz
Noise equivalent power	2.67 – 71.7 pW/√Hz

oscilloscope as the Rx was carried out. For transmission of the OOK signal, the LFTx daughterboard is mounted on the USRP Tx, to which the GNU Radio running PC is linked by an Ethernet connection. The output of the Tx is utilized to modulate the intensity of a red laser source via a current driver for transmission over a 50 cm-long free space channel. An optical Rx is utilized at the Rx to regenerate the electrical OOK signal, which is caught using a digital oscilloscope.

5.3.4 Recorded Data

The investigation of the relationship between the interpolation filter, bandwidth, and jitter of the received signals, as well as the evaluation of the system's performance under three different fog intensities and three turbulence situations, are conducted. Demonstration of the adaptability and capabilities of controlling the system by simply modifying its software-domain settings is also carried out. A series of experiments and measurements have been carried out by increasing the interpolation filter taps and interpolation rate while keeping the PC sample rate constant at 20 MHz (i.e., the sampling rate limit of the PC used). The system bandwidth was measured by measuring the rise and fall times of the received signal, while the jitter was determined by measuring the rise and fall time errors of the eye diagram, as shown in Table 5.3. Note that *sps* = 1 and is held constant throughout the experiment. *LR* and *LN* of 10 and a bandwidth of 4 MHz have the lowest jitter at 12.4 nanoseconds.

Table 5.3. Bandwidth and jitter of the received signal corresponding to the interpolation rate and taps.

Interpolation rate (*LR*)	**Interpolation taps (*LN*)**	**Bandwidth (MHz)**	**Eye jitter (ns)**
10	[1] × 10	4.0	12.4
12	[1] × 12	3.1	13.4
14	[1] × 14	2.6	14.7
16	[1] × 16	2.4	15.2
18	[1] × 18	2.1	16.0
20	[1] × 20	2.0	17.4

In addition, the examples of the captured received signal using an oscilloscope is provided in Figure 5.4, which depicts the acquired time-domain signals via the USRP (lower trace) and optical frontend (upper trace) for interpolation rates of 10, 12, 14, 16, 18, and 20. The signal waveform is observed to become less distorted as the interpolation factor increases. In order to evaluate the quality of the received signal, the eye diagrams in Figure 5.5 have been provided. Specifically, Figure 5.5(a) depicts the eye diagram for LR = 10 with the eye width and height of 397 ns and 26 mV, respectively while Figure. 5.5(b) corresponds to LR = 12 with the eye width and height of 495 ns and 22.4 mV, respectively. In addition, Figures 5.5(c)-(f) illustrate the eye diagram for LR and LN of 14, 16, 18, and 20, respectively. It is noted that the eye gradually shuts when LR and LN are increased and that the

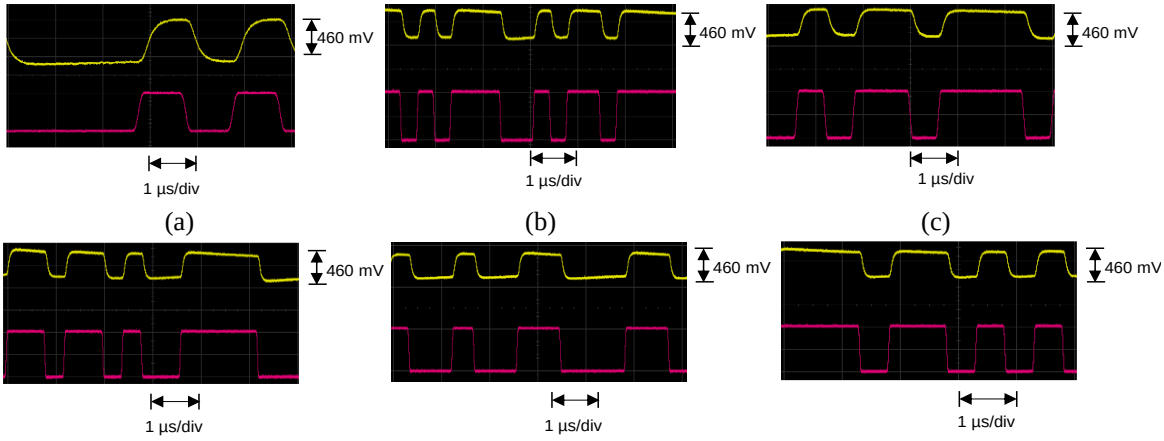

Figure 5.4. Received OOK-NRZ signals via USRP (lower trace, in red) and optical front end (upper trace, in yellow) with the interpolation filter length of: (a) 10, (b) 12, (c) 14, (d) 16, (e) 18, and (f) 20.

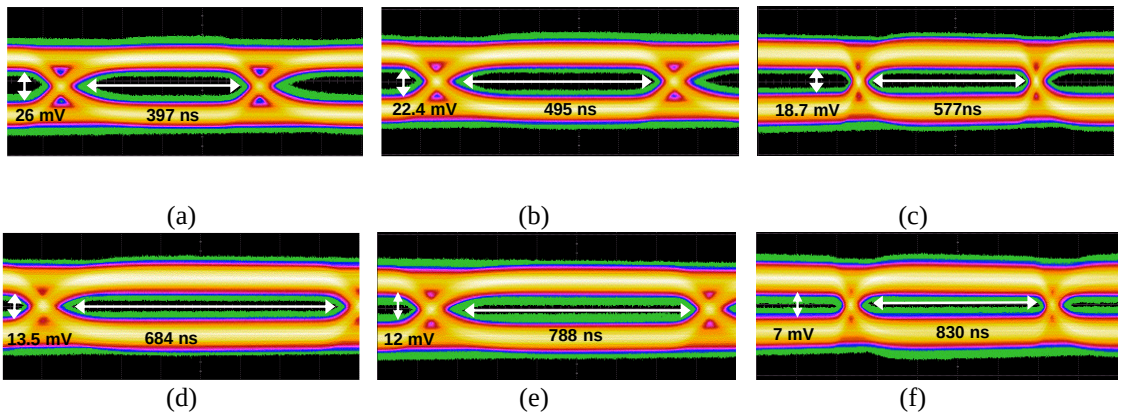

Figure 5.5. Eye diagrams of received OOK-NRZ via optical frontend with the interpolation filter rates of : (a) 10, (b) 12, (c) 14, (d) 16, (e) 18, and (f) 20.

eye is most open when *LR* and *LN* are the smallest. The signal is distorted due to the bias tee acting as a high pass filter.

Next, the atmospheric conditions of light, medium, and dense fog attenuations and weak, moderate, and strong turbulence regimes are considered. Initially, a clean channel with *V* of 20 km and 0 dB attenuation for a 200 m link length with transmit power P_{Tx} of 4.5 dBm and L_{Geo} of 1.7 dB is obtained, resulting in a received optical power of 3.8 dBm. For fog conditions, *V* of 5 km, 100 m, and 50 m are found, where the attenuation levels increased to 0.3, 17.7, and 34 dB for light, medium, and strong fog, respectively, with BER values of 10^{-6}, 10^{-5}, and 10^{-6}. Figure 5.6 depicts instances of collected signals at the Rx for all three fog conditions. The amplitude of the received signal decreased from 1.6 to 1.5 mV as the *V* decreased from 5 km to 100 m. At a distance of 50 m in dense fog, the signal amplitude decreased to 1.2 mV.

The turbulence regimes of $C_n^2 = 10^{-13}\mathrm{m}^{-2/3}$, $\sigma_I^2 = 0.03$ for weak, $C_n^2 = 10^{-12}\mathrm{m}^{-2/3}$, $\sigma_I^2 = 0.3$ for moderate, and $C_n^2 = 10^{-11}\mathrm{m}^{-2/3}$, $\sigma_I^2 > 1$ for strong turbulence is then investigated. Figures 5.7 (a), (b), and (c) exhibit the acquired received signals in light, moderate, and strong turbulence regimes, respectively. Under weak turbulence, the link functions with a BER of 10^{-5}, however moderate to strong turbulence will cause link failure with BER values of 10^{-2} and 0.5, respectively. Moreover, employing a software defined environment, similar BER values are obtained for both fog and turbulence situations compared to the purely experimental works described in a dedicated laboratory chamber in [273] and [287]. Using an experimental testbed, we validated the performance of the proposed system in situations of fog and turbulence. We demonstrated that the system could reach BER values of 10^{-6}, 10^{-5}, and 10^{-3} for light, moderate, and dense fog circumstances, respectively; and 10^{-5}, 10^{-2}, and 0.5 for weak, moderate, and high turbulence regimes, respectively, for a 200 m link span.

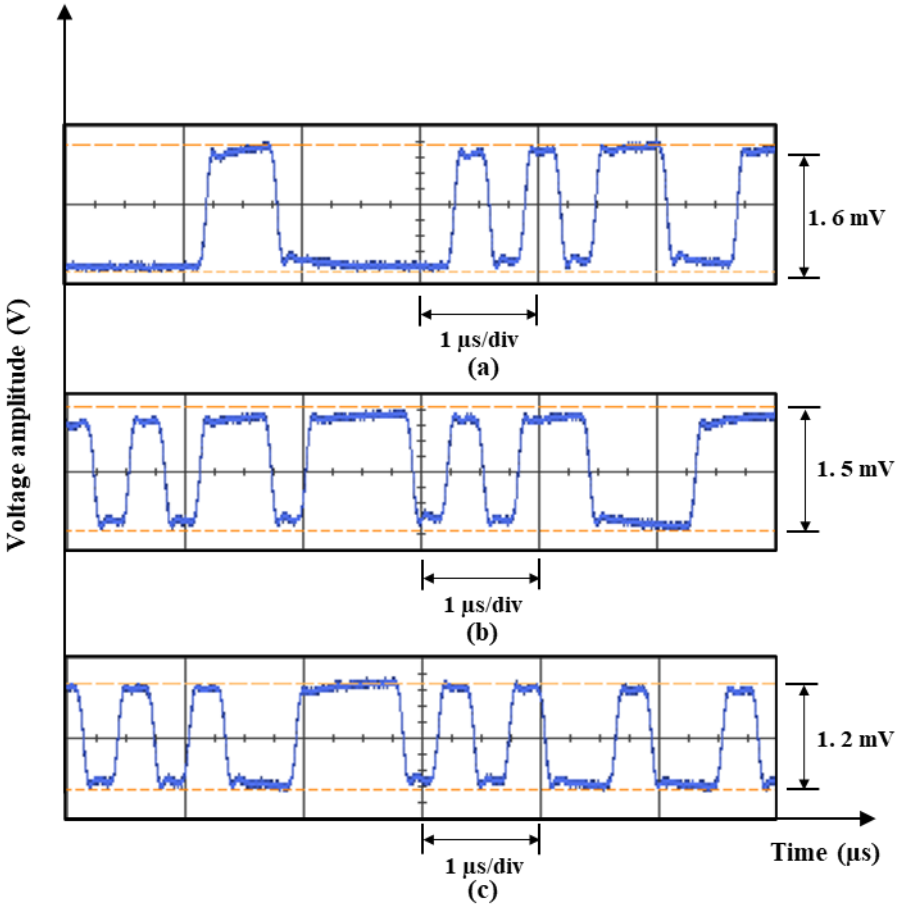

Figure 5.6. The received OOK signals transmitted via USRP and a red laser in a 200 m link for the: (a) light, (b) medium, and (c) dense fog conditions.

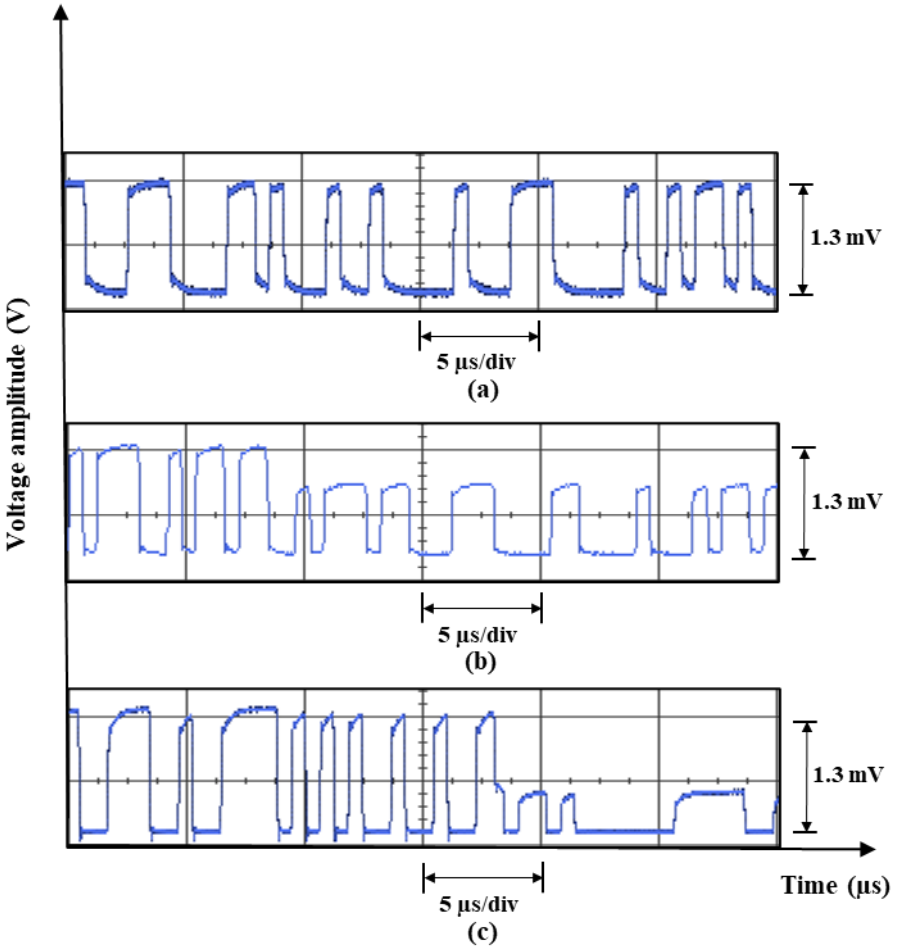

Figure 5.7. The received OOK signals transmitted via USRP and a red laser in a 200 m link under: (a) weak, (b) moderate, and (c) strong turbulence.

5.4 Experimental Implementation of Adaptive Switching in OWC

In the previous section, the implementation of OWC system and demonstration of the experimental testbed is explained and validated that the unique trait of FSO is subject to atmospheric conditions. Due to these conditions, the link availability becomes a major concern in FSO systems [288]. Despite both amplitude (power) and phase fluctuations of the optical wavefront while propagating through the free space channel, fog and turbulence contribute the most to the performance deterioration of the link. Techniques such as hybrid RF/FSO, MIMO FSO with SD, and relayed FSO systems have been presented in the literature [288] to mitigate the impact of the weather on the FSO link performance and to guarantee link availability at all times. Among the proposed methods, it has been demonstrated that SD approaches perform better than a single FSO connection in terms of BER performance to minimize the degradation caused by fog [19]. Different adaptive algorithms to overcome the aforementioned issues are also elaborated in chapter 4. In this section, the assessment and experimental demonstration of the MIMO FSO system using software-defined-based adaptive switching algorithms under different fog conditions will be discussed.

5.4.1 System Configuration and Specification

In the proposed system, two sets of Txs and Rxs are employed for the simultaneous transmission of duplicate data in order to ensure 99.999% link reliability under fog circumstances. Note, the link availability requirements generally depend on FSO deployment i.e., in an enterprise or carrier network. On the Tx side, a switching technique is proposed for enabling the additional Tx depending on the CSI received over the feedback link, i.e., the visibility estimation (VE) laser FSO link. To evaluate the performance of the connection, three different fog circumstances are considered. Figure 5.8 depicts the schematic diagram of the proposed MIMO FSO system with a feedback link. Link-1 is utilized for FSO-based data transfer, whereas Link-2 is based on a fibre link. Note, Link-2 can also be replaced with an FSO link. The Tx comprises of a client computer (i.e., Tx PC) that can be

considered as a data centre for generating random data sequences, which are packetized and sent through a Python script. This script transmits the user datagram protocol packets to the associated python script operating as the server at the Rx PC. The Tx PC is linked to the MC through a LAN/Ethernet cable in order to transform the 1 Gbps electrical signal into the optical domain using the fibre small form pluggable (SFP) transceiver module. The SFP output is connected to an optical coupler, which splits the incoming optical signal into two data streams for transmission via two single-mode fibres (SMFs). The first output of the coupler is applied to the collimator-1 through 3.25 m of SMF (with a core diameter of 9 m and a wavelength of 1550 nm), which partially compensates for the 16.2 ns delay caused by the OS in the second parallel channel. The second output of the coupler is connected to the optical subsystem and collimator 2. The outputs of the collimator are launched into the free space channel. Note that the OS is also connected to the Tx PC in order to switch on Tx-2 depending on the CSI in an adaptive manner. At the Rx, the incoming optical beams are caught by collimators 3 and 4, and their outputs are then combined using a 2x1 optical coupler. The output of the coupler is applied via SFP to the MC module to regenerate the electrical signal. Using the packet error rate tester (PERT) [30], the Rx PC is used to evaluate the link's performance. The VE laser utilized at the Rx is for estimating the fog attenuation/CSI experienced by the link. The measured power of the received VE laser beam $P_{\mathrm{VE-Rx}}$ is treated as the input to the power meter module in GNURadio, whose output is the input to the OS module.

For the switching algorithm in OS, the software-based Schmitt trigger thresholding method is adopted based on the maximum received power of the VE laser. Note, if $P_{\mathrm{VE-Rx}} < P_{\mathrm{VE-Lo}}$ (i.e., the lower limit of the received VE laser power) the Tx-2 is on, whereas for $P_{\mathrm{VE-Rx}} > P_{\mathrm{VE-Up}}$ (i.e., the upper limit of the received VE laser power) the Tx-2 is off and only the Tx-1 is on. Since the Schmitt trigger-based thresholding introduces hysteresis, several threshold levels are used to avoid unnecessary switching when the system is operating close to the threshold level. At the expense of an increase in P_{Tx}, the switching mechanism will ensure that the link's availability is maintained as feasible as possible in all-weather circumstances.

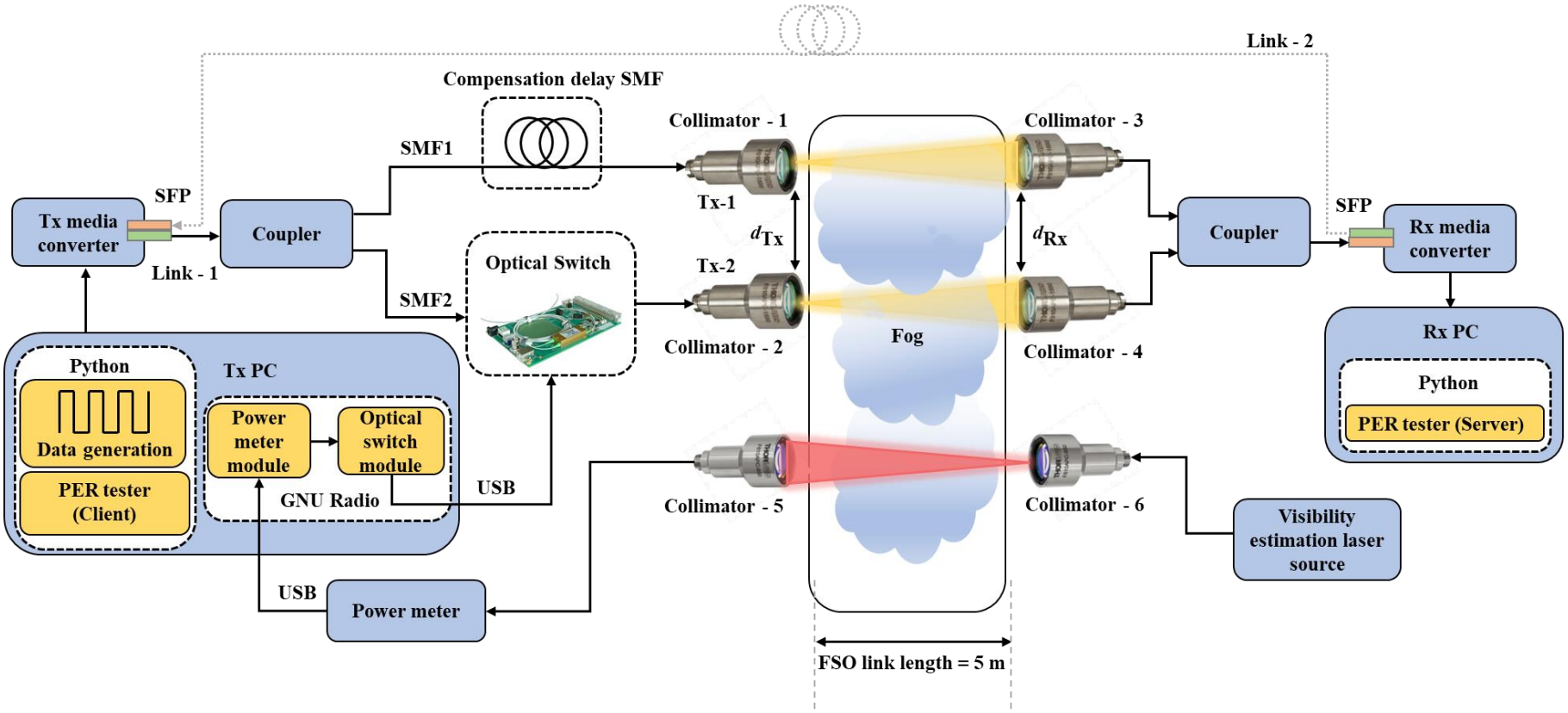

Figure 5.8. The schematic system block diagram of an experimental implementation of MIMO FSO with SDR based adaptive switching method.

Table 5.4. Key system parameters of MIMO FSO with adaptive switching set up.

Parameter	**Value**
Link length l	5 m
Data throughput	1 Gbps
SFP output power P_{Tx}	~4 dBm
Rx collimator diameter D_{Rx}	24 mm
Tx collimator diameter D_{Tx}	24 mm
Tx beam divergence θ	0.016°
Optical wavelength λ	1550 nm
SFP sensitivity	-23 dBm
Compensation delay SMF length	3.24 m
Collimator focal length *fl*	37.13 mm
Tx and Rx separation distance d_{Tx} and d_{Rx}	~8 cm

5.4.2 Switching Algorithm

The SDR-based decision-making blocks for the power meter and the optical switch in GNU Radio are built and implemented in order to accomplish the proposed adaptive switching. GNU Radio can be utilized not only as a real-time simulation environment for DSP applications but also to integrate and operate various hardware devices using the Python programming language. Using the flowchart depicted in Figure 5.9, a simulation to calculate the PER, jitter, and R_b as a function of V for single FSO and MIMO FSO lines with a length of 5 m under various fog situations is conducted. Figure 5.10 depicts the OOT modules used to create the power meter and operating system in the GNU Radio domain. The measured power levels received from the power meter f module are stored using the "File Sink" to determine the visibility, which is then applied to the "QT GUI Number Sink" to display the data in real-time, and the OS. In the OS, $P_{\mathrm{VE-Up}}$and $P_{\mathrm{VE-Lo}}$threshold levels are set to 0.275 and 0.225 mW, respectively, corresponding to the predicted L_{Atm} of 1.6 and 2.5 dB for a single clear FSO connection with $P_{\mathrm{VE-Max}}$ of 0.4 mW and a link margin of 8.6 dB. Before switching to

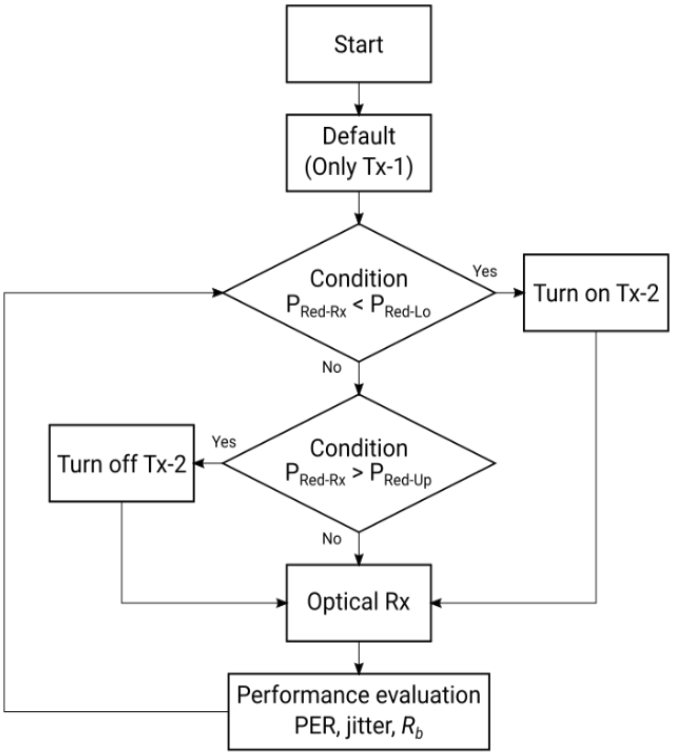

Figure 5.9. System flow chart of experimental GbE MIMO FSO with adaptive switching.

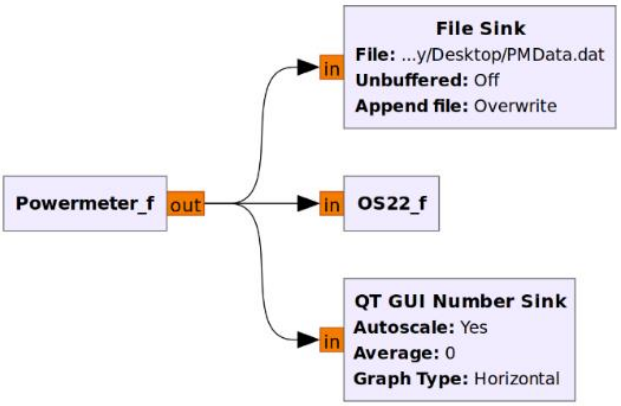

Figure 5.10. The OOT modules for the power meter and optical switch in the GNU Radio platform.

path 2, the link margin before considering L_{Atm} is 6.1 dB. To ensure link reliability, $P_{\mathrm{VE-Up}}$ and $P_{\mathrm{VE-Lo}}$ are set to their respective values. Note that the OS is controlled by the OS22 module.

Using the Schmitt trigger thresholding method and the given threshold values, the OS22 block determines the OS states. The performance of the proposed system is analyzed using a python tool based on iperf, as shown in Figure 5.11(a) and, (b), iperf is an open-source and widely used network testing tool for (*i*) measuring the maximum achievable R_{b}; (*ii*) testing the system performance in terms of PER and jitter; and (*iii*) measuring the end-to-end system throughput in one or both

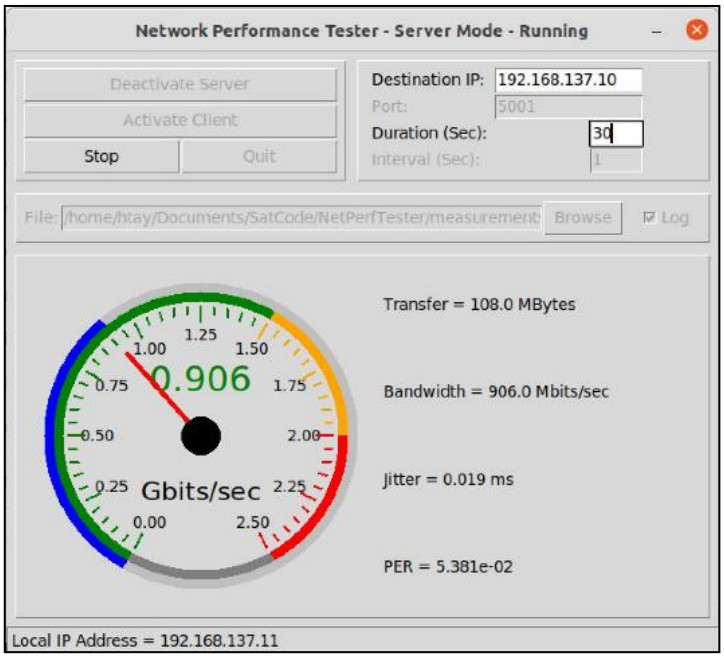

(a)

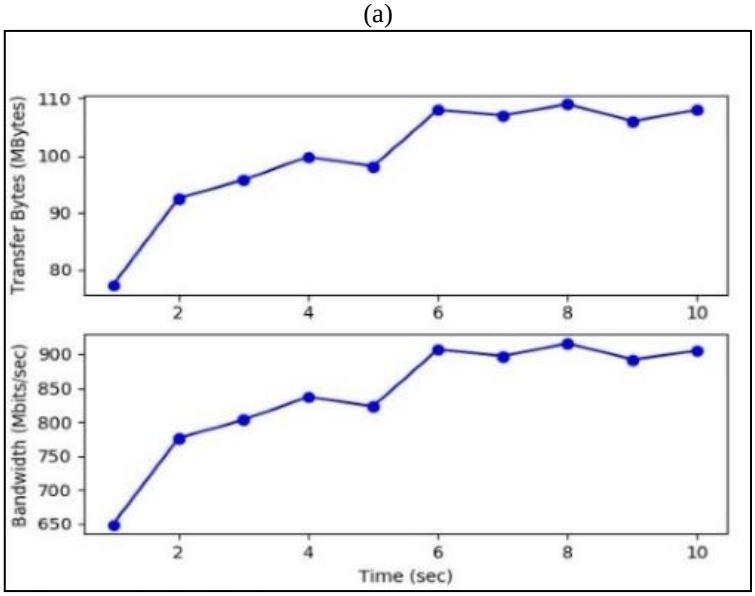

(b)

Figure 5.11. Screenshots of the developed python code for: (a) network performance tester for measuring the performance of the Ethernet FSO link, and (b) received data and bandwidth.

directions. For a back-to-back (B2B) link and under three different fog density conditions we have measured the key parameters including $R_{(b\text{-}Max)}$, jitter, and PER for 30 seconds each.

5.4.3 Experimental Setup

Figure 5.12 depicts the experimental testbed for the 1 Gbps MIMO FSO system with GNU Radio-based adaptive switching. Table 5.5 shows the key system specifications used in the experimental setup. As shown in Figure 5.12 (a), a PC is linked to the (*i*) power meter at the Tx; (*ii*) OS via a USB cable; and (*iii*) SFP, which is contained in the MC module, via an Ethernet cable. The coupler receives a 1 Gbps NRZ-OOK data from the output of the SFP through an SMF, with its outputs

connected to the compensation delay line and the OS supplying the Tx-1 and Tx-2 collimators. The purpose of the power meter is to estimate the *V* of the channel. The Rx in Figure 5.12(b) consists of a visibility estimation laser source, collimators, SMF cables, and a 2×1 optical coupler. The output of the coupler is applied to the SFP MC module, which is subsequently connected to the Rx PC. The generated optical signals are transmitted through a 40 × 40 × 500 cm^3 indoor atmospheric chamber, see Figure 5.13.

Table 5.5. Component specifications for the experimental demonstration of MIMO FSO with software defined adaptive switching.

Device	**Specification**
Media converter TP-Link MC220L)	IEEE 802.3ab, IEEE 802.3z, IEEE 802.3x
Small form factor pluggable module (SFP1000ZXST)	IEEE 802.3z 1000BASE -ZX Max data rate:1.25 Gbps Max range: 80 km SMF
Optical switch (OSW12-1310-E)	λ: 1280 -1625 nm Switching rate: <1 ms SMF 75 dB (Typical) Insertion loss: 0.7 dB
Power meter (PM100D - S120C)	λ: 400-1100 nm
Collimators 1-4 (F810APC – 1550)	Effective *fi*: 37.13 mm λ: 1550 nm
Collimators 5 and 6 (F810APC – 842)	Effective *fi*: 36.18 mm λ: 650-1050 nm
Coupler(s) (SC11C-002-0334 and 002-0354)	λ: 1310 -1550 nm Split ratio: 50:50 Insertion loss: 3.5 dB SMF
(Red) laser source (MCLS1-CUSTOM)	λ: 638 nm Laser class: 3B
SMF delay line	Core diameter: 9 μm

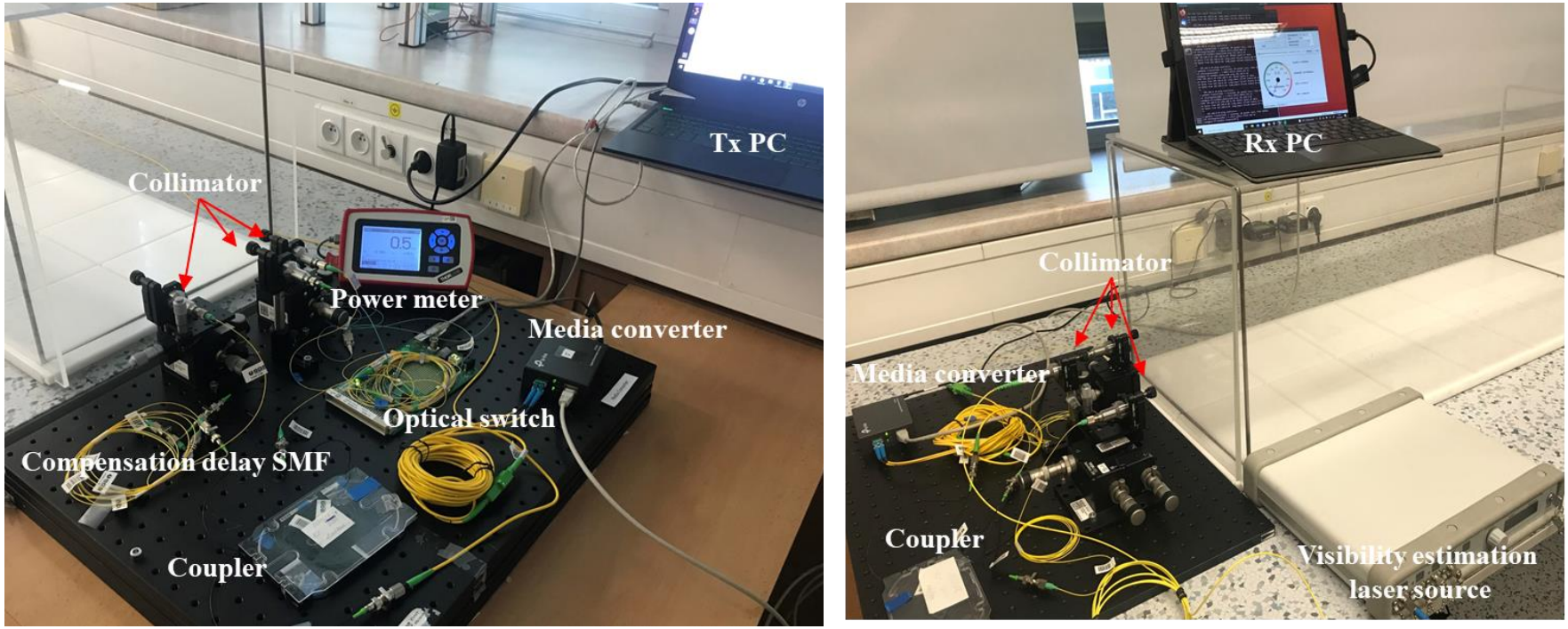

(a) (b)

Figure 5.12. Experimental setup of: (a) Tx with PC connected to MC to transmit data and power meter to receive the VE laser and estimate the visibility. Optical switch connected to the PC for adaptive switching according to received CSI from the power meter. (b) Rx setup with VE laser, two collimators for received signals, coupler to combine two received signals, and MC connected to the PC.

Figure 5.13. Experimental setup of Channel setup when fog is injected.

5.4.4 Link Power Budget

The link budget is one of the initial elements in the designing of the FSO system and serves numerous crucial purposes, including [289]:

- Predicting performance prior to establishing the connection.
- Determining whether there is enough optical power to traverse the link, often for a predefined worst-case scenario.
- Assisting with decision-making, trade-offs, and evaluations, such as the telescope aperture diameter or transmit laser power requirements necessary to sustain a specific BER.

To predict the system's performance, the link budget must include the characteristics of each component and assembly.

The link budget is a straightforward addition and subtraction of gains and losses generated from a given set of system characteristics and their tolerances (when values are converted to decibels). The link budget of an optical system consists of gains from antennas (telescopes) and the laser Tx, losses in propagation along the transmitting optical channel, losses across space or atmosphere, and losses along the receiving optical train to the PD. Typically, considering that there are no losses due to components, as a function of the transmitted power and losses, the received power is given as:

$$P_{\mathrm{Rx-Total}} = P_{\mathrm{Tx}} - L_{\mathrm{Geo}} - L_{\mathrm{Atm}} - L_{\mathrm{PE}}\,, \tag{5.1}$$

In this case, following the proposed experimental setup in Figure.5.8, the received power including all the losses experienced in the system can be represented and defined as:

$$\begin{aligned} P_{\mathrm{Rx-Total}} &= P_{\mathrm{Tx}} - L_{\mathrm{LC-\frac{FC}{APC}}} - 2L_{\mathrm{Cou}} \\ &+ 10\log\left(10^{\frac{-L_{\mathrm{Delay}}}{10}} + 10^{\frac{-L_{\mathrm{OS}}}{10}}\right) - L_{\mathrm{Geo}} - L_{\mathrm{PE}}\,, \end{aligned} \tag{5.2}$$

where $L_{\mathrm{LC-FC/APC}}$ and L_{Cou} are the LC-FC/APC connector loss and the coupler loss respectively. L_{Geo} and L_{PE} describe the geometric loss and the loss due to the pointing error. L_{Geo} and L_{PE} are neglected due to the free

space link length of 5 m and considering the specifications of the optics utilized in the configuration. L_{OS} and L_{Delay} are the losses at the optical switch line and delay line which can be expressed as:

$$L_{\mathrm{Delay}} = 5L_{\mathrm{FC/APC}} + L_{\mathrm{Col-1}} + L_{\mathrm{Col-3}}, \tag{5.3}$$

$$L_{\mathrm{OS}} = 2L_{\mathrm{FC/APC}} + L_{\mathrm{Col-2}} + L_{\mathrm{Col-4}}, \tag{5.4}$$

where $L_{\mathrm{FC/APC}}$ denotes the FC/APC connector loss. The collimator losses are $L_{\mathrm{Col-1}}, L_{\mathrm{Col-2}}, L_{\mathrm{Col-3}}$, and $L_{\mathrm{Col-4}}$. The link budget analysis for both paths is shown in Table 4.6. The link margin is assumed to be 10 dB to account for any additional losses, such as increased component losses and the received power fluctuation between a maximum of -4.6 dBm and a minimum of -12.9 dBm caused by the coherent combination of the two optical waves and random phase shifts in between.

Table 5.6. Link budget analysis of a combined link.

Parameter	**Value**	
	Path 1 (OS path)	Path 2 (Compensation delay path)
Transmit power P_{Tx}	0.25 dBm	0.25 dBm
Losses		
$L_{\mathrm{FC/APC}}$	0.35 dB	0.88 dB
$L_{\mathrm{LC-FC/APC}}$	0.15 dB	0.15 dB
L_{Cou}	3.75 dB	3.75 dB
$L_{\mathrm{Col-1}}, L_{\mathrm{Col-3}}, L_{\mathrm{Col-4}}$	0.5 dB	1.8 dB
$L_{\mathrm{Col-2}}$	3.6 dB	2.6 dB
Receiver sensitivity	-23 dBm	
Total average received power $P_{\mathrm{Rx-Avg}}$	-5.7 dBm	
Total minimum received power $P_{\mathrm{Rx-Min}}$	-12.9 dBm	
Link margin	10.1 dB	

5.4.5 Recorded Data

This section discusses the performance of the proposed MIMO FSO link with the adaptive switching algorithm implemented in the GNU Radio platform in the experimental domain. The adaptive switching algorithm is implemented using the OOT blocks described in 5.4.2. Before evaluating the system performance in atmospheric conditions, it is a good practice to test the system in back-to-back and clear conditions in order to determine the tolerance of the system. A series of experiments and measurements in clear and foggy channel conditions for the three scenarios of B2B, SISO, and MIMO FSO are carried out. Note that, V of 358 m is set for the clear channel and only the miscellaneous loss L_{misc} is considered as L_{Geo} is negligible. Figure 5.14 illustrates PER, jitter, and R_b as a function of V for 5 m long SISO and MIMO FSO links. The three distinctive visibility ranges of $38 < V_1 < 45$ m, $11 < V_2 < 38$ m,

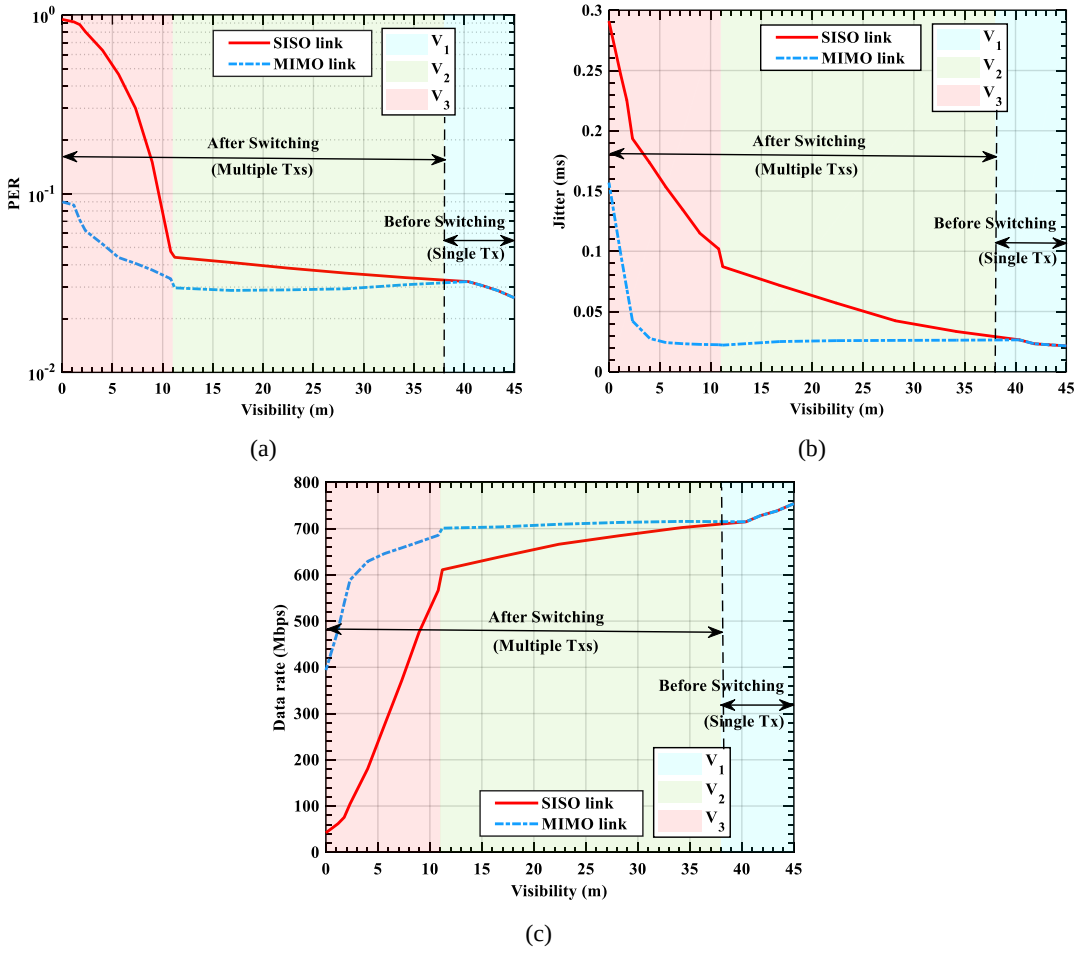

Figure 5.14. Visibility vs.: (a) PER, (b) Jitter, and (c) data rate for 5 m SISO and MIMO FSO links under fog conditions.

and 0 < V_3 <11 m are highlighted in this experiment. Figure 5.14(a) demonstrates that MIMO outperforms SISO in terms of PER for V_1 and V_2. The PER of the SISO starts to increase at V < 38 m, whereas for the MIMO link, the PER of 2×10^{-2} remains constant until V of 11 m, which is due to turning on the additional Tx (i.e., the Tx-2). Beyond V < 11 m, the PER increases for both cases with MIMO increasing at a significantly slower rate than SISO. It is observed that for V < 5 m, the PER for SISO is 0.55, indicating link failure, whereas the MIMO connection works exceptionally well. Similar patterns may be seen for the jitter and R_b plots as illustrated in Figures 5.14(b) and (c). To observe the same system performance in terms of L_{Atm} vs. PER, jitter, and bandwidth, additional plots are also provided, see Figure.

5.15.

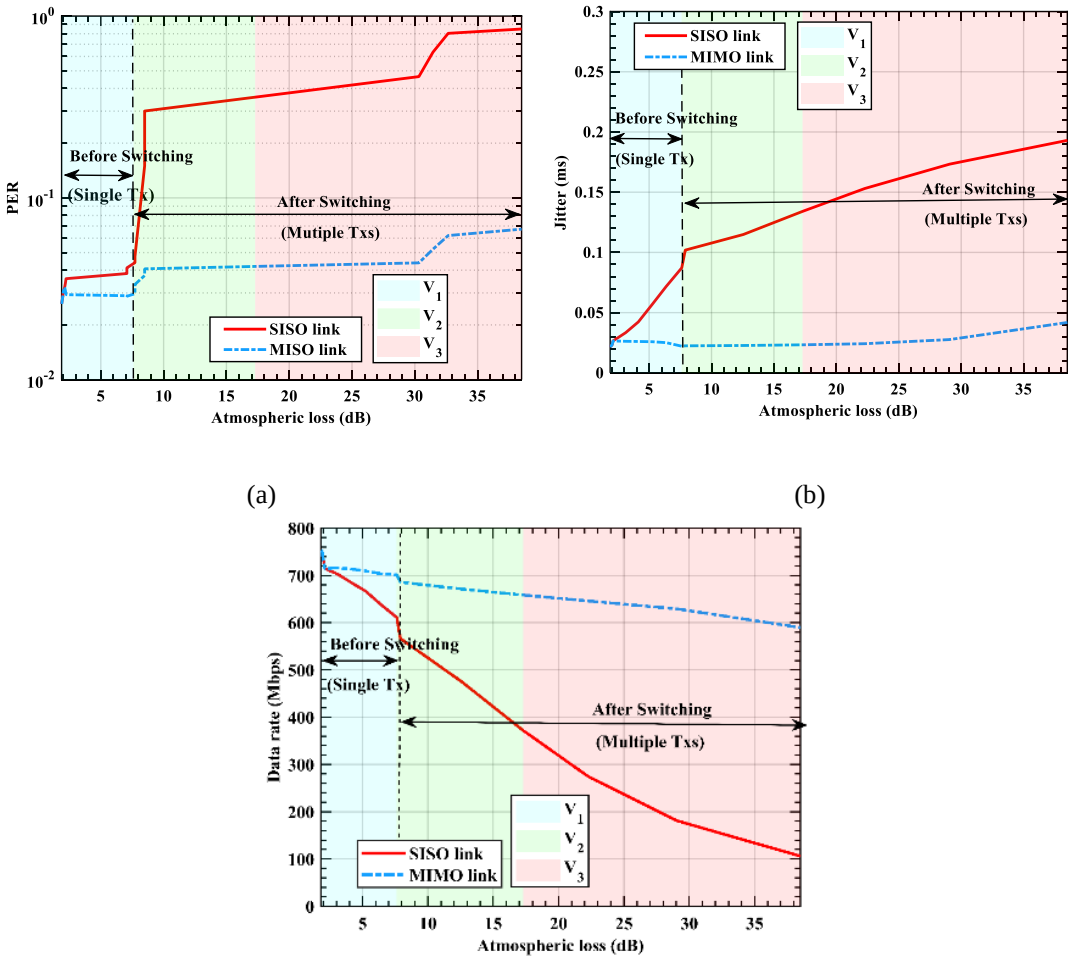

Figure 5.15. Atmospheric loss vs.: (a) PER, (b) Jitter, and (c) data rate for 5 m SISO and MIMO FSO links under fog conditions.

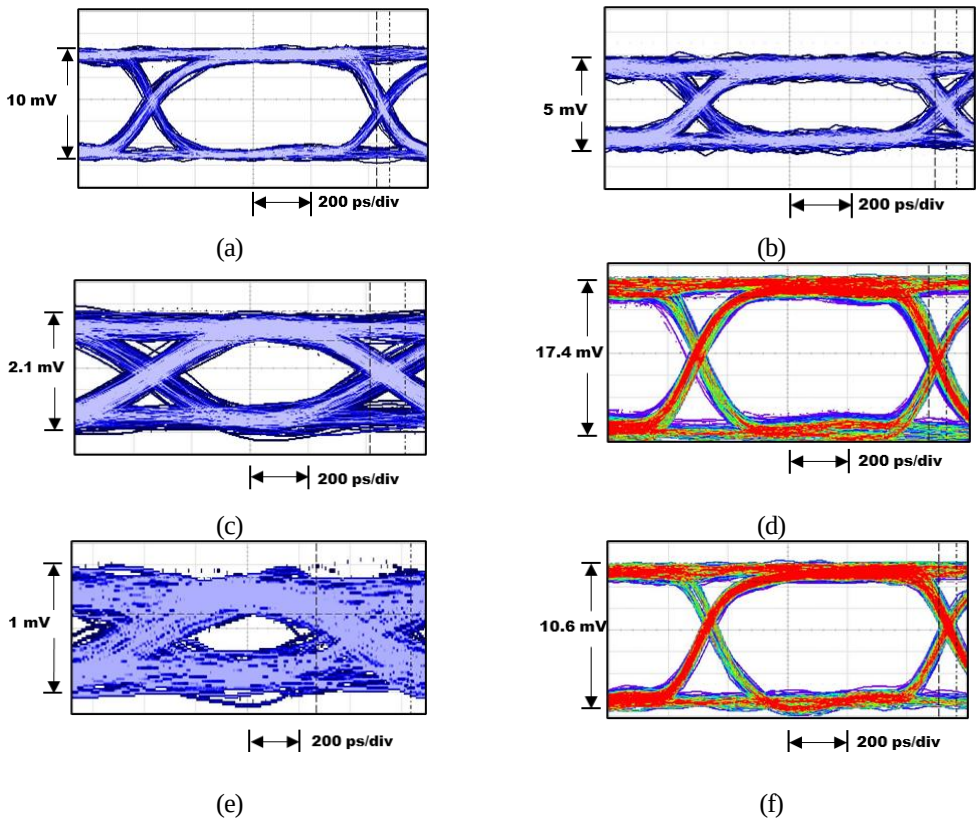

Figure 5.16. Eye diagrams of the single FSO link: (a) under clear channel, (b) V_1, (c) V_2, and (e) V_3; MIMO link for: (d) V_2, and (f) V_3.

Moreover, the measured eye diagrams for SISO and MIMO links for a range of V (i.e., fog conditions) can be seen in Figure 5.16. The eye diagrams for SISO under clear and foggy channels (i.e., 38 m < V_1 < 45 m) respectively, where the system is operating in the default state (i.e., using only the Tx-1) can be seen in Figure 5.16(a) and (b). As expected, the best eye diagram with a wide eye opening is observed under the clear channel. Figures 5.16(c) and (e) show the eye diagrams for 11 m < V_2 < 38 m and 0 < V_3 < 11 m, respectively for the SISO FSO link. Figures 5.16(d) and (f) illustrate the eye diagrams for the MIMO system showing the effectiveness of adopting multiple Txs. Note that, since the link margin of ~ 10 dB is sufficient to compensate for the fog induced attenuation For V < 38 m, MIMO is at the default state with noticeably reduced R_b of 643 Mbps and the jitter of 4.489×10^{-5} for the same PER of 2.3×10^{-2}. For 11 m < V_2 < 38 m the measured $R_{b-\max}$ is 630 Mbps for a PER of 4.06×10^{-2}. At this stage with $P_{\mathrm{VE-Rx}} < P_{\mathrm{VE-Lo}}$, the Tx-2 is switched on, i.e., the link is MIMO. Next, for 0 m < V_3 < 11 m, the PER, jitter, and $R_{b-\max}$ of

Table 5.7. Statistics of the system performance metrics for the B2B, clear and increasing fog density conditions of V_1, V_2 and, V_3.

Channel condition	**Parameter**	**Standard deviation**	**Mean**	**Maximum**	**Minimum**
B2B	PER	1.9×10^{-2}	2.1×10^{-2}	5.7×10^{-2}	2.2×10^{-6}
	R_b (Mbps)	78	846	929	612
	Jitter (ms)	8.6×10^{-6}	2.3×10^{-5}	3.5×10^{-5}	2×10^{-6}
Clear	PER	1.4×10^{-2}	2.9×10^{-2}	5.8×10^{-2}	1.1×10^{-3}
	R_b (Mbps)	81.3	703.8	845	543
	Jitter (ms)	4.4×10^{-6}	2.3×10^{-5}	3.7×10^{-5}	1×10^{-5}
V_1 $V \in$ (38, 45) m	PER	2.3×10^{-2}	3.3×10^{-2}	9.5×10^{-2}	1.7×10^{-3}
	R_b (Mbps)	126	643	803	426
	Jitter (ms)	1.1×10^{-4}	4.5×10^{-5}	2.2×10^{-4}	1.8×10^{-5}
V_2 $V \in$ (11, 38) m	PER	2.3×10^{-2}	4.1×10^{-2}	11.5×10^{-2}	4.6×10^{-3}
	R_b (Mbps)	118	630	802	404
	Jitter (ms)	1.8×10^{-4}	6.1×10^{-5}	4.2×10^{-4}	1.9×10^{-5}
V_3 $V <$ 11 m	PER	7.2×10^{-2}	8.4×10^{-2}	29.7×10^{-2}	8.3×10^{-3}
	R_b (Mbps)	117	620.5	791	315
	Jitter (ms)	5.5×10^{-4}	8.5×10^{-5}	8.6×10^{-4}	2×10^{-5}

8.42×10^{-2}, 8.54×10^{-5} ms, and 620.5 Mbps are measured respectively compared to SISO with 0.8, 2×10^{-4}ms, and 84.9 Mbps.

In addition, a series of tests and measurements are conducted for the B2B link, clear and foggy channels using an iperf-based FSO performance so performance tester, the results of which are shown in Table 5.7. The switching mechanism's behaviour is observed to be dependent on atmospheric attenuation, and hence the link length, rather than *V*. Finally, for practical applications, the longer link lengths of 500 m, 1, and 2 km are evaluated with the same atmospheric losses and theoretically determined that *V* of 1, 2, and 4 km are the point of switching, respectively. Furthermore, as compared to previous work [19] and [290], a similar improvement in system performance under fog situations is observed.

5.5 Summary

In this chapter, the real time implementation of software defined optical communications systems and system performance evaluation were discussed. The proposed switching algorithm was also implemented employing off the shelf components. By using the software defined based adaptive switching method, the FSO system was protected against the severe fog regime, supporting the flexible configuration and providing the easily implementable design. It was also discussed that the software defined FSO system can be utilized to evaluate the system performance in real time for very long-distance communications without the need of physical space for the required distance. Under fog conditions the additional FSO link was turned on and the link performance was investigated based on the real time data from the power meter. Link assessment was performed to investigate the effect of FSO data rate, PER and jitter on the link availability. It was observed that the proposed MIMO FSO with adaptive switching in heavy fog condition can operate much more effectively with nearly similar performance as SISO under a clear channel. In conclusion, the following can be stated: (*i*) MIMO with the synchronised parallel transmission can successfully minimise the fog generated losses while a short delay (ns) can lead an oscillation in amplitude when two parallel signals are combined; (*ii*) the randomness of the fog attenuation can create amplitude variations in the results; and (*iii*) implementing adaptive algorithms in GNU Radio allows a great degree of flexibility in design and implementation of the SDR based systems.

Chapter 6. Conclusions and Future Work

6.1 Conclusions

This thesis has provided an overview of the design, optimization, and evaluation of the SDR-based MIMO FSO system with adaptive switching by utilizing an SDR-based ecosystem called GNU Radio. The proposed system is robust, and reconfigurable and takes advantage of an additional FSO backup link to maintain high-speed transmission in cases of harsh weather conditions. Additionally, an adaptive method to reduce the effects of severe atmospheric conditions such as fog and turbulence losses has been proposed. The introduction to FSO was followed by a discussion of the impact of channels such as fog and turbulence on the performance and link availability. The literature on the mitigation techniques to combat the effect of atmospheric conditions was presented along with the combining methods of MIMO systems. Further introduced were the basics of software defined systems and the potential area of applications along with the off-the-shelf commercially available frontends to provide reconfigurability and cost-efficiency. Additionally, a very brief introduction of SDN was also discussed. Moreover, software defined optical communications systems and various adaptive systems, such as adaptive equalization, adaptive modulation, and adaptive power allocation were introduced and the demonstration and implementation of MIMO FSO system with adaptive switching algorithm based on scintillation index coefficient and atmospheric loss experience in the channel in SDR ecosystem is later presented for a real-time emulation. BERT is utilized to perform a bit-by-bit comparison with the GNURadio signal processing block. The system performance of SISO, MIMO, and the proposed system in terms of BER in 100, 200, and 300 m links were evaluated, assessed, and compared. It was shown that the switching mechanism was found to effectively mitigate fog and turbulence-induced attenuation. The MIMO FSO with adaptive switching technique has been shown to operate effectively in dense

fog, whereas in moderately turbulent conditions it experienced a peak turnover degradation after switching in 200 and 300 m. According to the results obtained, the switching mechanism, i.e., activating additional Txs, can only mitigate turbulence up to a certain level. In order to perform the adaptive switching technique a real-time decision-making feedback link using the estimated BER and the thresholding methods to support the decision-making process was also proposed.

The experimental investigations were later carried out to validate the proposed concept of implementing OWC systems in an SDR environment to overcome the hardware limitation, provide flexibility, and as a proof of concept. The OOT modules for the OOK signal generator, FSO channel, fog, turbulence, geometric loss, BERT, etc., were all built from scratch in GNURadio and experimentally implemented using optical frontends such as LD and PD. The system was evaluated for a 199.5 m linkspan in the GNURadio domain and a 50 cm in a real experimental setup under different atmospheric conditions. The operation speed (bandwidth) in this case since the signal generation was mainly from the PC (running GNURadio) was limited which mainly depends on the type of components utilized in the experimental setup. In addition, it was discussed that the software defined FSO system can be used to evaluate the system's performance in real-time for very long-distance communications without the need for the required amount of physical space.

Furthermore, a practical MIMO FSO with software-defined-based system was proposed and evaluated. The proposed switching algorithm was implemented using commercially available components. Using a software defined adaptive switching method, the FSO system was protected against the severe fog regime, allowing for a flexible configuration and a design that is simple to implement. Under conditions of fog, the additional FSO link was activated, and the link performance was evaluated using real-time data from the power meter. Link evaluation was conducted to determine the influence of FSO data rate, PER, and jitter on link availability. Observations indicated that the proposed MIMO FSO with adaptive switching can operate significantly more effectively with nearly comparable performance to SISO when the

channel is clear. The proposed system offered up to 1 Gbps. As expected, the data rate of the system decreased while maintaining the link availability to provide the data transmission with 99.999% availability with a PER and a data rate of 7.2×10^{-2} and ~120 Mbps, respectively, under extremely harsh fog conditions with V of < 11 m.

6.2 Future Works

Although the objectives outlined in the first chapter of this dissertation have been met, the work was never intended to be self-contained and rigorous enough to cover all FSO aspects using SDR. Since the amount of effort and time required is beyond the scope of this thesis, the author will now suggest additional research that can be conducted to extend the work reported here.

Adaptive algorithms – As a logical progression of the work presented here, the investigation and experimental demonstration of adaptive algorithms such as the equalization and modulation using SDR in Radio over FSO (RoFSO) systems could prove extremely useful. This may provide interesting insights into the integration of SDR and FSO with radio over fibre systems. The experimental investigation can further demonstrate the real application of SDR-RoFSO in the last-mile access networks to offer increased transmission capacity, and link availability.

System performance analysis – It would be an interesting work to evaluate the proposed system theoretically in GNURadio for a real-time emulation of pointing errors and other atmospheric conditions. Th experimental evaluation can be done and mitigation of the pointing error concept can be carried out by using a different lens such as ball lens to collimate the beam instead of a solid lens.

Combining methods – The thesis mainly focuses on optical combining with SD. Adopting other combining methods for different applications such as spatial multiplexing, EGC, SelC

and MLC, etc., could provide increased data rates and improved performance. Theoretical comparison and simulation could be investigated followed by the experimental demonstration.

Different configuration - An alternative configuration could be considered using the proposed experimental implemented system by changing the direction of Txs and Rxs to change the channel conditions. An investigation of improved system performance could be carried out in this configuration.

Data rate – The maximum achievable data rate of 1 Gbps, demonstrated using off-the-shelf components and providing the flexibility of the system using a software- defined environment in this thesis could be improved by using components that support higher speed to demonstrate the same concept. Using programmable evaluation boards with high-speed optical frontends can perform adaptive algorithms and achieve high-speed transmission.

Lower cost - Since integrating SDR to provide flexible FSO systems supports cost efficiency, the feasibility of integrating 850 nm VCSELs needs investigating to reduce costs compared with 1550 nm-based systems, which are widely investigated and reported.

ML and ANN in SDR - The evaluation of FSO in a real channel condition could also be carried out using only the PC as discussed in Section 5.3.2 but with a higher spec PC to avoid the limitation of bandwidth. In this way, the FSO system transmitting the optical beam using different and advanced modulations, including ML and ANN techniques on-the-fly could be investigated.

References

[1] W. Popoola, "Subcarrier intensity modulated free-space optical communication systems," Doctoral, School of Computing, Engineering and Information Sciences, Northumbria University, 2009.

[2] A. G. Bell, "On the production and reproduction of sound by light," *American Journal of Science,* vol. s3-20, pp. 305 - 324.

[3] X. Tang, "Polarisation shift keying modulated free-space optical communication systems," 2012.

[4] F. E. Goodwin, "A review of operational laser communication systems," *Proceedings of the IEEE,* vol. 58, no. 10, pp. 1746-1752, 1970, doi: 10.1109/PROC.1970.7998.

[5] A. K. M. Arockia Bazil Raj, "Historical perspective of free space optical communications: from the early dates to today's developments," *IET Communications,* vol. 13, no. 16, 2019, doi: 10.1049/iet-com.2019.0051.

[6] S. Rajbhandari, "Application of wavelets and artificial neural network for Indoor optical wireless communication systems," Doctoral, School of Computing, Engineering and Information Sciences, Northumbria University, 2009.

[7] L. B. Stotts, *Free space optical systems engineering: Design and analysis*. Wiley, 2017.

[8] S. V. Kartalopoulos, *Free space optical networks for ultra-broad band services*. Wiley, 2011.

[9] H. A. Willebrand and B. S. Ghuman, "Free space optics: Enabling optical connectivity in today's networks," 2001.

[10] M. Toyoshima *et al.*, "Ground-to-satellite laser communication experiments," *IEEE Aerospace and Electronic Systems Magazine,* vol. 23, 2008.

[11] H. Hemmati, *Deep space optical communications*. Wiley, 2006.

[12] A. Jooshesh, T. A. Gulliver, and S. Uysal, "Space to ground optical power transmission," in *2012 Seventh International Conference on Broadband, Wireless Computing, Communication and Applications,* 12-14 Nov. 2012 2012, pp. 302-307, doi: 10.1109/BWCCA.2012.57.

[13] Z. Ghassemlooy, W. Popoola, and S. Rajbhandari, *Optical wireless communications: system and channel modelling with MATLAB,* . New York, NY, USA: Taylor & Francis, 2012.

[14] I. Kim, B. McArthur, and E. Korevaar, "Comparison of laser beam propagation at 785 nm and 1550 nm in fog and haze for optical wireless communications," *Proc. SPIE,* vol. 4214, 02/01 2001, doi: 10.1117/12.417512.

[15] M. Bettayeb and S. F. A. Shah, "State of the art ultra-wideband technology for communication systems: a review," in *10th IEEE International Conference on Electronics, Circuits and Systems, 2003. ICECS 2003. Proceedings of the 2003*, 14-17 Dec. 2003 2003, vol. 3, pp. 1276-1279 Vol.3, doi: 10.1109/ICECS.2003.1301747.

[16] A. U. Mac Rae, J. N. Pelton, and R. De Paula, "Global satellite communications technology and systems," *Space Communications,* vol. 16, pp. 51-54, 2000.

[17] J. Machado Fernández, "Software defined radio: Basic principles and applications," *Revista Facultad de Ingenier'ia,* vol. 24, pp. 79-96, 01/01 2015, doi: 10.19053/01211129.3160.

[18] W. H. Tuttlebee, *Software defined radio: enabling technologies*. John Wiley & Sons, 2003.

[19] Z. Htay, Z. Ghassemlooy, M. M. Abadi, A. Burton, N. Mohan, and S. Zvanovec, "Performance analysis and software defined implementation of real-time MIMO FSO With adaptive switching in GNURadio platform," *IEEE Access,* vol. 9, pp. 92168-92177, 2021, doi: 10.1109/ACCESS.2021.3092968.

[20] W. Hussain, H. F. Ugurdag, and M. Uysal, *Software defined VLC System: Implementation and Performance Evaluation*. 2015.

[21] J. Nappier, D. J. Zeleznikar, A. C. Wroblewski, R. Tokars, B. L. Schoenholz, and N. C. Lantz, "A COTS RF/Optical software defined radio for the integrated radio and optical communications test bed," 2016.

[22] P. Deng and M. Kavehrad, "Adaptive real-time software defined MIMO visible light communications using spatial multiplexing and spatial diversity," in *2016 IEEE International Conference on Wireless for Space and Extreme Environments (WiSEE)*, 26-28 Sept. 2016 2016, pp. 111-116, doi: 10.1109/WiSEE.2016.7877314.

[23] P. Chen and Y. Rong, "A Software-defined optical wireless OFDM system for underwater video communication," in *OCEANS 2022, Hampton Roads*, 17-20 Oct. 2022 2022, pp. 1-5, doi: 10.1109/OCEANS47191.2022.9977077.

[24] A. Gruber, S. S. Muhammad, and E. Leitgeb, "A software defined free space optics (SD-FSO) platform based on an analog optical frontend," in *Proceedings of the 11th International Conference on Telecommunications*, 15-17 June 2011 2011, pp. 363-366.

[25] F. Peng, S. Zhang, S. Cao, and S. Xu, "A prototype performance analysis for V2V communications using USRP-based software defined radio platform," in *2018 IEEE Global Conference on Signal and Information Processing (GlobalSIP)*, 26-29 Nov. 2018 2018, pp. 1218-1222, doi: 10.1109/GlobalSIP.2018.8646490.

[26] L. Wansink, "Global fixed broadband - Key statistics and insights," Budde Comm, 2019.

[27] P. Taylor, "Quarterly growth of FTTH broadband subscribers in the 4th quarter 2020, by leading fibre broadband markets," Statista, 2022.

[28] C.-H. Cheng, "Signal processing for optical communication," *Signal Processing Magazine, IEEE*, vol. 23, pp. 88-96, 02/01 2006, doi: 10.1109/MSP.2006.1593341.

[29] C. C. Davis, I. I. Smolyaninov, and S. D. Milner, "Flexible optical wireless links and networks," *IEEE Communications Magazine*, vol. 41, no. 3, pp. 51-57, 2003, doi: 10.1109/MCOM.2003.1186545.

[30] A. Nordbotten, "LMDS systems and their application," *IEEE Communications Magazine*, vol. 38, no. 6, pp. 150-154, 2000, doi: 10.1109/35.846087.

[31] R. C. Qiu, H. Liu, and X. Shen, "Ultra-wideband for multiple access communications," *IEEE Communications Magazine*, vol. 43, no. 2, pp. 80-87, 2005, doi: 10.1109/MCOM.2005.1391505.

[32] D. Kedar and S. Arnon, "Optical wireless communication through fog in the presence of pointing errors," *Appl. Opt.*, vol. 42, no. 24, pp. 4946-4954, 2003/08/20 2003, doi: 10.1364/AO.42.004946.

[33] T. Kamalakis and T. Sphicopoulos, "Estimation of power scintillation probability density function in free space optical links using multi-canonical Monte Carlo sampling," 2010.

[34] D. Kedar and S. Arnon, "Urban optical wireless communication networks: the main challenges and possible solutions," *IEEE Communications Magazine*, vol. 42, no. 5, pp. S2-S7, 2004, doi: 10.1109/MCOM.2004.1299334.

[35] Z. Xiaoming and J. M. Kahn, "Free-space optical communication through atmospheric turbulence channels," *IEEE Transactions on Communications*, vol. 50, no. 8, pp. 1293-1300, 2002, doi: 10.1109/TCOMM.2002.800829.

[36] R. G. W. Brown, "Optical channels. fibers, clouds, water and the atmosphere," *Journal of Modern Optics*, vol. 36, no. 4, pp. 552-552, 1989/04/01 1989, doi: 10.1080/09500348914550651.

[37] S. H. Bloom, E. J. Korevaar, J. J. Schuster, and H. A. Willebrand, "Understanding the performance of free-space optics [Invited]," *Journal of Optical Networking*, vol. 2, pp. 178-200, 2003.

[38] H. Izadpanah, T. ElBatt, V. Kukshya, F. Dolezal, and B. K. Ryu, "High-availability free space optical and RF hybrid wireless networks," *IEEE Wireless Communications*, vol. 10, no. 2, pp. 45-53, 2003, doi: 10.1109/MWC.2003.1196402.

[39] D.-N. Nguyen, J. Bohata, S. Zvanovec, L. Nguyen, and Z. Ghassemlooy, "Turbulence mitigation in a 28 GHz radio-over-free-space optics link using an integrated Mach–Zehnder interferometer and a diversity combining receiver," *IET Communications*, vol. 14, no. 19, pp. 3373-3379, 2020, doi: https://doi.org/10.1049/iet-com.2019.1166.

[40] Z. Ahmad, J. Mirza, A. Jeza Aljohani, A. Salman, and S. Ghafoor, "A Mach–Zehnder modulator based novel regenerator for employment in relays used in free space optical communication," *Transactions on Emerging Telecommunications Technologies*, vol. 33, no. 4, p. e4405, 2022, doi: https://doi.org/10.1002/ett.4405.

[41] C. H. Yeh, Y. R. Xie, C. M. Luo, and C. W. Chow, "Integration of FSO traffic in ring-topology bidirectional fiber access network with fault protection," *IEEE Communications Letters*, vol. 24, no. 3, pp. 589-592, 2020, doi: 10.1109/LCOMM.2019.2960221.

[42] Z. Htay, N. Mohan, M. M. Abadi, Z. Ghassemlooy, A. Burton, and S. Zvanovec, "Implementation and evaluation of a 10 Gbps real-time FSO link," in *2020 3rd West Asian Symposium on Optical and Millimeter-wave Wireless Communication (WASOWC)*, 24-25 Nov. 2020 2020, pp. 1-7, doi: 10.1109/WASOWC49739.2020.9410045.

[43] M. A. Khalighi and M. Uysal, "Survey on free space optical communication: A communication theory perspective," *IEEE Communications Surveys & Tutorials*, vol. 16, no. 4, pp. 2231-2258, 2014, doi: 10.1109/COMST.2014.2329501.

[44] M. Uysal and H. Nouri, "Optical wireless communications — An emerging technology," in *2014 16th International Conference on Transparent Optical Networks (ICTON)*, 6-10 July 2014 2014, pp. 1-7, doi: 10.1109/ICTON.2014.6876267.

[45] A. B. Raj and A. K. Majumder, "Historical perspective of free space optical communications: from the early dates to today's developments," *IET Communications*, vol. 13, no. 16, pp. 2405-2419, 2019, doi: https://doi.org/10.1049/iet-com.2019.0051.

[46] A. Abdulsalam Ghalib and A. Khaleel Saeed, "Free space optical communications — Theory and practices," in *Contemporary Issues in Wireless Communications*, K. Mutamed Ed. Rijeka: IntechOpen, 2014, p. Ch. 5.

[47] H. Hemmati, *Near-earth laser communications*, Second Edition ed. Boca Raton: CRC Press, 2020.

[48] A. K. Majumdar, Z. Ghassemlooy, and A. Arockia Bazil Raj, *Principles and applications of free space optical communications*. Institution of Engineering and Technology, 2019.

[49] H. Tataria, M. Shafi, A. F. Molisch, M. Dohler, H. Sjöland, and F. Tufvesson, "6G wireless systems: Vision, requirements, challenges, insights, and opportunities," *Proceedings of the IEEE*, vol. 109, no. 7, pp. 1166-1199, 2021, doi: 10.1109/JPROC.2021.3061701.

[50] L. Di Gregorio, *Latency in 5G networks*. 2015.

[51] G. C. Garry Kranz. "What is 6G? Overview of 6G networks & technology."

[52] "Breaking Down the RF Spectrum – Which Bandwidth is Best for Your Application?" Bliley Technologies.

[53] Rajiv. "What are 5G frequency bands." RF Page

[54] O. Aboelala, I. E. Lee, and G. C. Chung, "A survey of hybrid free space optics (FSO) communication networks to achieve 5G connectivity for backhauling," *Entropy*, vol. 24, no. 11, doi: 10.3390/e24111573.

[55] I. A. Alimi and N. J. Muga, "Simple and robust transmit diversity based free-space optical communications for 5G and beyond networks," *Optics Communications*, vol. 476, p. 126306, 2020/12/01/ 2020, doi: 10.1016/j.optcom.2020.126306.

[56] S. Rao, J. Digge, and B. U. Rindhe, "Free space optics for 5G and beyond," in *2021 6th International Conference for Convergence in Technology (I2CT)*, 2-4 April 2021 2021, pp. 1-5, doi: 10.1109/I2CT51068.2021.9418147.

[57] E. Leitgeb, S. S. Muhammad, C. Chlestil, M. Gebhart, and U. Birnbacher, "Reliability of FSO links in next generation optical networks," in *Proceedings of 2005 7th*

International Conference Transparent Optical Networks, 2005., 7-7 July 2005 2005, vol. 1, pp. 394-401 Vol. 1, doi: 10.1109/ICTON.2005.1505829.

[58] S. A. Al-Gailani *et al.*, "A survey of free space optics (FSO) communication systems, Links, and Networks," *IEEE Access*, vol. 9, pp. 7353-7373, 2021, doi: 10.1109/ACCESS.2020.3048049.

[59] M. Z. Chowdhury, M. Shahjalal, S. Ahmed, and Y. M. Jang, "6G wireless communication systems: Applications, requirements, technologies, challenges, and research directions," *IEEE Open Journal of the Communications Society*, vol. 1, pp. 957-975, 2020, doi: 10.1109/OJCOMS.2020.3010270.

[60] A. K. Majumdar, *Optical wireless communications for broadband global internet connectivity*. Elsevier, 2019, pp. 259-268.

[61] "Coherent free space optics for ground and space applications."

[62] M. Z. Chowdhury, M. T. Hossan, A. Islam, and Y. M. Jang, "A Comparative survey of optical wireless technologies: Architectures and applications," *IEEE Access*, vol. 6, pp. 9819-9840, 2018, doi: 10.1109/ACCESS.2018.2792419.

[63] I. Kim. "10 G FSO systems position technology for the future." Lightwaveonline.

[64] L. Rakotondrainibe, Y. Kokar, G. Zaharia, and G. E. Zein, "60 GHz High data rate wireless communication system," in *VTC Spring 2009 - IEEE 69th Vehicular Technology Conference*, 26-29 April 2009 2009, pp. 1-5, doi: 10.1109/VETECS.2009.5073281.

[65] A. Sikora and V. F. Groza, "Coexistence of IEEE802.15.4 with other systems in the 2.4 GHz-ISM-Band," in *2005 IEEE Instrumentationand Measurement Technology Conference Proceedings*, 16-19 May 2005 2005, vol. 3, pp. 1786-1791, doi: 10.1109/IMTC.2005.1604479.

[66] J. M. Kahn and J. R. Barry, "Wireless infrared communications," *Proceedings of the IEEE*, vol. 85, no. 2, pp. 265-298, 1997, doi: 10.1109/5.554222.

[67] R. Ramirez-Iniguez, S. M. Idrus, and Z. Sun, *Optical wireless communications : IR for wireless connectivity*. Auerbach Publications, 2008.

[68] K. Biesecker, "The promise of broadband wireless," *IT Professional*, vol. 2, pp. 31-39, 12/01 2000, doi: 10.1109/6294.888014.

[69] N. Cvijetic, D. Qian, and T. Wang, "10Gb/s free-space optical transmission using OFDM," in *OFC/NFOEC 2008 - 2008 Conference on Optical Fiber Communication/National Fiber Optic Engineers Conference*, 24-28 Feb. 2008 2008, pp. 1-3, doi: 10.1109/OFC.2008.4528442.

[70] D. Killinger, "Free space optics for laser communication through the air," *Opt. Photon. News*, vol. 13, no. 10, pp. 36-42, 2002/10/01 2002, doi: 10.1364/OPN.13.10.000036.

[71] A. Malik and P. Singh, "Free space optics: Current Applications and future challenges," *International Journal of Optics*, vol. 2015, pp. 1-7, 11/17 2015, doi: 10.1155/2015/945483.

[72] Y. Alfadhli *et al.*, "Real-Time FPGA demonstration of hybrid bi-directional MMW and FSO fronthaul architecture," in *2019 Optical Fiber Communications Conference and Exhibition (OFC)*, 3-7 March 2019 2019, pp. 1-3.

[73] H. A. Fadhil *et al.*, "Optimization of free space optics parameters: An optimum solution for bad weather conditions," *Optik*, vol. 124, no. 19, pp. 3969-3973, 2013/10/01/ 2013, doi: 10.1016/j.ijleo.2012.11.059.

[74] E. Gulsen, E. Olivetti, L. C. Kimerling, and R. Kirchain, "Energy concerns in information and communication technology and the potential for photonics integration," in *Proceedings of the 2010 IEEE International Symposium on Sustainable Systems and Technology*, 17-19 May 2010 2010, pp. 1-1, doi: 10.1109/ISSST.2010.5507699.

[75] L. Xian, "Secrecy capacity of wireless links subject to log-normal fading," in *7th International Conference on Communications and Networking in China*, 8-10 Aug. 2012 2012, pp. 167-172, doi: 10.1109/ChinaCom.2012.6417469.

[76] L. F. Abdulameer, J. Jignesh D., U. Sripati, and M. Kulkarni, "Enhancement of security for free space optics based on reconfigurable chaotic technique," in *Other Conferences*, 2012.

[77] J. M. Kahn, "Modulation and detection techniques for optical communication systems," in *Optical Amplifiers and Their Applications/Coherent Optical Technologies and Applications*, Whistler, 2006/06/25 2006: Optica Publishing Group, in Technical Digest (CD), p. CThC1, doi: 10.1364/COTA.2006.CThC1.

[78] T. Berceli, M. Csornyei, B. J. Klein, and T. Bánky, "Nonlinear effects in optical-wireless OFDM signal transmission," *2002 International Topical Meeting on Microwave Photonics*, pp. 225-228, 2002.

[79] P. Yue, X. Yi, R. Zheng, and D. Xu, "Performance analysis of a LDPC coded OAM-based UCA FSO system exploring linear equalization with channel estimation over atmospheric turbulence," *Opt. Express*, vol. 28, no. 2, pp. 816-820, 2020/01/20 2020, doi: 10.1364/OE.28.000816.

[80] M. V. Kumar and V. Kumar, "Investigation of a coherent dual-polarized 16-QAM 16-channel WDM FSO gamma–gamma fading system under various atmospheric losses," *Journal of Modern Optics*, vol. 69, no. 12, pp. 665-676, 2022/07/12 2022, doi: 10.1080/09500340.2022.2074160.

[81] K. Mallick, P. Mandal, G. C. Mandal, R. Mukherjee, B. Das, and A. S. Patra, "Hybrid MMW-over fiber/OFDM-FSO transmission system based on doublet lens scheme and POLMUX technique," *Optical Fiber Technology*, vol. 52, p. 101942, 2019/11/01/ 2019, doi: 10.1016/j.yofte.2019.101942.

[82] J. J. O, apos, Reilly, P. M. Lane, and M. H. Capstick, "Optical generation and delivery of modulated mm-waves for mobile communications," in *Telecommunications, Analogue Optical Fibre Communications*: Institution of Engineering and Technology, 1995, pp. 229-256.

[83] K. Sato and K. Asatani, "Speckle noise reduction in fiber optic analog video transmission using semiconductor laser diodes," *IEEE Transactions on Communications*, vol. 29, no. 7, pp. 1017-1024, 1981, doi: 10.1109/TCOM.1981.1095084.

[84] Y. Ai *et al.*, "The analysis of 7.5Gbps 40 Km FSO experiments," in *2012 IEEE Photonics Society Summer Topical Meeting Series*, 9-11 July 2012 2012, pp. 128-129, doi: 10.1109/PHOSST.2012.6280759.

[85] O. Bouchet, H. Sizun, C. Boisrobert, F. Fornel, and P. N. Favennec, "Free-space optics: Propagation and communication," *Free-Space Optics: Propagation and Communication*, 01/05 2010, doi: 10.1002/9780470612095.

[86] *Free space optics system design*, LightPoint-White and P. Series, 2009.

[87] M. Ijaz, Z. Ghassemlooy, H. L. Minh, S. Rajbhandari, and J. Perez, "Analysis of fog and smoke attenuation in a free space optical communication link under controlled laboratory conditions," in *2012 International Workshop on Optical Wireless Communications (IWOW)*, 22-22 Oct. 2012 2012, pp. 1-3, doi: 10.1109/IWOW.2012.6349680.

[88] B. E. A. Saleh and J. M. Minkowski, "On the spatial coherence of laser beams," *Journal of Physics A*, vol. 8, pp. 120-125, 1975.

[89] T. Sasaki, M. Toyoshima, and H. Takenaka, "Fading simulator for satellite-to-ground optical communication," vol. 59, pp. 95-102, 03/01 2012.

[90] S. M. I. Roberto Ramirez-Iniguez, Ziran Sun, *Optical wireless communications: IR for wireless connectivity*, 1st Edition ed. New York: Auerbach Publications., 2008.

[91] S. Hranilovic, "Wireless optical intensity channels," in *Wireless Optical Communication Systems*, S. Hranilovic Ed. New York, NY: Springer New York, 2005, pp. 9-37.

[92] O. Kharraz and D. Forsyth, "Performance comparisons between PIN and APD photodetectors for use in optical communication systems," *Optik*, vol. 124, no. 13, pp. 1493-1498, 2013/07/01/ 2013, doi: 10.1016/j.ijleo.2012.04.008.

[93] C. Pernechele, *Encyclopedia of Modern Optics*. 2005.

[94] S. Arnon, *Optical wireless communication through random media* (SPIE LASE). SPIE, 2011.
[95] F. Fidler, M. Knapek, J. Horwath, and W. R. Leeb, "Optical communications for high-altitude platforms," *IEEE Journal of Selected Topics in Quantum Electronics*, vol. 16, no. 5, pp. 1058-1070, 2010, doi: 10.1109/JSTQE.2010.2047382.
[96] W. K. Pratt, *Laser communications systems*, 1st ed ed. New York: John Wiley & Sons, Inc., 1969.
[97] O. G.R, "Optical detection theory for laser applications," 07/01 2002.
[98] S. K. Robert M. Gagliardi, *Optical Communications*, 2nd ed. (Wiley Series in Telecommunications and Signal Processing). 1995.
[99] S. Rajbhandari, Z. Ghassemlooy, P. A. Haigh, T. Kanesan, and X. Tang, "Experimental error performance of modulation schemes under a controlled laboratory Turbulence FSO Channel," *Journal of Lightwave Technology*, vol. 33, no. 1, pp. 244-250, 2015, doi: 10.1109/JLT.2014.2377155.
[100] M. A. Khalighi, N. Aitamer, N. Schwartz, and S. Bourennane, "Turbulence mitigation by aperture averaging in wireless optical systems," in *2009 10th International Conference on Telecommunications*, 8-10 June 2009 2009, pp. 59-66.
[101] L. C. Andrews, R. L. Phillips, and C. Y. Hopen, "Laser Beam Scintillation with Applications," 2001.
[102] S. M. Navidpour, M. Uysal, and M. Kavehrad, "BER performance of Free-space optical transmission with spatial diversity," *IEEE Transactions on Wireless Communications*, vol. 6, no. 8, pp. 2813-2819, 2007, doi: 10.1109/TWC.2007.06109.
[103] H. Kaushal *et al.*, "Experimental study on beam wander under varying atmospheric turbulence conditions," *IEEE Photonics Technology Letters*, vol. 23, no. 22, pp. 1691-1693, 2011, doi: 10.1109/LPT.2011.2166113.
[104] J.-H. Lee and S.-H. Hwang, "Selection diversity-aided subcarrier intensity modulation/spatial modulation for free-space optical communication," *IET Optoelectronics*, vol. 9, no. 2, pp. 116-124, 2015, doi: 10.1049/iet-opt.2014.0016.
[105] L. C. Andrews and R. L. Phillips, "Laser beam propagation through random media," 1998.
[106] M. A. Khalighi, N. Schwartz, N. Aitamer, and S. Bourennane, "Fading reduction by aperture averaging and spatial diversity in optical wireless systems," *Journal of Optical Communications and Networking*, vol. 1, no. 6, pp. 580-593, 2009, doi: 10.1364/JOCN.1.000580.
[107] Z. Wang, W. D. Zhong, S. Fu, and C. Lin, "Performance comparison of different modulation formats over free-space optical (FSO) turbulence links with space diversity reception technique," *IEEE Photonics Journal*, vol. 1, no. 6, pp. 277-285, 2009, doi: 10.1109/JPHOT.2009.2039015.
[108] N. D. Chatzidiamantis and G. K. Karagiannidis, "On the distribution of the sum of Gamma-Gamma variates and applications in RF and Optical Wireless Communications," *IEEE Transactions on Communications*, vol. 59, no. 5, pp. 1298-1308, 2011, doi: 10.1109/TCOMM.2011.020811.090205.
[109] Z. Xiaoming and J. M. Kahn, "Markov chain model in maximum-likelihood sequence detection for free-space optical communication through atmospheric turbulence channels," *IEEE Transactions on Communications*, vol. 51, no. 3, pp. 509-516, 2003, doi: 10.1109/TCOMM.2003.809787.
[110] Z. Chen, S. Yu, T. Wang, G. Wu, S. Wang, and W. Gu, "Channel correlation in aperture receiver diversity systems for free-space optical communication," *Journal of Optics*, vol. 14, no. 12, p. 125710, 2012/11/13 2012, doi: 10.1088/2040-8978/14/12/125710.
[111] F. S. Vetelino, C. Young, L. Andrews, and J. Recolons, "Aperture averaging effects on the probability density of irradiance fluctuations in moderate-to-strong turbulence," *Appl. Opt.*, vol. 46, no. 11, pp. 2099-2108, 2007/04/10 2007, doi: 10.1364/AO.46.002099.

[112] J. Watson, "Tip tilt corection for astronomical telescopes using adaptive control," presented at the Conference: Wescon integrated circuit expo 1997, Santa Clara, CA (United States), 5-6 Nov 1997; Other Information: PBD: 17 Apr 1997, United States, 1997.

[113] E. Arikan, "Channel polarization: A method for constructing capacity-achieving codes," in *2008 IEEE International Symposium on Information Theory*, 6-11 July 2008 2008, pp. 1173-1177, doi: 10.1109/ISIT.2008.4595172.

[114] I. B. Djordjevic, "LDPC-coded optical communication over the atmospheric turbulence channel," in *2007 Conference Record of the Forty-First Asilomar Conference on Signals, Systems and Computers*, 4-7 Nov. 2007 2007, pp. 1903-1909, doi: 10.1109/ACSSC.2007.4487567.

[115] J. Fang *et al.*, "Polar-coded MIMO FSO communication system over gamma-gamma turbulence channel with spatially correlated fading," *Journal of Optical Communications and Networking*, vol. 10, no. 11, pp. 915-923, 2018, doi: 10.1364/JOCN.10.000915.

[116] T. Ohtsuki, "Turbo-coded atmospheric optical communication systems," in *2002 IEEE International Conference on Communications. Conference Proceedings. ICC 2002 (Cat. No.02CH37333)*, 28 April-2 May 2002 2002, vol. 5, pp. 2938-2942 vol.5, doi: 10.1109/ICC.2002.997378.

[117] T. Adiono, Y. Aska, S. Fuada, and A. Purwita, "Design of an OFDM system for VLC with a Viterbi decoder," *IEIE Transactions on Smart Processing and Computing*, vol. 6, pp. 455-465, 12/30 2017, doi: 10.5573/IEIESPC.2017.6.6.455.

[118] N. Mohan *et al.*, "The BER performance of a FSO system with polar codes under weak turbulence," *IET Optoelectronics*, vol. 16, no. 2, pp. 72-80, 2022, doi: 10.1049/ote2.12058.

[119] G. S. M. DAVID ROCKWELL. "Optical wireless: Low-cost, broadband, optical access."

[120] T. A. Tsiftsis, H. G. Sandalidis, G. K. Karagiannidis, and M. Uysal, "FSO links with spatial diversity over strong atmospheric turbulence channels," in *2008 IEEE International Conference on Communications*, 19-23 May 2008 2008, pp. 5379-5384, doi: 10.1109/ICC.2008.1008.

[121] M. Razavi and J. H. Shapiro, "Wireless optical communications via diversity reception and optical preamplification," *IEEE Transactions on Wireless Communications*, vol. 4, no. 3, pp. 975-983, 2005, doi: 10.1109/TWC.2005.847102.

[122] M. A. Kashani, M. Uysal, and M. Kavehrad, "A Novel statistical channel model for turbulence-induced fading in free-space optical systems," *Journal of Lightwave Technology*, vol. 33, no. 11, pp. 2303-2312, 2015, doi: 10.1109/JLT.2015.2410695.

[123] M. Abramowitz, I. A. Stegun, and D. M. Miller, "Handbook of mathematical functions with formulas, graphs and mathematical tables (National Bureau of Standards Applied Mathematics Series No. 55)," *Journal of Applied Mechanics*, vol. 32, pp. 239-239, 1964.

[124] A. A. Abu-Dayya and N. C. Beaulieu, "Comparison of methods of computing correlated lognormal sum distributions and outages for digital wireless applications," in *Proceedings of IEEE Vehicular Technology Conference (VTC)*, 8-10 June 1994 1994, pp. 175-179 vol.1, doi: 10.1109/VETEC.1994.345143.

[125] T. A. Tsiftsis, H. G. Sandalidis, G. K. Karagiannidis, and M. Uysal, "Optical wireless links with spatial diversity over strong atmospheric turbulence channels," *IEEE Transactions on Wireless Communications*, vol. 8, no. 2, pp. 951-957, 2009, doi: 10.1109/TWC.2009.071318.

[126] T. Eng, K. Ning, and L. B. Milstein, "Comparison of diversity combining techniques for Rayleigh-fading channels," *IEEE Transactions on Communications*, vol. 44, no. 9, pp. 1117-1129, 1996, doi: 10.1109/26.536918.

[127] M. D. M. D. C. J. M. D. Nordel, "Laser relay for free space optical communications," United States Patent Appl. 13/855,602 2013.

[128] H. Kaushal and G. Kaddoum, "Optical communication in space: challenges and mitigation techniques," *IEEE Communications Surveys & Tutorials*, vol. 19, no. 1, pp. 57-96, 2017, doi: 10.1109/COMST.2016.2603518.
[129] E. Bayaki, D. S. Michalopoulos, and R. Schober, "EDFA-based all-optical relaying in free-space optical systems," in *2011 IEEE 73rd Vehicular Technology Conference (VTC Spring)*, 15-18 May 2011 2011, pp. 1-5, doi: 10.1109/VETECS.2011.5956657.
[130] R. Li, T. Chen, L. Fan, and A. Dang, "Performance analysis of a multiuser dual-hop amplify-and-forward relay system with FSO/RF Links," *J. Opt. Commun. Netw.*, vol. 11, no. 7, pp. 362-370, 2019/07/01 2019, doi: 10.1364/JOCN.11.000362.
[131] A. A. A. Haija and C. Tellambura, "Outage and decoding delay analysis of full-duplex DF relaying: Backward or sliding window decoding," *2016 IEEE Global Communications Conference (GLOBECOM)*, pp. 1-6, 2016.
[132] M. K. El-Nayal, M. M. Aly, H. A. Fayed, and R. A. AbdelRassoul, "Adaptive free space optic system based on visibility detector to overcome atmospheric attenuation," *Results in Physics*, vol. 14, p. 102392, 2019/09/01/ 2019, doi: 10.1016/j.rinp.2019.102392.
[133] H. C. v. d. Hulst, *Light Scattering by Small Particles*. New York: Wiley, 1957.
[134] L. D. M. P. W. Kruse, and R. B. McQuistan, *Elements of infrared technology: Generation, transmission, and detection* 1963.
[135] R. Paudel, Z. Ghassemlooy, H. Le-Minh, and S. Rajbhandari, "Modelling of free space optical link for ground-to-train communications using a Gaussian source," *IET Optoelectronics*, vol. 7, no. 1, pp. 1-8, 2013, doi: 10.1049/iet-opt.2012.0047.
[136] M. Ijaz, Z. Ghassemlooy, J. Pesek, O. Fiser, H. L. Minh, and E. Bentley, "Modeling of fog and smoke attenuation in free space optical communications link under Controlled Laboratory Conditions," *Journal of Lightwave Technology*, vol. 31, no. 11, pp. 1720-1726, 2013, doi: 10.1109/JLT.2013.2257683.
[137] IEC. "Safety of laser products - Part 1: Equipment classification and requirements." International Electrotechnical Commission,. (accessed.
[138] S. Hranilovic, *Wireless Optical Communication Systems*. Boston: Springer, 2005.
[139] M. M. Abadi, Z. Ghassemlooy, S. Zvanovec, M. R. Bhatnagar, and Y. Wu, "Hard switching in hybrid FSO/RF link: Investigating data rate and link availability," in *2017 IEEE International Conference on Communications Workshops (ICC Workshops)*, 21-25 May 2017 2017, pp. 463-468, doi: 10.1109/ICCW.2017.7962701.
[140] Y. Tang, M. Brandt-Pearce, and S. G. Wilson, "Link adaptation for throughput optimization of parallel channels with application to hybrid FSO/RF systems," *IEEE Transactions on Communications*, vol. 60, no. 9, pp. 2723-2732, 2012, doi: 10.1109/TCOMM.2012.061412.100460.
[141] Z. Kolka, Z. Kincl, V. Biolkova, and D. Biolek, "Hybrid FSO/RF test link," in *2012 IV International Congress on Ultra Modern Telecommunications and Control Systems*, 3-5 Oct. 2012 2012, pp. 502-505, doi: 10.1109/ICUMT.2012.6459718.
[142] B. H. Walker, "Optical Engineering Fundamentals," 1995.
[143] E. J. Oughton and W. Lehr, "Surveying 5G techno-economic research to inform the evaluation of 6G wireless technologies," *IEEE Access*, vol. 10, pp. 25237-25257, 2022, doi: 10.1109/ACCESS.2022.3153046.
[144] A. L. G. Reis, A. F. Barros, K. G. Lenzi, L. G. P. Meloni, and S. E. Barbin, "Introduction to the software-defined radio approach," *IEEE Latin America Transactions*, vol. 10, no. 1, pp. 1156-1161, 2012.
[145] CableFree. "An overview of software defined radio, SDR" CableFree.
[146] F. H. P. Fitzek, P. Seeling, T. Höschele, and B. Jacobfeuerborn, "On the need of computing in future communication networks," in *Computing in Communication Networks*, F. H. P. Fitzek, F. Granelli, and P. Seeling Eds.: Academic Press, 2020.
[147] W. H. W. Tuttlebee, "Software defined radio : origins, drivers and international perspectives," 2002.
[148] T. A. Sturman, "An Evaluation of Software defined radio – Main Document," QinetiQ, Defence and Technology Systems, 2006.

[149] T. Ulversoy, "Software defined radio: challenges and opportunities," *IEEE Communications Surveys & Tutorials,* vol. 12, no. 4, pp. 531-550, 2010, doi: 10.1109/SURV.2010.032910.00019.
[150] J. Mitola, "Cognitive radio architecture," in *Cooperation in Wireless Networks: Principles and Applications: Real Egoistic Behavior is to Cooperate!*, F. H. P. Fitzek and M. D. Katz Eds. Dordrecht: Springer Netherlands, 2006, pp. 243-311.
[151] J. Mitola and G. Q. Maguire, "Cognitive radio: making software radios more personal," *IEEE Personal Communications,* vol. 6, no. 4, pp. 13-18, 1999, doi: 10.1109/98.788210.
[152] J. Mitola, "Cognitive radio an integrated agent architecture for software defined radio," 2000.
[153] F. K. Jondral, "Software-defined radio—Basics and evolution to cognitive radio," *EURASIP Journal on Wireless Communications and Networking,* vol. 2005, no. 3, p. 652784, 2005/08/01 2005, doi: 10.1155/WCN.2005.275.
[154] W. H. W. Tuttlebee, *Software defined radio: enabling technologies*. John Wiley & Sons Ltd., 2002.
[155] K. M. Markus Dillinger, Nancy Alonistioti, *Software defined radio: architectures, systems and functions*. John Wiley & Sons Ltd, 2005.
[156] X. Wei *et al.*, "Software Defined Radio Implementation of a non-orthogonal multiple access system towards 5G," *IEEE Access,* vol. 4, pp. 9604-9613, 2016, doi: 10.1109/ACCESS.2016.2634038.
[157] E. Grayver, *Implementing software defined radio*. Springer, 2013.
[158] R. Akeela and B. Dezfouli, "Software-defined radios: Architecture, state-of-the-art, and challenges," *Computer Communications,* vol. 128, pp. 106-125, 2018/09/01/ 2018, doi: 10.1016/j.comcom.2018.07.012.
[159] V. J. K. John Bard, Jr, *Software Defined Radio: The software communications Architecture*. John Wiley & Sons, Ltd, 2007.
[160] R. Chávez-Santiago, K. Chomu, L. Gavrilovska, and I. Balasingham, "Applications of software-defined radio (SDR) technology in hospital environments," *Conference proceedings : ... Annual International Conference of the IEEE Engineering in Medicine and Biology Society. IEEE Engineering in Medicine and Biology Society. Conference,* vol. 2013, pp. 1266-1269, 07/01 2013, doi: 10.1109/EMBC.2013.6609738.
[161] B. McHugh. "SDRs for low latency and time sensitive industrial internet of things (IIoT) applications." Embedded Computing Design.
[162] H. H. Cho, C. F. Lai, T. K. Shih, and H. C. Chao, "Integration of SDR and SDN for 5G," *IEEE Access,* vol. 2, pp. 1196-1204, 2014, doi: 10.1109/ACCESS.2014.2357435.
[163] G. Quintana and R. Birkeland, Software defined radios in satellite communications. 2018.
[164] R. W. Stewart, K. W. Barlee, D. S. Atkinson, and L. H. Crockett, *Software defined radio using MATLAB & Simulink and the RTL-SDR*. 2015.
[165] J. C. Vito Giannini, Andrea Baschirotto, *Baseband analog circuits for software defined radio*. Springer, 2008.
[166] M. Dillinger, K. Madani, and N. Alonistioti, *Software defined radio: Architectures, systems and functions*. John Wiley & Sons, 2005.
[167] P. Cruz, N. B. Carvalho, and K. A. Remley, "Designing and testing software-defined radios," *IEEE Microwave Magazine,* vol. 11, no. 4, pp. 83-94, 2010, doi: 10.1109/MMM.2010.936493.
[168] M. Arief, S. Mohd Adib, F. Norsheila, Y. Sharifah Kamilah Syed, and R. A. Rashid, "Experimental study of OFDM implementation utilizing GNU Radio and USRP - SDR," in *2009 IEEE 9th Malaysia International Conference on Communications (MICC)*, 15-17 Dec. 2009 2009, pp. 132-135, doi: 10.1109/MICC.2009.5431480.
[169] R. Schiphorst, F. Hoeksema, and C. Slump, "The Front end of software-defined radio: Possibilities and challenges," *Proceedings of The IEEE - PIEEE,* 01/01 2001.

[170] X. Lu, L. Ni, S. Jin, C. K. Wen, and W. J. Lu, "SDR implementation of a real-time testbed for future multi-antenna smartphone applications," *IEEE Access*, vol. 5, pp. 19761-19772, 2017, doi: 10.1109/ACCESS.2017.2751622.
[171] T. Izydorczyk, F. M. L. Tavares, G. Berardinelli, and P. Mogensen, "A USRP-Based multi-antenna testbed for reception of multi-site cellular signals," *IEEE Access*, vol. 7, pp. 162723-162734, 2019, doi: 10.1109/ACCESS.2019.2952094.
[172] B. S. K. Reddy, "Experimental validation of timing, frequency and phase correction of received signals using software defined radio testbed," *Wireless Personal Communications*, vol. 101, no. 4, pp. 2085-2103, 2018/08/01 2018, doi: 10.1007/s11277-018-5806-2.
[173] C. Lahoud, S. Ehsanfar, M. Gabriel, P. Küffner, and K. Mößner, "Experimental Testbed Results on LTE/5G-V2I Communication using Software Defined Radio," in *ICC 2022 - IEEE International Conference on Communications*, 16-20 May 2022 2022, pp. 2894-2899, doi: 10.1109/ICC45855.2022.9838411.
[174] S. Sun, M. Kadoch, L. Gong, and B. Rong, "Integrating network function virtualization with SDR and SDN for 4G/5G networks," *IEEE Network*, vol. 29, no. 3, pp. 54-59, 2015, doi: 10.1109/MNET.2015.7113226.
[175] H. Feng, J. Wu, and X. Gong, "SOUP: Advanced SDR platform for 5G communication," in *2017 IEEE/CIC International Conference on Communications in China (ICCC)*, 22-24 Oct. 2017 2017, pp. 1-5, doi: 10.1109/ICCChina.2017.8330392.
[176] M. Agiwal, A. Roy, and N. Saxena, "Next generation 5G wireless networks: A comprehensive survey," *IEEE Communications Surveys & Tutorials*, vol. 18, no. 3, pp. 1617-1655, 2016, doi: 10.1109/COMST.2016.2532458.
[177] RTL-SDR.COM. "About RTL-SDR." rtl-sdr.com. https://www.rtl-sdr.com/about-rtl-sdr/
[178] S. a. Elizabeth. "HackRF One - Great Scott Gadgets." greatscottgadgets.com. https://greatscottgadgets.com/ (accessed Dec. 12, 2022).
[179] L. Microsystems. "Software defined radio technology for wireless networks." (accessed Nov. 23, 2022).
[180] RedPitaya. "Swiss Army Knife for Engineers." https://redpitaya.com/ (accessed Jan. 01, 2023).
[181] Airspy. "The dependable VHF/UHF Radio for your projects." https://airspy.com/airspy-r2/ (accessed Jan. 02, 2023).
[182] Nuand. "bladeRF 2.0 micro." https://www.nuand.com/bladerf-2-0-micro/ (accessed Oct. 26, 2022).
[183] KiwiSDR. "KiwiSDR: Wide-band SDR + GPS cape for the BeagleBone Black." http://kiwisdr.com/ (accessed Oct. 26, 2022).
[184] Analog Devices. "ADALM-PLUTO." https://www.analog.com/en/design-center/evaluation-hardware-and-software/evaluation-boards-kits/adalm-pluto.html#eb-overview (accessed Oct. 26, 2022).
[185] WB5RVZ.org. "Ensemble RXTX - Home page band: 30, 20, 17m." http://www.wb5rvz.org/ensemble_rxtx/index?projectId=14 (accessed Oct. 26, 2022).
[186] SDRplay. "RSPduo." https://www.sdrplay.com/rspduo/ (accessed Oct. 26, 2022).
[187] F. Dongle. "The FUNcube Dongle Pro+: LF to L band software-defined radio." http://www.funcubedongle.com/ (accessed Nov. 16, 2022).
[188] N. Instruments. "USRP Software Defined Radio Device." https://www.ni.com/en-gb/shop/hardware/products/usrp-software-defined-radio-device.html (accessed Dec. 15, 2022).
[189] E. Research. "USRP X310." https://www.ettus.com/all-products/x310-kit/ (accessed Dec. 22, 2022).
[190] E. Research. " USRP N320." https://www.ettus.com/all-products/usrp-n320/ (accessed 16. Nov, 2022).
[191] A. Devices. "AD9371." https://www.analog.com/en/products/ad9371.html#product-overview (accessed Dec. 16, 2022).

[192] Lime Microsystems. "LMS8001 Companion." https://limemicro.com/products/boards/lms8001-companion/ (accessed Dec. 18, 2022).
[193] GNURadio. "GNURadio." https://www.gnuradio.org/ (accessed Dec. 02, 2022).
[194] RTL-SDR.COM. "SDRSHARP BIG GUIDE BOOK UPDATED TO V5.3." https://www.rtl-sdr.com/tag/sdrsharp/ (accessed Dec. 03, 2022).
[195] A. Csete. "Gqrx SDR." https://gqrx.dk/ (accessed Dec. 01, 2022).
[196] HDSDR. "HDSDR : High Definition Software Defined Radio." https://www.hdsdr.de/ (accessed Oct. 13, 2022).
[197] SDR-Radio.com. "SDR Console : The main program in the SDR-radio.com suite." https://www.sdr-radio.com/console (accessed Dec. 14, 2022).
[198] SDR-J. "Software defined radio : DAB, drm and other software." https://www.sdr-j.tk/index.html (accessed Nov. 04, 2022).
[199] P. Kamboj and S. Pal, "Software-defined networking in data centers," in *Software Defined Internet of Everything*, G. S. Aujla, S. Garg, K. Kaur, and B. Sikdar Eds. Cham: Springer International Publishing, 2022, pp. 177-203.
[200] S. Bera, S. Misra, and A. V. Vasilakos, "Software-defined networking for internet of things: A survey," *IEEE Internet of Things Journal*, vol. 4, no. 6, pp. 1994-2008, 2017, doi: 10.1109/JIOT.2017.2746186.
[201] R. Jain and S. Paul, "Network virtualization and software defined networking for cloud computing: a survey," *IEEE Communications Magazine*, vol. 51, no. 11, pp. 24-31, 2013, doi: 10.1109/MCOM.2013.6658648.
[202] Y. Miao, Z. Cheng, W. Li, H. Ma, X. Liu, and Z. Cui, "Software defined integrated satellite-terrestrial network: A survey," in *Space Information Networks*, Singapore, Q. Yu, Ed., 2017// 2017: Springer Singapore, pp. 16-25.
[203] S. K. Routray and K. P. Sharmila, "Software defined networking for 5G," in *2017 4th International Conference on Advanced Computing and Communication Systems (ICACCS)*, 6-7 Jan. 2017 2017, pp. 1-5, doi: 10.1109/ICACCS.2017.8014576.
[204] W. Xia, Y. Wen, C. H. Foh, D. Niyato, and H. Xie, "A Survey on software-defined networking," *IEEE Communications Surveys & Tutorials*, vol. 17, no. 1, pp. 27-51, 2015, doi: 10.1109/COMST.2014.2330903.
[205] D. Kreutz, F. M. V. Ramos, P. E. Veríssimo, C. E. Rothenberg, S. Azodolmolky, and S. Uhlig, "Software-defined networking: A comprehensive survey," *Proceedings of the IEEE*, vol. 103, no. 1, pp. 14-76, 2015, doi: 10.1109/JPROC.2014.2371999.
[206] H. Farhady, H. Lee, and A. Nakao, "Software-Defined Networking: A survey," *Computer Networks*, vol. 81, pp. 79-95, 2015/04/22/ 2015, doi: 10.1016/j.comnet.2015.02.014.
[207] M. K. Shin, K. H. Nam, and H. J. Kim, "Software-defined networking (SDN): A reference architecture and open APIs," in *2012 International Conference on ICT Convergence (ICTC)*, 15-17 Oct. 2012 2012, pp. 360-361, doi: 10.1109/ICTC.2012.6386859.
[208] Z. Chunrong, "What Is NETCONF?," in *IP Encyclopedia*, ed, 2022.
[209] "OpenFlow Protocol Library Developer Guide." OpenDaylight Project.
[210] "OpenDaylight Controller Overview." OpenDaylight Project.
[211] A. Koshibe. "The ONOS Web GUI.".
[212] A. Koshibe. "The ONOS CLI."
[213] C. Trois, M. D. D. Fabro, L. C. E. d. Bona, and M. Martinello, "A Survey on SDN programming languages: Toward a taxonomy," *IEEE Communications Surveys & Tutorials*, vol. 18, no. 4, pp. 2687-2712, 2016, doi: 10.1109/COMST.2016.2553778.
[214] Y. Maleh, Y. Qasmaoui, K. El Gholami, Y. Sadqi, and S. Mounir, "A comprehensive survey on SDN security: threats, mitigations, and future directions," *Journal of Reliable Intelligent Environments*, 2022/02/08 2022, doi: 10.1007/s40860-022-00171-8.
[215] D. Kafetzis, S. Vassilaras, G. Vardoulias, and I. Koutsopoulos, "Software-defined networking meets software-defined radio in mobile ad hoc networks: State of the art

and future directions," *IEEE Access*, vol. 10, pp. 9989-10014, 2022, doi: 10.1109/ACCESS.2022.3144072.

[216] S. Hitam, M. K. Abdullah, M. A. Mahdi, H. Harun, A. Sali, and M. Fauzi, "Impact of increasing threshold level on higher bit rate in free space optical communications," *Journal of Optical and Fiber Communications Research*, vol. 6, no. 1, pp. 22-34, 2009/12/01 2009, doi: 10.1007/s10297-009-9004-6.

[217] P. Deng and M. Kavehrad, "Software defined adaptive MIMO visible light communications after an obstruction," in *2017 Optical Fiber Communications Conference and Exhibition (OFC)*, 19-23 March 2017 2017, pp. 1-3.

[218] D. Peng and M. Kavehrad, "Real-time software-defined single-carrier QAM MIMO visible light communication system," in *2016 Integrated Communications Navigation and Surveillance (ICNS)*, 19-21 April 2016 2016, pp. 5A3-1-5A3-11, doi: 10.1109/ICNSURV.2016.7486354.

[219] Y. Su, F. Fu, and S. Guo, "Resource allocation in communications and computing," *Journal of Electrical and Computer Engineering*, vol. 2013, 01/01 2013, doi: 10.1155/2013/328395.

[220] L. M. John Paul Mueller, *Machine Learning For Dummies*. John Wiley & Sons, Inc., 2021.

[221] B. Aly, M. Elamassie, B. Kebapci, and M. Uysal, "Experimental evaluation of a software defined visible light communication system," in *2020 IEEE International Conference on Communications Workshops (ICC Workshops)*, 7-11 June 2020 2020, pp. 1-6, doi: 10.1109/ICCWorkshops49005.2020.9145145.

[222] A. Vanderka *et al.*, "Utilization of software defined radio for laser beam modulation of OWC by influence of simulated atmospheric phenomena," in *2016 18th International Conference on Transparent Optical Networks (ICTON)*, 10-14 July 2016 2016, pp. 1-8, doi: 10.1109/ICTON.2016.7550489.

[223] A. Costanzo, V. Loscri, and M. Biagi, "Adaptive modulation control for visible light communication systems," *Journal of Lightwave Technology*, vol. 39, no. 9, pp. 2780-2789, 2021, doi: 10.1109/JLT.2021.3056177.

[224] Radek Martinek, Lukas Danys and Rene Jaros "Adaptive software defined equalization techniques for indoor visible light communication," *Sensors*, vol. 20, no. 6, 2020, doi: https://doi.org/10.3390/s20061618.

[225] W. Hussain, H. F. Ugurdag, and M. Uysal, "Software defined VLC system: implementation and performance evaluation," in *2015 4th International Workshop on Optical Wireless Communications (IWOW)*, 7-8 Sept. 2015 2015, pp. 117-121, doi: 10.1109/IWOW.2015.7342278.

[226] H. Technologies. "LiFi R&D Kit." http://www.hyperiontechs.com/lifi-rd-kit/ (accessed 17 Nov 2020, 2020).

[227] H. Boeglen, S. Joumessi-Demeffo, S. Sahuguede, P. Combeau, D. Sauveron, and A. Julien-Vergonjanne, "Optical front-ends for USRP radios," 2018.

[228] P. Deng, "Real - time software - defined sdaptive MIMO visible light communications," 2017.

[229] A. Costanzo and V. Loscri, "Visible light indoor positioning in a noise-aware environment," in *2019 IEEE Wireless Communications and Networking Conference (WCNC)*, 15-18 April 2019 2019, pp. 1-6, doi: 10.1109/WCNC.2019.8885607.

[230] S. Barua, Y. Rong, S. Nordholm, and P. Chen, "Real-time adaptive modulation schemes for underwater acoustic OFDM communications," *Sensors*, vol. 22, no. 9, p. 3436, 2022.

[231] E. Schmidt, D. Inupakutika, R. Mundlamuri, and D. Akopian, "SDR-Fi: Deep-learning-based indoor positioning via software defined radio," *IEEE Access*, vol. 7, pp. 145784-145797, 2019, doi: 10.1109/ACCESS.2019.2945929.

[232] R. Martinek, L. Danys, and R. Jaros, "Visible light communication system based on software defined radio: performance study of intelligent transportation and indoor applications," *Electronics*, vol. 8, no. 4, p. 433, 2019.

[233] S. G. Anavatti, F. Santoso, and M. Garratt, *Adaptive control systems: Past, present, and future*. 2015.

[234] A. Paul, M. Akar, M. G. Safonov, and U. Mitra, "Adaptive power control for wireless networks using multiple controllers and switching," *IEEE Transactions on Neural Networks*, vol. 16, no. 5, pp. 1212-1218, 2005, doi: 10.1109/TNN.2005.853420.

[235] Q. Xiaoxin and K. Chawla, "On the performance of adaptive modulation in cellular systems," *IEEE Transactions on Communications*, vol. 47, no. 6, pp. 884-895, 1999, doi: 10.1109/26.771345.

[236] D. Li, H. Zhang, M. S. Khan, and F. Mi, "A self-adaptive frequency selection common spatial pattern and least squares twin support vector machine for motor imagery electroencephalography recognition," *Biomedical Signal Processing and Control*, vol. 41, pp. 222-232, 2018/03/01/ 2018, doi: 10.1016/j.bspc.2017.11.014.

[237] P. Sadeghi, D. Traskov, and R. Koetter, "Adaptive network coding for broadcast channels," in *2009 Workshop on Network Coding, Theory, and Applications*, 15-16 June 2009 2009, pp. 80-85, doi: 10.1109/NETCOD.2009.5191398.

[238] S. Rajbhandari, Z. Ghassemlooy, and M. Angelova, "Effective denoising and adaptive equalization of indoor optical wireless channels with artificial light using discrete wavelet transform and artificial neural network," *J. Lightwave Technol.*, vol. 27, no. 20, pp. 4493-4500, 2009/10/15 2009.

[239] R. W. Lucky, "Techniques for adaptive equalization of digital communication systems," *Bell System Technical Journal*, vol. 45, no. 2, pp. 255-286, 1966/02/01 1966, doi: 10.1002/j.1538-7305.1966.tb00020.x

[240] A. Zafar, A. Khalid, and H. Asif, *Equalization techniques for visible light communication system*. 2017, pp. 1-5.

[241] M. Atef and H. Zimmermann, "Equalization techniques," in *Optical Communication over Plastic Optical Fibers: Integrated Optical Receiver Technology*, M. Atef and H. Zimmermann Eds. Berlin, Heidelberg: Springer Berlin Heidelberg, 2013, pp. 23-40.

[242] "Equalization," in *Wireless Communications*, A. Goldsmith Ed. Cambridge: Cambridge University Press, 2005, pp. 351-373.

[243] J. Li, C. Lim, and A. Nirmalathas, "Indoor optical wireless communication using few-mode based uniform beam shaping and LMS based adaptive equalization," in *2020 IEEE Photonics Conference (IPC)*, 28 Sept.-1 Oct. 2020 2020, pp. 1-2, doi: 10.1109/IPC47351.2020.9252273.

[244] P. F. Cui, Y. Yu, Y. Liu, W. J. Lu, and H. B. Zhu, "Joint RLS and LMS adaptive equalization for indoor wireless communications under staircase environments," in *2015 International Conference on Wireless Communications & Signal Processing (WCSP)*, 15-17 Oct. 2015 2015, pp. 1-5, doi: 10.1109/WCSP.2015.7341115.

[245] S. U. H. Qureshi, "Adaptive equalization," *Proceedings of the IEEE*, vol. 73, no. 9, pp. 1349-1387, 1985, doi: 10.1109/PROC.1985.13298.

[246] O. Macchi and E. Eweda, "Convergence analysis of self-adaptive equalizers," *IEEE Transactions on Information Theory*, vol. 30, no. 2, pp. 161-176, 1984, doi: 10.1109/TIT.1984.1056896.

[247] X. Chen, W. Lyu, Z. Zhang, J. Zhao, and J. Xu, "56-m/3.31-Gbps underwater wireless optical communication employing Nyquist single carrier frequency domain equalization with noise prediction," *Opt. Express*, vol. 28, no. 16, pp. 23784-23795, 2020/08/03 2020, doi: 10.1364/OE.399794.

[248] S. Rajbhandari *et al.*, "Neural network-based joint spatial and temporal equalization for MIMO-VLC system," *IEEE Photonics Technology Letters*, vol. 31, no. 11, pp. 821-824, 2019, doi: 10.1109/LPT.2019.2909139.

[249] R. Kisacik, M. Y. Yagan, M. Uysal, A. E. Pusane, and A. D. Yalcinkaya, "A New LED response model and its application to pre-equalization in VLC systems," *IEEE Photonics Technology Letters*, vol. 33, no. 17, pp. 955-958, 2021, doi: 10.1109/LPT.2021.3100924.

[250] G. H. Tanudjaja, M. A. Ramadhan, R. Mulyawan, I. Syafalni, N. Sutisna, and T. Adiono, "Analysis of MMSE equalizer for VLC OFDM system sample frequency

offset compensation," in *2021 International Symposium on Intelligent Signal Processing and Communication Systems (ISPACS)*, 16-19 Nov. 2021 2021, pp. 1-2, doi: 10.1109/ISPACS51563.2021.9651040.

[251] L. C. Mathias, J. C. Marinello Filho, and T. Abrao, "Predistortion and pre-equalization for nonlinearities and low-pass effect mitigation in OFDM-VLC systems," *Appl. Opt.*, vol. 58, no. 19, pp. 5328-5338, 2019/07/01 2019, doi: 10.1364/AO.58.005328.

[252] Y. Cai *et al.*, "Experimental demonstration of 16QAM/QPSK OFDM-NOMA VLC with LDPC codes and analog pre-equalization," *Appl. Opt.*, vol. 61, no. 19, pp. 5585-5591, 2022/07/01 2022, doi: 10.1364/AO.460839.

[253] B. Mortada *et al.*, "Optical wireless communication performance enhancement using Hamming coding and an efficient adaptive equalizer with a deep-learning-based quality assessment," *Appl. Opt.*, vol. 60, no. 13, pp. 3677-3688, 2021/05/01 2021, doi: 10.1364/AO.418438.

[254] R. Martinek, L. Danys, and R. Jaros, "Adaptive software defined equalization techniques for indoor visible light communication," *Sensors*, vol. 20, no. 6, p. 1618, 2020. [Online]. Available: https://www.mdpi.com/1424-8220/20/6/1618.

[255] R. Martinek, L. Danys, R. Jaros, D. Mozny, P. Siska, and J. Latal, "VLC channel equalization simulator based on LMS algorithm and virtual instrumentation," in *2019 International Symposium on Advanced Electrical and Communication Technologies (ISAECT)*, 27-29 Nov. 2019 2019, pp. 1-6, doi: 10.1109/ISAECT47714.2019.9069713.

[256] Y. Q. Rice, "Demo : A sfotware defined visible light communications system with WARP," 2014.

[257] S. Schmid, B. v. Deschwanden, S. Mangold, and T. R. Gross, "Adaptivesoftware defined visible light communications networks," in *2017 IEEE/ACM Second International Conference on Internet-of-Things Design and Implementation (IoTDI)*, 18-21 April 2017 2017, pp. 109-120.

[258] F. Peng, J. Zhang, and W. E. Ryan, "Adaptive modulation and coding for IEEE 802.11n," in *2007 IEEE Wireless Communications and Networking Conference*, 11-15 March 2007 2007, pp. 656-661, doi: 10.1109/WCNC.2007.126.

[259] T. Keller and L. Hanzo, "Adaptive modulation techniques for duplex OFDM transmission," *IEEE Transactions on Vehicular Technology*, vol. 49, no. 5, pp. 1893-1906, 2000, doi: 10.1109/25.892592.

[260] Q. Fu and A. Song, "Adaptive modulation for underwater acoustic communications based on reinforcement learning," in *OCEANS 2018 MTS/IEEE Charleston*, 22-25 Oct. 2018 2018, pp. 1-8, doi: 10.1109/OCEANS.2018.8604746.

[261] A. E. Ekpenyong and H. Yih-Fang, "Feedback-detection strategies for adaptive modulation systems," *IEEE Transactions on Communications*, vol. 54, no. 10, pp. 1735-1740, 2006, doi: 10.1109/TCOMM.2006.881352.

[262] L. Jinsock, R. Arnott, K. Hamabe, and N. Takano, "Adaptive modulation switching level control in high speed downlink packet access transmission," in *Third International Conference on 3G Mobile Communication Technologies*, 8-10 May 2002 2002, pp. 156-159, doi: 10.1049/cp:20020380.

[263] I. B. Djordjevic, "Adaptive modulation and coding for free-space optical channels," *J. Opt. Commun. Netw.*, vol. 2, no. 5, pp. 221-229, 2010/05/01 2010, doi: 10.1364/JOCN.2.000221.

[264] F. Sipahioglu, V. Ozduran, and S. B. Yarman, "An adaptive modulation for relay-assisted wireless optical network," in *2018 Advances in Wireless and Optical Communications (RTUWO)*, 15-16 Nov. 2018 2018, pp. 6-11, doi: 10.1109/RTUWO.2018.8587883.

[265] I. B. Djordjevic and G. T. Djordjevic, "On the communication over strong atmospheric turbulence channels by adaptive modulation and coding," *Opt. Express*, vol. 17, no. 20, pp. 18250-18262, 2009/09/28 2009, doi: 10.1364/OE.17.018250.

[266] D. Peng, "Real-time software-defined adaptive MIMO visible light communications," in *Visible Light Communications*, W. Jin-Yuan Ed. Rijeka: IntechOpen, 2017, p. Ch. 2.
[267] M. Gubergrits, R. E. Goot, U. Mahlab, and S. Arnon, "Adaptive power control for satellite to ground laser communication," *International Journal of Satellite Communications and Networking*, vol. 25, no. 4, pp. 349-362, 2007, doi: https://doi.org/10.1002/sat.878.
[268] N. B. Hassan and M. D. Matinfar, "On the implemetation aspects of adaptive power control algorithms in free-space optical communications," in *2014 Iran Workshop on Communication and Information Theory (IWCIT)*, 7-8 May 2014 2014, pp. 1-5, doi: 10.1109/IWCIT.2014.6842485.
[269] H. Safi, A. A. Sharifi, M. T. Dabiri, I. S. Ansari, and J. Cheng, "Adaptive channel coding and power control for practical FSO communication systems under channel Estimation Error," *IEEE Transactions on Vehicular Technology*, vol. 68, no. 8, pp. 7566-7577, 2019, doi: 10.1109/TVT.2019.2916843.
[270] A. Zappone, L. Sanguinetti, G. Bacci, E. Jorswieck, and M. Debbah, "Energy-efficient power control: A look at 5G wireless technologies," *IEEE Transactions on Signal Processing*, vol. 64, no. 7, pp. 1668-1683, 2016, doi: 10.1109/TSP.2015.2500200.
[271] A. H. Sodhro, Y. Li, and M. A. Shah, "Energy-efficient adaptive transmission power control for wireless body area networks," *IET Communications*, vol. 10, no. 1, pp. 81-90, 2016, doi: https://doi.org/10.1049/iet-com.2015.0368.
[272] I. K. Isaac and J. K. Eric, "Availability of free-space optics (FSO) and hybrid FSO/RF systems," in *Proc.SPIE*, 2001, vol. 4530, doi: 10.1117/12.449800. [Online]. Available: https://doi.org/10.1117/12.449800
[273] M. M. Abadi, Z. Ghassemlooy, N. Mohan, S. Zvanovec, M. R. Bhatnagar, and R. Hudson, "Implementation and evaluation of a Gigabit Ethernet FSO link for 'The Last Metre and Last Mile Access Network'," in *2019 IEEE International Conference on Communications Workshops (ICC Workshops)*, 20-24 May 2019 2019, pp. 1-6, doi: 10.1109/ICCW.2019.8757150.
[274] R. L. P. Larry C. Andrews, *Laser beam propagation through random media* Second Edition ed. Bellingham, Washington 98227-0010 USA SPIE—The International Society for Optical Engineering, 2005.
[275] M. Mansour Abadi, Z. Ghassemlooy, M. R. Bhatnagar, S. Zvanovec, M.-A. Khalighi, and M. P. J. Lavery, "Differential signalling in free-space optical communication systems," *Applied Sciences*, vol. 8, no. 6, p. 872, 2018.
[276] S. Zvanovec, J. Perez, Z. Ghassemlooy, S. Rajbhandari, and J. Libich, "Route diversity analyses for free-space optical wireless links within turbulent scenarios," *Opt. Express*, vol. 21, no. 6, pp. 7641-7650, 2013/03/25 2013, doi: 10.1364/OE.21.007641.
[277] M. Abaza, R. Mesleh, A. Mansour, and E. M. Aggoune, "Spatial diversity for FSO communication systems over atmospheric turbulence channels," in *2014 IEEE Wireless Communications and Networking Conference (WCNC)*, 6-9 April 2014 2014, pp. 382-387, doi: 10.1109/WCNC.2014.6952038.
[278] M. Uysal, "Visible light communications: from theory to industrial standardization," in *2019 Optical Fiber Communications Conference and Exhibition (OFC)*, 3-7 March 2019 2019, pp. 1-3.
[279] "Cisco Annual Internet Report (2018–2023) White Paper," March 9, 2020.
[280] V. K. J. Jürgen Franz, V. K. Jain, *Optical communications: components and systems : analysis--design--optimization--application*. CRC press, 2000.
[281] L. Xiaolong, H. Weihong, H. Yousefi'zadeh, and A. Qureshi, "A case study of a MIMO SDR implementation," in *MILCOM 2008 - 2008 IEEE Military Communications Conference*, 16-19 Nov. 2008 2008, pp. 1-7, doi: 10.1109/MILCOM.2008.4753441.
[282] B. Bloessl, M. Segata, C. Sommer, and F. Dressler, "Performance assessment of IEEE 802.11p with an open source SDR-based prototype," *IEEE Transactions on*

Mobile Computing, vol. 17, no. 5, pp. 1162-1175, 2018, doi: 10.1109/TMC.2017.2751474.

[283] C. O. Boakye-Mensah, D. V. Vann, J. J. Ramsey, and H. Guo, "(POSTER) A Software-defined underwater visible light communication testbed," in *2022 18th International Conference on Distributed Computing in Sensor Systems (DCOSS)*, 30 May-1 June 2022 2022, pp. 72-74, doi: 10.1109/DCOSS54816.2022.00024.

[284] O. R. B. Sayco and A. C. Gordillo, "Design and implementation for a USRP – Based visible light communications transceiver," in *2019 UNSA International Symposium on Communications (UNSA ISCOMM)*, 28-29 March 2019 2019, pp. 1-5, doi: 10.1109/UNSAISC.2019.8712826.

[285] R. Martinek, L. Danys, and R. Jaros, "Visible light communication system based on software defined radio: Performance Study of Intelligent Transportation and Indoor Applications," *Electronics*, vol. 8, no. 4, 2019, doi: 10.3390/electronics8040433.

[286] J. G. Proakis, *Digital signal processing: principles algorithms and applications*. Pearson Education India, 2001.

[287] M. Ijaz, Z. Ghassemlooy, H. L. Minh, S. Rajbhandari, J. Perez, and A. Gholami, "Bit error rate measurement of free space optical communication links under laboratory-controlled fog conditions," in *2011 16th European Conference on Networks and Optical Communications*, 20-22 July 2011 2011, pp. 52-55.

[288] A. K. Majumdar, Z. Ghassemlooy, and A. A. B. Raj, "Principles and applications of free space optical communications," (in English), 2019.

[289] T. L. a. A. E. W. Ivan P. Kaminow, *Optical fiber telecommunications systems and networks*, Sixth Edition ed. Academic Press, 2013.

[290] M. Singh, "Mitigating the effects of fog attenuation in FSO communication link using multiple transceivers and EDFA," *Journal of Optical Communications*, vol. 38, no. 2, pp. 169-174, 2017, doi: doi:10.1515/joc-2016-0061.